Eindhoven University of Technology

MASTER

The effect of rear-wheel steering on advanced driver assistance systems

Neilen, T.

Award date:
2020

Link to publication

MASTER THESIS

The Effect of Rear-Wheel Steering on Advanced Driver Assistance Systems

Author:

T. Neilen

Coordinators:

prof.dr. H. Nijmeijer

prof.dr.ir. P.W.A. Zegelaar

TU/e

EINDHOVEN UNIVERSITY OF TECHNOLOGY
DEPARTMENT OF MECHANICAL ENGINEERING

DYNAMICS AND CONTROL
DC 2020.009

10 FEBRUARY 2020

Abstract

The interest of the automotive industry in rear-wheel steering is gradually rising with several car manufacturers implementing it in recent years. With rear-wheel steering, not only the front wheels are steered, but also the rear wheels, affecting the driving characteristics of the vehicle. This master thesis combines rear-wheel steering with another automotive development, namely advanced driver assistance systems.

Vehicles with advanced driver assistance systems are rapidly entering the consumer market. Advanced driver assistance systems are developed to automate, adapt, and enhance vehicle systems for safety and better driving. These systems have the potential to greatly improve traffic safety by minimising the human error. This report discusses, implements and simulates two advanced driver assistance systems, Lane Centring and Automated Lane Change.

Combining rear-wheel steering and advanced driver assistance systems in a vehicle creates a challenge. The motion and orientation of a vehicle change due to rear-wheel steering, possibly affecting the operation and thus the required control of advanced driver assistance systems. To know if the control needs to be retuned, this research quantifies the effect of rear-wheel steering on advanced driver assistance systems.

For the quantification of this effect, multiple control methods for rear-wheel steering are investigated, as well as the two advanced driver assistance systems, Lane Centring and Automated Lane Change. These systems are modelled using path tracking control. With the use of a simulation model, the effect of the various rear-wheel steering control methods on advanced driver assistance systems is quantified. Analysing the path tracking performance, the largest change in lateral offset due to rear-wheel steering is found to be slightly over 4 cm. Therefore, it is concluded that the control of the advanced driver assistance systems does not have to be retuned when rear-wheel steering is added.

Nomenclature

Roman Symbols

a	Distance from the centre of gravity to the front axle	[m]
a_x	Longitudinal acceleration	[m/s^2]
a_y	Lateral acceleration	[m/s^2]
b	Distance from the centre of gravity to the rear axle	[m]
C	Cornering stiffness	[N/rad]
c_φ	Roll damping	[N·m·s/rad]
e	Error	[m]
F_x	Longitudinal force	[N]
F_y	Lateral force	[N]
F_z	Vertical force	[N]
g	Acceleration due to gravity	[m/s^2]
G	Steady-state yaw rate gain	[s^{-1}]
h	Height from the centre of gravity to the ground	[m]
h'	Height from the centre of gravity to the roll axis	[m]
h_φ	Roll centre height	[m]
I	Moment of inertia	[kg·m^2]
i	Ratio	[-]
K	Gain	[-]
k	Steering angle ratio	[-]
k_φ	Roll stiffness	[N·m/rad]
L	Length	[m]
l	Wheelbase; length; distance	[m]
M	Torque	[N·m]
M_z	Self-aligning torque	[N·m]
m	Mass	[kg]
O	Overshoot	[%]
P	Point	[-]
Q_i	Generalised force	[-]
q_i	Generalised coordinate	[-]
R	Radius	[m]
r	Yaw rate	[rad/s]
s	Half track width	[m]
T	Kinetic energy	[J]
t	Time	[s]
U	Potential energy	[J]
V	Velocity	[m/s]
v_x	Longitudinal velocity	[m/s]
v_y	Lateral velocity	[m/s]
x	Position coordinate; x-coordinate	[m]
y	Position coordinate; y-coordinate; lateral offset	[m]
z	Position coordinate; z-coordinate	[m]

Greek Symbols

α	Axle side-slip angle; wheel side-slip angle	[rad]
β	Side-slip angle	[rad]
γ	Angle	[rad]
δ	Steering angle	[rad]
ζ	Damping ratio	[-]
η	Understeer coefficient	[-]
θ	Roll axis inclination angle	[rad]
κ	Curvature	[m^{-1}]
τ	Time constant	[s]
φ	Roll angle	[rad]
ψ	Yaw angle	[rad]
ω	Angular natural frequency	[rad/s]

Subscripts

a	Look-ahead; at the look-ahead point
c	Controller; determined by the controller
D	Derivative
d	Damped
e	At the centre of gravity
F-150	Ford F-150
Fiesta	Ford Fiesta
g	Global; with respect to the global coordinate system
I	Integral
init	Initial
L	Left tyre; left wheel
max	Maximum
n	Undamped
P	Proportional
p	Peak
pr	Projection
R	Right tyre; right wheel
ri	Rise
rel	Relative; between the path and vehicle
se	Settling
st	Steering
sw	Steering wheel
sat	Saturation value

Abbreviations

ADAS	Advanced Driver Assistance Systems
ALC	Automated Lane Change
ILC	Iterative Learning Control
LC	Lane Centring
MPC	Model Predictive Control
ODE	Ordinary Differential Equation
PID	Proportional-Derivative-Integral
RMSE	Root-Mean-Square Error
RWS	Rear-Wheel Steering

Contents

Chapter 1

Introduction

This master thesis combines two automotive developments, rear-wheel steering (RWS) and advanced driver assistance systems (ADAS). Both will be briefly addressed in this introduction, along with the problem definition, research goal, report outline, and the sign convention used in the report.

1.1 Rear-Wheel Steering

Around the 1980s, a relatively large amount of research was conducted regarding RWS. After that, the interest in it seemed to be somewhat diluted. However, the interest in RWS seems to be back, because several car manufacturers have implemented RWS in recent years. With RWS, not only the front wheels are steered, but also the rear wheels. This affects the driving characteristics of the vehicle. It provides the capability to make the vehicle more agile or increase its stability.

There are many control methods for RWS researched, tested, and applied throughout the years. Some methods control the steering angle of the rear wheels independently of the front wheels. This could have potential benefits in certain situations. For example, during a lane change, the steering angles of the front and rear wheels may be the same, causing the car to change lanes with a crab-like movement. However, this research solely focusses on RWS control methods where the rear-wheel steering angle is proportional to the front-wheel steering angle and depends on the vehicle speed.

1.2 Advanced Driver Assistance Systems

Vehicles with ADAS are rapidly entering the consumer market and the impact of these features are transforming traffic safety. ADAS are systems developed to automate, adapt, and enhance vehicle systems for safety and better driving. ADAS are able to reduce road fatalities by minimising the human error [1].

It becomes clear how large the potential impact of ADAS on traffic safety is if one looks at the figures. For example, systems that prevent unintentional lane departures could prevent or mitigate 179,000 crashes in the United States each year, including up to 7,500 fatal crashes. Moreover, forward collision mitigation systems are potentially applicable to around 1.2 million crashes in the United States each year. About 66,000 of these are serious and moderate injury crashes [2].

Adding RWS to a vehicle changes the vehicle's motion and position in the lane. As a result, the following ADAS might be affected:

- **Lane Centring:** this system can detect the lane markings to help the driver with keeping the vehicle in the lane centre [3]. In this research, Lane Centring is modelled to track predefined paths as closely as possible.

- **Automated Lane Change:** a vehicle equipped with Automated Lane Change is able to autonomously perform a lane change. This system will be simulated by letting the vehicle follow a predefined path of a lane change manoeuvre.

- **Automated Parking:** this system is able to locate a suitable parking space and autonomously park the vehicle during perpendicular and parallel parking [4]. Automated Parking will not be further discussed, since it is chosen to focus on Lane Centring and Automated Lane Change during this research.

ADAS are only able to control the vehicle's total steering effort. The steering system chooses the distribution between the front-wheel ans rear-wheel steering angles, as long as the difference in steering angles between front and rear wheels is equal to the total steering effort. This way, the total steering effort determined by an ADAS controller does not change when RWS is added.

1.3   Expected Effect of Rear-Wheel Steering

RWS poses a challenge for the control of ADAS as the motion and the orientation of the vehicle change due to RWS. It is expected that RWS will have an influence on:

- **Steering wheel angle:** the total steering effort stays the same when adding RWS, as explained in the previous section. So the front-wheel steering angle has to change due to the added steering effort at the rear wheels. The steering wheel angle is coupled to the front-wheel steering angle and will therefore also change, which means ADAS that use the steering wheel angle in any way could be affected.

- **Steering wheel torque:** since the steering wheel angle is expected to change, the steering wheel torque could also change. Some ADAS control a trajectory indirectly via the steering wheel torque. These systems will be affected.

- **Yaw angle:** it is expected that if the rear wheels are also steered, the yaw angle of the vehicle changes. If the yaw angle changes, the vehicle orientation also changes. This would affect ADAS that base their trajectory on the heading angle from a camera in the vehicle, as this camera looks ahead of the vehicle and is used to determine the distance between the vehicle's direction of travel and the lane markings.

- **Manoeuvrability:** an enhancement in manoeuvrability is expected at low speeds, because generally, the rear wheels are steered in the opposite direction of the front wheels at low speeds. This means that the control of ADAS possibly has to be altered to fully benefit from this.

1.4   Research Goal

The goal of this research is to quantify the effect of RWS on ADAS and decide whether retuning of ADAS control is required.

RWS changes the vehicle's motion and orientation, altering the behaviour of ADAS, as explained in the previous section. Moreover, ADAS controllers are typically developed and tuned for vehicles without RWS. If retuning the ADAS control for a vehicle with RWS is not required, the development effort is reduced. Therefore, this research goal is set to possibly reduce the future development effort. The main steps taken to achieve the research goal are discussed in the following section.

1.5   Report Outline

This report is divided in six chapters, including this introduction. Chapter 2 introduces two vehicle models and compares these to decide which one should be used for the required simulations and the controller design of RWS and ADAS. Chapter 3 explains the design of multiple RWS control methods for two different vehicles. Next, Chapter 4 discusses the control of the two ADAS, Lane Centring and Automated Lane Change, and explains the corresponding simulation model, which also implements the developments of Chapters 2 and 3. In the following chapter, Chapter 5, the simulation model is used for a quantitative analysis of the effect of RWS on ADAS. Finally, Chapter 6 discusses the major findings in the conclusions and presents the recommendations for future research.

1.6   Sign Convention

This report uses the so-called adapted SAE sign convention. This sign convention is based on the SAE sign convention, but is adapted, as described in [6]. Figure 1.1 shows the x-axis, y-axis, and z-axis of the adapted SAE sign convention, including the positive direction of rotation around each axis. Compared to the SAE sign convention, the adapted SAE sign convention reverses the sign of the negative vertical force. So the vertical force is positive. Furthermore, the sign of the side-slip angle with respect to the SAE sign convention is reversed to enhance the similarity between the longitudinal and lateral slip characteristics. An overview of different sign conventions, along with more detailed information about the adapted SAE sign convention, can be found in Appendix A.
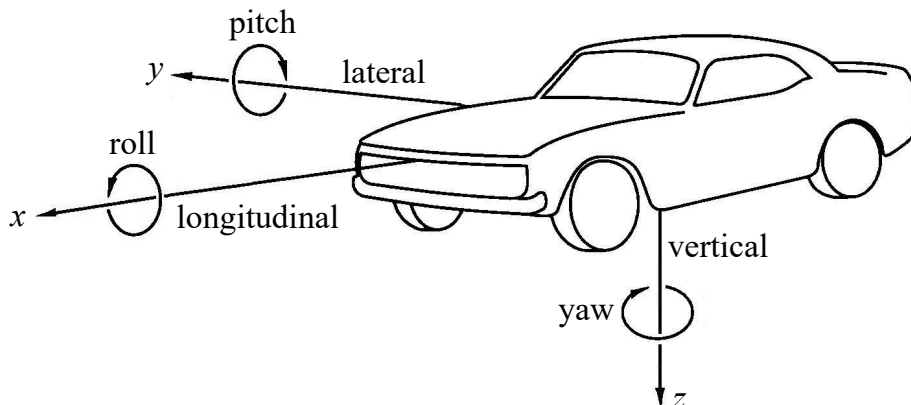
Figure 1.1: Adapted SAE sign convention. Adapted from [5].

3

Chapter 2

Vehicle Models

This chapter introduces two vehicle models. The first section presents a so-called linear single track vehicle model, which will be used to develop controllers for RWS and ADAS, and for linear simulations. Furthermore, the steady-state responses of the yaw rate, lateral acceleration, and side-slip angle are determined in the first section, using the linear single track vehicle model. The second section presents a more complex non-linear two track vehicle model, which is able to simulate non-linear manoeuvres more accurately. The third section compares the vehicle models and the final section gives a summary.

2.1   Single Track Vehicle Model

The linear single track vehicle model, shown in Figure 2.1, is used for the controller design of RWS and ADAS, and for all simulations, besides non-linear ones. This vehicle model is a mathematical model of a two-wheel in-plane vehicle with two degrees of freedom, yaw rate r and lateral velocity v_y. Multiple assumptions are made regarding the linear single track vehicle model [5] [6] [7]:

- The longitudinal velocity v_x is constant. Moreover, the linear single track vehicle model is simplified by using v_x instead of velocity V, because it is hard to precisely determine V in a vehicle due to v_y being difficult to measure.
- Roll and pitch are neglected, so no load transfer and thus constant vertical forces.
- The left and right tyre are combined into an equivalent tyre characteristic, which describes the axle's lateral tyre force as a linear function of the side-slip angle at the wheel, assuming the side-slip angle is small.
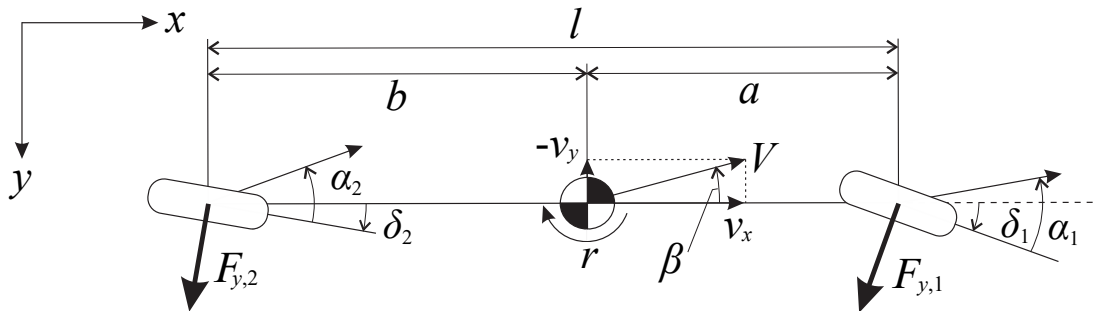- The lateral tyre forces are the only external forces on the vehicle.

Figure 2.1: Single track vehicle model. Adapted from [7].

5

The equations of motion of the linear single track vehicle model are [5] [6]:

$$m \left(\dot{v}_y + v_x r \right) = F_{y,1} + F_{y,2} \tag{2.1}$$

$$I_{zz} \dot{r} = a F_{y,1} - b F_{y,2} \tag{2.2}$$

with:

$$F_{y,1} = C_1 \alpha_1 \ , \quad F_{y,2} = C_2 \alpha_2 \tag{2.3}$$

$$\alpha_1 = \delta_1 - \frac{v_y + ar}{v_x} \ , \quad \alpha_2 = \delta_2 - \frac{v_y - br}{v_x} \tag{2.4}$$

where m is the mass, $F_{y,1}$ and $F_{y,2}$ are the lateral forces at the front and rear wheels respectively, I_{zz} is the moment of inertia about a vertical axis through the centre of gravity, a and b are the distances from the centre of gravity to the front and rear axle respectively, C_1 and C_2 are the cornering stiffness of the front and rear tyres respectively, α_1 and α_2 are the side-slip angles at the front and rear wheels respectively, and δ_1 and δ_2 are the front-wheel and rear-wheel steering angles respectively. Substituting (2.3) and (2.4) into (2.1) and (2.2) results in:

$$m \dot{v}_y + \frac{1}{v_x} \left(C_1 + C_2 \right) v_y + \left(m v_x + \frac{1}{v_x} \left(a C_1 - b C_2 \right) \right) r = C_1 \delta_1 + C_2 \delta_2 \tag{2.5}$$

$$I_{zz} \dot{r} + \frac{1}{v_x} \left(a^2 C_1 + b^2 C_2 \right) r + \frac{1}{v_x} \left(a C_1 - b C_2 \right) v_y = a C_1 \delta_1 - b C_2 \delta_2 \tag{2.6}$$

The model can be written in state-space form with state $\mathbf{x}$, input $\mathbf{u}$, and output $\mathbf{y}$:

$$\dot{\mathbf{x}} = \mathbf{A} \mathbf{x} + \mathbf{B} \mathbf{u} \tag{2.7}$$

$$\mathbf{y} = \mathbf{C} \mathbf{x} + \mathbf{D} \mathbf{u} \tag{2.8}$$

with:

$$\mathbf{x} = \begin{bmatrix} v_y \\ r \end{bmatrix}, \quad \mathbf{u} = \begin{bmatrix} \delta_1 \\ \delta_2 \end{bmatrix}, \quad \mathbf{y} = \begin{bmatrix} a_y \\ r \\ \beta \end{bmatrix} = \begin{bmatrix} \dot{v}_y + v_x r \\ r \\ -\dfrac{v_y}{v_x} \end{bmatrix}, \quad \mathbf{A} = \begin{bmatrix} -\dfrac{C_1 + C_2}{m v_x} & \dfrac{b C_2 - a C_1}{m v_x} - v_x \\ \dfrac{b C_2 - a C_1}{I_{zz} v_x} & -\dfrac{a^2 C_1 + b^2 C_2}{I_{zz} v_x} \end{bmatrix},$$

$$\mathbf{B} = \begin{bmatrix} \dfrac{C_1}{m} & \dfrac{C_2}{m} \\ \dfrac{a C_1}{I_{zz}} & -\dfrac{b C_2}{I_{zz}} \end{bmatrix}, \quad \mathbf{C} = \begin{bmatrix} -\dfrac{C_1 + C_2}{m v_x} & \dfrac{b C_2 - a C_1}{m v_x} \\ 0 & 1 \\ -\dfrac{1}{v_x} & 0 \end{bmatrix}, \quad \mathbf{D} = \begin{bmatrix} \dfrac{C_1}{m} & \dfrac{C_2}{m} \\ 0 & 0 \\ 0 & 0 \end{bmatrix} \tag{2.9}$$

where a_y is the lateral acceleration and β is the side-slip angle.

Now the steady-state responses are determined, which will be used in Chapter 3 to assess the effect of RWS on the vehicle's handling characteristics.

2.1.1 Steady-State Yaw Rate Response

To find the yaw rate response for a vehicle with RWS during steady-state cornering, the steady-state yaw rate gain without RWS is determined first. This is done by setting all time derivatives to zero in (2.5) and (2.6) and neglecting the rear-wheel steering angle. After rewriting, one finds the steady-state yaw rate gain for a vehicle without RWS, provided that $\delta_1 \neq 0$:

$$\frac{r}{\delta_1} = \frac{C_1 C_2 v_x l}{C_1 C_2 l^2 - m v_x^2 (a C_1 - b C_2)} \tag{2.10}$$

which can be rewritten as:

$$\frac{r}{\delta_1} = \frac{v_x/l}{1 + \dfrac{\eta}{gl} v_x^2} \tag{2.11}$$

where l is the wheelbase, η is the understeer coefficient, and g is the acceleration due to gravity. Doing the same for a vehicle that only steers the rear wheels results in the same expression as (2.11), except that r is divided by δ_2 instead of δ_1, provided that $\delta_2 \neq 0$. Combining this with (2.11), the steady-state yaw rate response with RWS is:

$$r = \frac{v_x/l}{1 + \dfrac{\eta}{gl} v_x^2} (\delta_1 - \delta_2) \tag{2.12}$$

Using the RWS control methods, explained in Chapter 3, the rear-wheel steering angle can be expressed as a constant term multiplied by the front-wheel steering angle. This makes it possible to obtain the steady-state yaw rate gain r/δ_1 with (2.12).

2.1.2 Steady-State Lateral Acceleration Response

During steady-state cornering, $\dot{v}_y$ is zero. So using (2.9), one finds that $a_y = v_x r$. With that expression and the steady-state yaw rate response in (2.12), the steady-state lateral acceleration response for a vehicle with RWS is found to be:

$$a_y = \frac{v_x^2/l}{1 + \dfrac{\eta}{gl} v_x^2} (\delta_1 - \delta_2) \tag{2.13}$$

Again, the rear-wheel steering angle can be expressed as a constant term multiplied by the front-wheel steering angle to obtain the steady-state lateral acceleration gain a_y/δ_1.

2.1.3 Steady-State Side-Slip Angle Response

To determine the side-slip angle response for a vehicle with RWS during steady-state cornering, the method of subsection 2.1.1 is used. So the steady-state side-slip angle gain without RWS is determined first. This is done by setting all time derivatives to zero in (2.5) and (2.6), neglecting the rear-wheel steering angle, and knowing that $\beta = -v_y/v_x$.

After rewriting, one finds the steady-state side-slip angle gain for a vehicle without RWS, provided that $\delta_1 \neq 0$:

$$\frac{\beta}{\delta_1} = \frac{C_1 amv_x^2 - C_1 C_2 lb}{C_1 C_2 l^2 - mv_x^2 (aC_1 - bC_2)} \tag{2.14}$$

which can be rewritten as:

$$\frac{\beta}{\delta_1} = \frac{\dfrac{amv_x^2}{C_2 l^2} - \dfrac{b}{l}}{1 + \dfrac{\eta}{gl} v_x^2} \tag{2.15}$$

For a vehicle that only steers the rear wheels and provided that $\delta_2 \neq 0$, the expression is:

$$\frac{\beta}{\delta_2} = \frac{\dfrac{bmv_x^2}{C_1 l^2} + \dfrac{a}{l}}{1 + \dfrac{\eta}{gl} v_x^2} \tag{2.16}$$

Combining (2.15) and (2.16), the steady-state side-slip angle response with RWS is:

$$\beta = \frac{\left(\dfrac{amv_x^2}{C_2 l^2} - \dfrac{b}{l}\right) \delta_1 - \left(\dfrac{bmv_x^2}{C_1 l^2} + \dfrac{a}{l}\right) \delta_2}{1 + \dfrac{\eta}{gl} v_x^2} \tag{2.17}$$

As stated in subsection 2.1.1, the rear-wheel steering angle can be expressed as a constant term multiplied by the front-wheel steering angle. This makes it possible to obtain the steady-state side-slip angle gain β/δ_1 using (2.17).

2.1.4 Simulation Model

A simulation model of the linear single track vehicle model is implemented in MATLAB and created for a vehicle with RWS. If a vehicle without RWS has to be simulated, the rear-wheel steering angle can be set to zero. The model's main input is the front-wheel steering angle, which is used, along with the predefined longitudinal velocity, to determine the rear-wheel steering angle if RWS is used. RWS will be addressed in Chapter 3.

The front-wheel steering angle is a predefined input vector as a function of time. To find the angle at each time step, the `linear` interpolation method is used, which means that the interpolated value at a query point is based on linear interpolation of the values at neighbouring grid points in each respective dimension [8]. A similar approach is done for the rear-wheel steering angle and longitudinal velocity, but this velocity can only increase slowly, because the vehicle model assumes a constant longitudinal velocity.

Based on the inputs and states, $\dot{v}_y$ and $\dot{r}$ are calculated using the equations of motion, shown in (2.5) and (2.6). These are integrated with the `ode45` ordinary differential equation (ODE) solver with a variable step size. This solver is based on an explicit Runge-Kutta formula, namely the Dormand-Prince method [9]. Having the lateral velocity and yaw rate, the lateral acceleration and side-slip angle are found using their expressions in output **y** of (2.9).

2.2   Two Track Vehicle Model

The non-linear two track vehicle model will be used to simulate non-linear manoeuvres, as it can do this more accurately than the linear single track vehicle model. Figures 2.2 and 2.3 show the non-linear two track vehicle model. This vehicle model has four degrees of freedom, longitudinal velocity v_x, lateral velocity v_y, yaw rate r, and roll angle φ. Point P_{pr} in Figures 2.2 and 2.3 is the projection on the ground plane of the centre of gravity if the roll angle is zero. The vehicle body can roll around the roll axis, which is a virtual axis defined by the roll centre height of the front axle $h_{\varphi,1}$ and the roll centre height of the rear axle $h_{\varphi,2}$. Both roll centres contain springs and dampers to simulate the roll stiffness and roll damping.
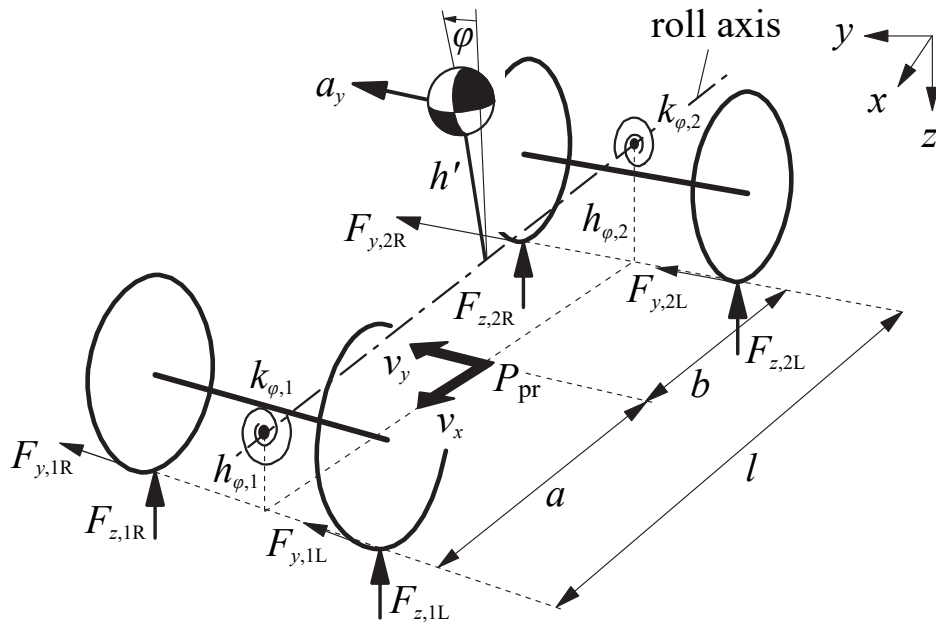

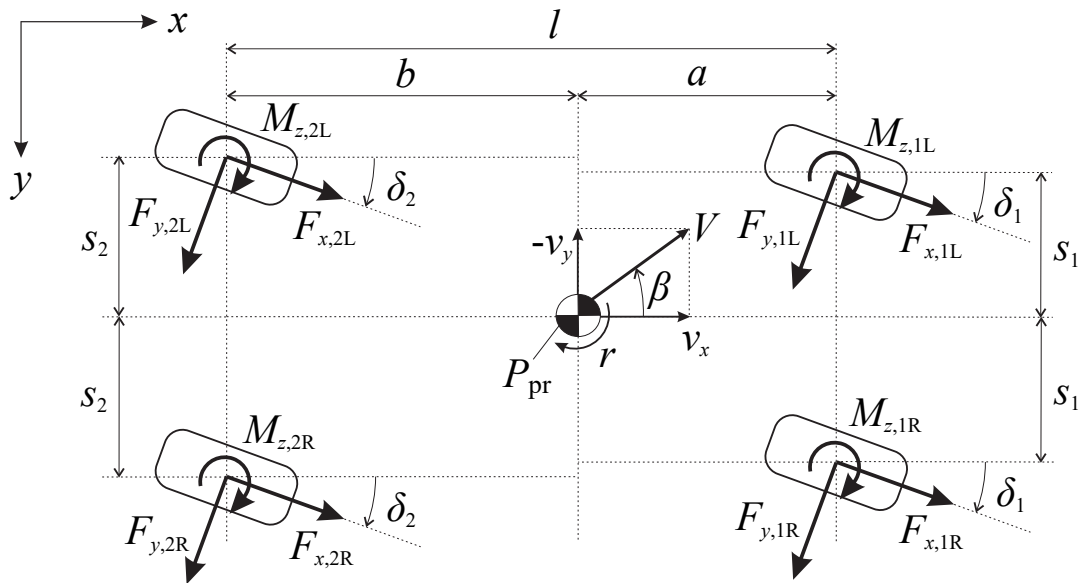**Figure 2.2:** Two track vehicle model. Adapted from [6].

Figure 2.3: Top view of two track vehicle model. Adapted from [7].

9

Now the equations of motion for the non-linear two track vehicle model are determined. For a system with n degrees of freedom, n generalised coordinates q_i are selected. These describe the kinetic energy T and potential energy U of the system. External generalised forces Q_i associated with the generalised coordinates q_i may act on the system. For coordinate q_i, the Lagrangian equation is defined as [5] [6]:

$$\frac{\mathrm{d}}{\mathrm{d}t} \frac{\partial T}{\partial \dot{q}_i} - \frac{\partial T}{\partial q_i} + \frac{\partial U}{\partial q_i} = Q_i \tag{2.18}$$

The generalised motion variables are v_x, v_y, and r, in addition to the coordinate φ. The following set of modified Lagrangian equations are obtained [5] [6]:

$$\frac{\partial}{\partial t} \frac{\partial T}{\partial v_x} - r \frac{\partial T}{\partial v_y} = Q_{v_x} \tag{2.19}$$

$$\frac{\partial}{\partial t} \frac{\partial T}{\partial v_y} + r \frac{\partial T}{\partial v_x} = Q_{v_y} \tag{2.20}$$

$$\frac{\partial}{\partial t} \frac{\partial T}{\partial r} - v_y \frac{\partial T}{\partial v_x} + v_x \frac{\partial T}{\partial v_y} = Q_r \tag{2.21}$$

$$\frac{\partial}{\partial t} \frac{\partial T}{\partial \dot{\varphi}} - \frac{\partial T}{\partial \varphi} + \frac{\partial U}{\partial \varphi} = Q_\varphi \tag{2.22}$$

The non-conservative generalised forces Q_i follow from the virtual work as a result of the virtual displacement. Using Figure 2.3, these forces are [5] [6] [7]:

$$\begin{aligned} Q_{v_x} = \sum F_x &= (F_{x,1L} + F_{x,1R})\cos\delta_1 - (F_{y,1L} + F_{y,1R})\sin\delta_1 \\ &+ (F_{x,2L} + F_{x,2R})\cos\delta_2 - (F_{y,2L} + F_{y,2R})\sin\delta_2 \end{aligned} \tag{2.23}$$

$$\begin{aligned} Q_{v_y} = \sum F_y &= (F_{x,1L} + F_{x,1R})\sin\delta_1 + (F_{y,1L} + F_{y,1R})\cos\delta_1 \\ &+ (F_{x,2L} + F_{x,2R})\sin\delta_2 + (F_{y,2L} + F_{y,2R})\cos\delta_2 \end{aligned} \tag{2.24}$$

$$\begin{aligned} Q_r = \sum M_z &= M_{z,1L} + M_{z,1R} + M_{z,2L} + M_{z,2R} \\ &+ a\,(F_{x,1L} + F_{x,1R})\sin\delta_1 + a\,(F_{y,1L} + F_{y,1R})\cos\delta_1 \\ &- b\,(F_{x,2L} + F_{x,2R})\sin\delta_2 - b\,(F_{y,2L} + F_{y,2R})\cos\delta_2 \\ &+ (F_{x,1L}\cos\delta_1 - F_{y,1L}\sin\delta_1)\,s_1 - (F_{x,1R}\cos\delta_1 - F_{y,1R}\sin\delta_1)\,s_1 \\ &+ (F_{x,2L}\cos\delta_2 - F_{y,2L}\sin\delta_2)\,s_2 - (F_{x,2R}\cos\delta_2 - F_{y,2R}\sin\delta_2)\,s_2 \end{aligned} \tag{2.25}$$

$$Q_\varphi = \sum M_\varphi = -\left(c_{\varphi,1} + c_{\varphi,2}\right)\dot{\varphi} \tag{2.26}$$

where $F_{x,1L}$, $F_{x,1R}$, $F_{x,2L}$, and $F_{x,2R}$ are the longitudinal forces, $F_{y,1L}$, $F_{y,1R}$, $F_{y,2L}$, and $F_{y,2R}$ are the lateral forces, and $M_{z,1L}$, $M_{z,1R}$, $M_{z,2L}$, and $M_{z,2R}$ are the self-aligning torques of each tyre. Furthermore, s_1 and s_2 are half of the front and rear track widths respectively, and $c_{\varphi,1}$ and $c_{\varphi,2}$ are the roll damping at the front and rear axle respectively.

The vehicle's kinetic energy T is expressed as [5] [6]:

$$
\begin{aligned}
T = \frac{1}{2}\, m \left((v_x - h'\varphi r)^2 + (v_y + h'\dot\varphi)^2 \right) + \frac{1}{2}\, I_{xx}\dot\varphi^2 \\
+ \frac{1}{2}\, I_{yy}(\varphi r)^2 + \frac{1}{2}\, I_{zz}\left(r^2 - \varphi^2 r^2 + 2\theta r\dot\varphi \right) - I_{xz} r\dot\varphi
\end{aligned}
\tag{2.27}
$$

where h' is the height from the centre of gravity to the roll axis, I_{xx}, I_{yy}, I_{zz}, and I_{xz} are the moments of inertia in different directions, and θ is the roll axis inclination angle. The vehicle's potential energy U becomes [5] [6]:

$$
U = \frac{1}{2}\left(k_{\varphi,1} + k_{\varphi,2} \right)\varphi^2 - \frac{1}{2}\, mgh'\varphi^2
\tag{2.28}
$$

where $k_{\varphi,1}$ and $k_{\varphi,2}$ are the roll stiffness at the front and rear axle respectively. Using (2.23) to (2.28), the equations of motion with RWS are found:

$$
\begin{aligned}
m \left(\dot v_x - rv_y - h'\varphi\dot r - 2h'r\dot\varphi \right) = (F_{x,1L} + F_{x,1R})\cos\delta_1 - (F_{y,1L} + F_{y,1R})\sin\delta_1 \\
+ (F_{x,2L} + F_{x,2R})\cos\delta_2 - (F_{y,2L} + F_{y,2R})\sin\delta_2
\end{aligned}
\tag{2.29}
$$

$$
\begin{aligned}
m \left(\dot v_y + rv_x + h'\ddot\varphi - h'r^2\varphi \right) = (F_{x,1L} + F_{x,1R})\sin\delta_1 + (F_{y,1L} + F_{y,1R})\cos\delta_1 \\
+ (F_{x,2L} + F_{x,2R})\sin\delta_2 + (F_{y,2L} + F_{y,2R})\cos\delta_2
\end{aligned}
\tag{2.30}
$$

$$
\begin{aligned}
I_{zz}\dot r + (I_{zz}\theta - I_{xz})\ddot\varphi - mh'(\dot v_x - rv_y)\varphi = M_{z,1L} + M_{z,1R} + M_{z,2L} + M_{z,2R} \\
+ a\,(F_{x,1L} + F_{x,1R})\sin\delta_1 + a\,(F_{y,1L} + F_{y,1R})\cos\delta_1 \\
- b\,(F_{x,2L} + F_{x,2R})\sin\delta_2 - b\,(F_{y,2L} + F_{y,2R})\cos\delta_2 \\
+ (F_{x,1L}\cos\delta_1 - F_{y,1L}\sin\delta_1)\, s_1 - (F_{x,1R}\cos\delta_1 - F_{y,1R}\sin\delta_1)\, s_1 \\
+ (F_{x,2L}\cos\delta_2 - F_{y,2L}\sin\delta_2)\, s_2 - (F_{x,2R}\cos\delta_2 - F_{y,2R}\sin\delta_2)\, s_2
\end{aligned}
\tag{2.31}
$$

$$
\begin{aligned}
\left(I_{xx} + mh'^2 \right)\ddot\varphi + mh'(\dot v_y + rv_x) + (I_{zz}\theta - I_{xz})\dot r - \left(mh'^2 + I_{yy} - I_{zz} \right)\varphi r^2 \\
+ (c_{\varphi,1} + c_{\varphi,2})\dot\varphi + (k_{\varphi,1} + k_{\varphi,2} - mgh')\varphi = 0
\end{aligned}
\tag{2.32}
$$

The roll angle φ and roll axis inclination angle θ are assumed to be small. The non-linear two track vehicle model is implemented in SIMULINK. The simulation model described in [5] is used as a basis. Figure 2.4 shows a high-level overview of the model.
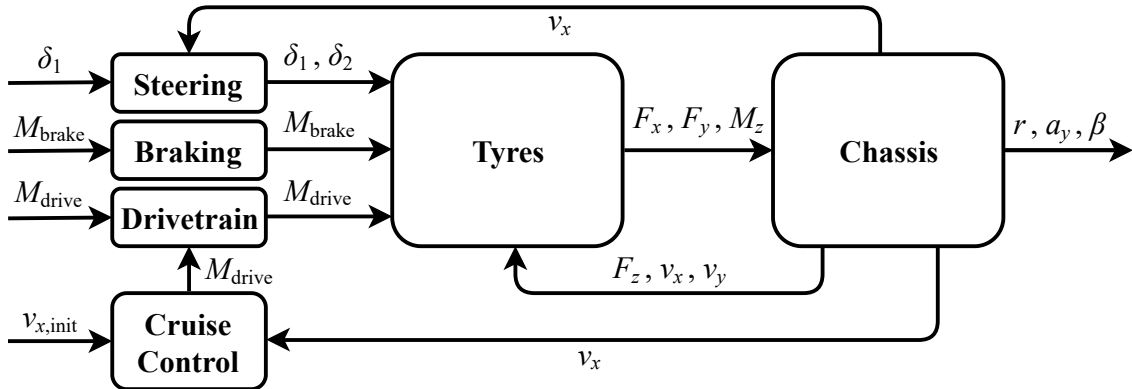

Figure 2.4: Overview of the two track vehicle model as implemented in SIMULINK.

The model described in [5] is optimised for this research. The major changes are:

- RWS is added in the steering block using a so-called MATLAB function block. In the MATLAB function block, the front-wheel steering angle and longitudinal velocity, which are the inputs, are used to determine the rear-wheel steering angle with one of the RWS control methods that will be explained in Chapter 3. Also, a gain is added after the block, which can be set to 1 for RWS and to 0 for no RWS.

- The cornering stiffness of the tyres used in the Magic Formula is adjusted so that it represents the cornering stiffness of the simulated vehicle. The adjustment of the cornering stiffness is made using the scaling factors of the Magic Formula [6]. All other tyre parameters and the relaxation length of the tyres are unchanged.

- The option to switch between front-wheel, rear-wheel, and all-wheel drive is added. By default, the model splits the driving torque M_{drive}, which is a model input, to all four wheels using a gain of 0.25, so 25 % to each wheel. This gain is replaced by four separate gains in the drivetrain block. This makes it also possible to send all driving torque to either the front or rear wheels.

- The model is changed to be able to use predefined input vectors for front-wheel steering angle δ_1, driving torque M_{drive}, and brake torque M_{brake} as model inputs. This is done by changing out the model's input blocks to blocks that can load predefined input vectors, which are so-called from workspace blocks.

The model is simulated using the `ode45` ODE solver with a variable step size, which is based on the Dormand-Prince method [9]. As can be seen in Figure 2.4, there are four model inputs, front-wheel steering angle δ_1, driving torque M_{drive}, brake torque M_{brake}, and initial longitudinal velocity $v_{x,\text{init}}$.

The front-wheel steering angle, along with the longitudinal velocity from the chassis block, is used in the steering system block to determine the rear-wheel steering angle before going to the tyres block. The driving torque needed to maintain a certain speed is determined in the cruise control block by comparing the value of $v_{x,\text{init}}$ with the current longitudinal velocity. The driving torque is sent to the drivetrain block and there split between the wheels. Another option is to turn off cruise control and use a predefined driving torque and brake torque, which are split between the wheels in the drivetrain block and braking block respectively, and determine if the vehicle accelerates or brakes. The steering angles, drive torque, and brake torque are sent to the tyres block.

In the tyres block, the drive torque, brake torque, and longitudinal forces are used to determine the angular acceleration of the wheels, which is integrated to obtain the rotation speed of the wheels. Furthermore, v_x and v_y from the chassis block are converted to velocities at the wheels. All three velocities are used to find the side-slip angles and longitudinal slip of the wheels. These are then used, along with the vertical forces F_z from the chassis block, in the Magic Formula to calculate the lateral forces, longitudinal forces, and the self-aligning torques of the tyres [6]. These forces are converted to chassis forces and sent to the chassis block, along with the self-aligning torques of the tyres.

The chassis block uses the chassis forces and self-aligning torques in the equations of motion, shown in (2.29) to (2.32), to find $\dot{v}_x$, $\dot{v}_y$, $\dot{r}$, and $\ddot{\varphi}$. These results are integrated right after the chassis block to find the longitudinal and lateral velocity, yaw rate, and roll angle. Finally, all other desired outputs can be determined using the results of the equations of motion and their integrated values.

2.3 Comparison of Vehicle Models

This section compares the linear single track vehicle model in MATLAB and the non-linear two track vehicle model in SIMULINK. This is done by discussing the differences in assumptions and vehicle response between the vehicle models.

2.3.1 Differences in Assumptions

This subsection discusses the differences in assumptions between the linear single track and non-linear two track vehicle model, which can divided in three major categories:

- **Longitudinal velocity:** for the linear single track vehicle model, the longitudinal velocity is assumed to be constant. On the other hand, the longitudinal velocity can vary for the non-linear two track vehicle model, meaning that simulating acceleration and braking is possible. Moreover, cruise control can be used to maintain a certain longitudinal velocity, as explained in the previous section.
- **Roll:** the roll in the linear single track vehicle model is neglected, meaning the roll angle φ and its derivative are set equal to zero. The non-linear two track vehicle model does include roll, which results in load transfer.
- **Tyres:** as the non-linear Magic Formula in the non-linear two track vehicle model accurately describes the tyre characteristics up to high levels of slip, this tyre model can be used for simulating manoeuvres with higher levels of lateral acceleration. This in contrast to the linear single track vehicle model, in which the lateral tyre force of each tyre has a linear relation with the side-slip angle at each wheel, due to the assumption that these angles are small.

Furthermore, in [5], test data of vehicle tests is shown, in which an actual vehicle is compared to results of the linear single track vehicle model. It is concluded in [5] that the linear single track vehicle model represents lateral vehicle dynamics quite accurately up to 4 m/s^2. Higher lateral accelerations give non-linear results from the actual vehicle, which are not obtained from the linear single track vehicle model. For these simulations, the non-linear two track vehicle model is suggested. To further investigate the differences between the vehicle models, the next subsection discusses the difference in vehicle response between the linear single track and non-linear two track vehicle model during different circumstances.

2.3.2 Differences in Vehicle Response

To compare the vehicle response using the vehicle models, three simulations will be discussed as an example. For the simulations, the vehicle parameters of a Ford Fiesta are taken, which can be found in Appendix B. During the first simulation, it is chosen to simulate an acceleration from 0 km/h to 200 km/h in 500 s. Due to the fact that the longitudinal velocity should be constant for the linear single track model, the longitudinal acceleration is chosen to be low ($a_x = 0.11$ m/s^2), closely approaching steady-state driving. During the simulation, the steering wheel angle δ_{sw} is kept at 5°, which is chosen to keep the maximum lateral acceleration around 1 m/s^2, so well within the linear part of the Magic Formula, making the simulation results more comparable. So the simulation inputs are the longitudinal velocity and the front-wheel steering angle, which is determined using δ_{sw}. For the non-linear two track vehicle model, $v_{x,\text{init}}$ is predefined, which the cruise control will use as a reference, as explained in the previous section.
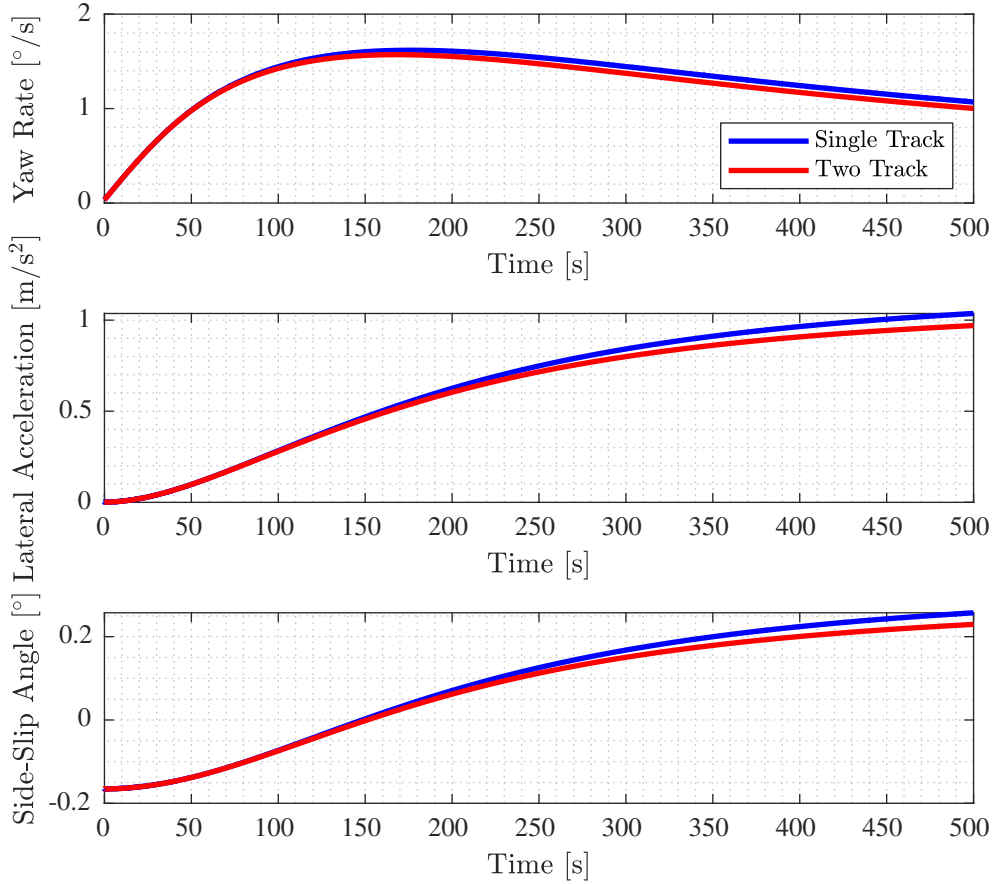
Figure 2.5: Accelerating from 0 km/h to 200 km/h with δ_{sw} at 5°.

The simulation results are shown in Figure 2.5, in which both vehicle models include RWS, which will be explained in Chapter 3. As can be seen, the results of both vehicle models are close to each other at low speeds. However, when the speed increases, the deviation between the results also increases. The roll angle in the non-linear two track vehicle model is equal to $-0.38°$ at its maximum, which is the main cause of the difference. The difference is hardly caused by the different tyre models used in each vehicle model, since the simulation stays well within the linear part of the Magic Formula. Table 2.1 shows the root-mean-square error (RMSE) values and deviations at 200 km/h.

Table 2.1: RMSE and deviation between the single track and two track vehicle model.

Parameter	RMSE [-]	Deviation at 200 km/h [%]
Yaw rate	$9.97 \cdot 10^{-4}$	6.40
Lateral acceleration	0.0388	6.39
Side-slip angle	$2.82 \cdot 10^{-4}$	10.8

The second simulation performs a so-called step response, meaning that the vehicle drives straight at constant speed and at a certain time, a certain input value is chosen and maintained. In this case, the vehicle drives straight at 100 km/h and then steers with a steering wheel angle of 7°. This angle is chosen to stay within the Magic Formula's linear part, as explained before. So the simulation inputs are the longitudinal velocity and the front-wheel steering angle, which is determined using δ_{sw}. Figure 2.6 shows the results.
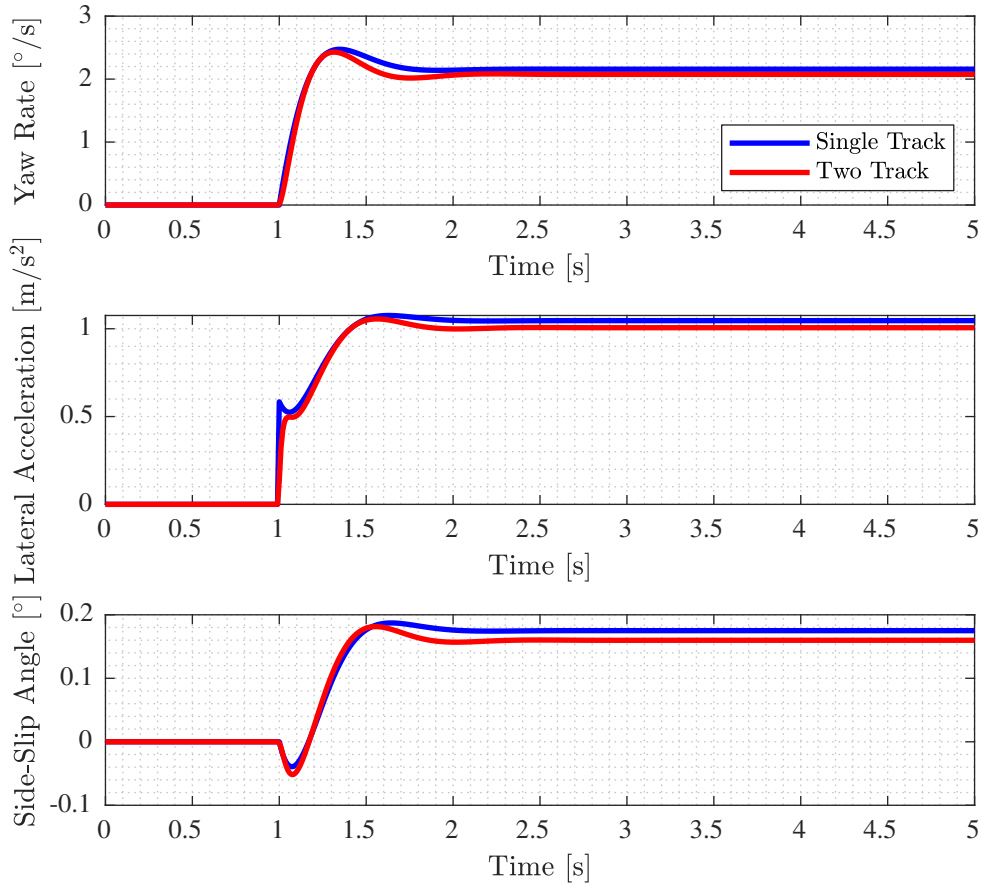
Figure 2.6: Step steer test at 100 km/h with δ_{sw} at 7°.

The non-linear two track vehicle model reacts slightly slower compared to the linear single track vehicle model. This is caused by the relaxation length of the tyres in the tyre model of the non-linear two track vehicle model, which is not implemented in the linear single track vehicle model. Furthermore, the results of the non-linear two track vehicle model show more dynamics and are less damped, which can be declared by the difference in roll. As explained in the previous subsection, the linear single track vehicle model neglects roll instead of taking roll into account, like the non-linear two track vehicle model.

After the step, there is a slight deviation in the steady-state values, which is mainly caused by differences between the vehicle models regarding roll. At around 2 s, the vehicle settles and the roll angle in the non-linear two track vehicle model settles to −0.40°. The RMSE values between the vehicle models are shown in Table 2.2, along with the RMSE values for a step response with a steering wheel angle of 45°. The results of this step response are shown in Figure 2.7.

Table 2.2: RMSE between the single track and two track vehicle model.

Parameter	RMSE [-]	
	$\delta_{sw} = 7°$	$\delta_{sw} = 45°$
Yaw rate	0.00144	0.0304
Lateral acceleration	0.0418	0.832
Side-slip angle	$2.27 \cdot 10^{-4}$	0.00122

15
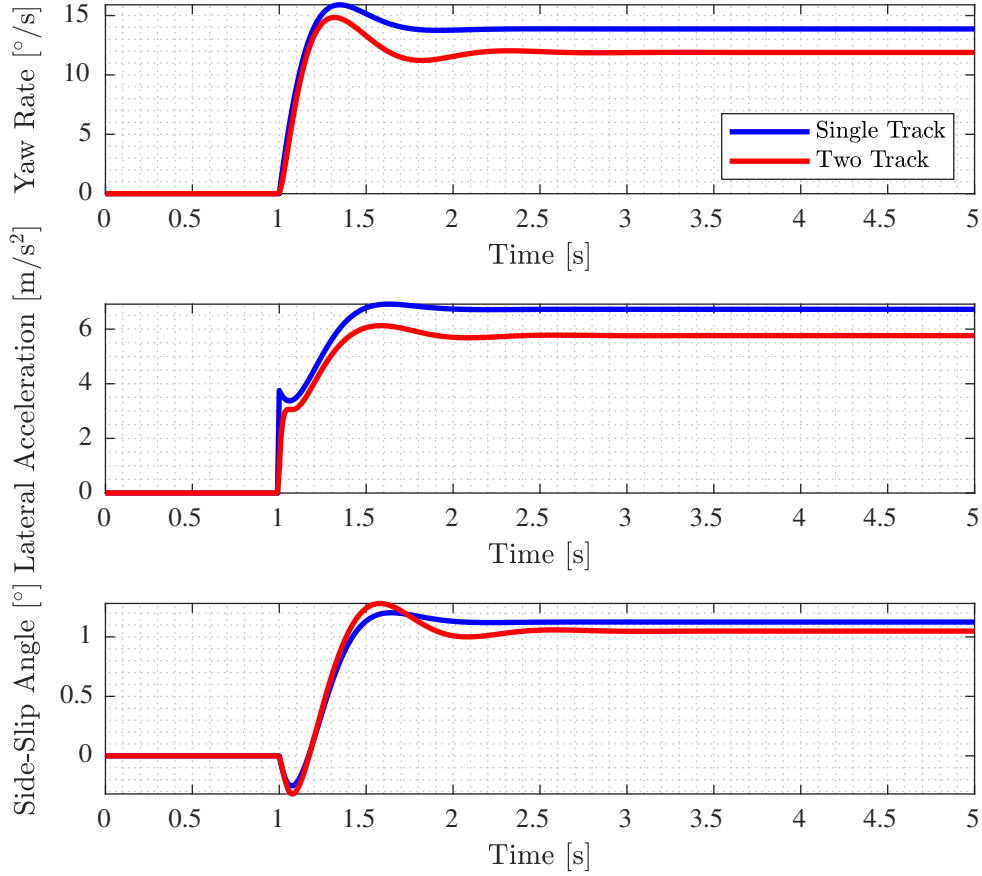
Figure 2.7: Step response at 100 km/h with δ_{sw} at 45°.

As could be expected, the step response with the larger steering wheel angle results in considerably larger RMSE values. For the non-linear two track vehicle model, the tyres now enter the non-linear area of the Magic Formula and the roll angle settles at $-2.3°$. So both effects are far more influential, resulting in a larger difference, and thus a larger RMSE. Furthermore, the differences between the vehicle models during the step, which are already discussed for Figure 2.6, are far more noticeable in Figure 2.7. All in all, the general vehicle behaviour differs more substantially during this second step response compared to the first step response. The extent to which the differences between vehicle models affect the results is further investigated in Appendix C.

It can be concluded that the differences between the models are relatively small and that the same general vehicle characteristics are evident using both vehicle models. However, it should be kept in mind that during non-linear manoeuvres with the lateral acceleration meeting or exceeding 4 m/s², the deviation between the vehicle models becomes noticeably larger.

The non-linear two track vehicle model will only be utilised for several simulations in Chapter 3. During these simulations, the lateral acceleration meets or exceeds 4 m/s². For all other simulations, during which the lateral acceleration is well under 4 m/s², the linear single track vehicle model is used, because of its relative simplicity. So it will also be used for all ADAS simulations.

2.4 Summary

A linear single track vehicle model is implemented in MATLAB, which will be used to develop controllers for RWS and ADAS. The model is simplified by making several assumptions. The steady-state responses of the yaw rate, lateral acceleration, and side-slip angle are obtained using this vehicle model, which will be used in Chapter 3 to assess the effect of RWS on the vehicle's handling characteristics.

Furthermore, a more complex non-linear two track vehicle model is implemented in SIMULINK. Comparing the vehicle models shows that the differences in simulation results are relatively small and that the same general vehicle characteristics are evident using both vehicle models. However, if the lateral acceleration during simulations meets or exceeds 4 m/s^2, the deviation between the models becomes noticeably larger. It is decided that the linear single track vehicle model will be used for all simulations during which the lateral acceleration stays under 4 m/s^2. When this value is met or exceeded, the non-linear two track vehicle model will be used.

Chapter 3

Rear-Wheel Steering

This chapter introduces RWS. The first section presents a literature survey on RWS and RWS control methods. The second section discusses the implemented methods. A total of four RWS control methods is implemented to quantify the effect of RWS on ADAS. This way, the outcome is not based on just one method. To get a better understanding of RWS and its effects, RWS control methods are developed for a small and large vehicle, namely a Ford Fiesta and a Ford F-150 respectively. The third section explains the implementation of the RWS control methods for the two vehicles. The fourth section discusses RWS simulations and the final section gives a summary.

3.1 Literature Survey

This section discusses the RWS control methods researched in literature, but first a brief explanation of RWS itself. A vehicle with RWS cannot only steer its front wheels, but also its rear wheels, introducing a rear-wheel steering angle. This angle depends on the front-wheel steering angle and the longitudinal velocity. The rear-wheel steering angle increases when the front-wheel steering angle increases. The longitudinal velocity affects the rear-wheel steering angle differently. Typically, the rear wheel steer in the opposite direction of the front wheels at low speeds and in the same direction at higher speeds. Countersteering effectively reduces the wheelbase and generates a higher yaw rate, which results in increased agility, improved manoeuvrability, and a smaller turning circle. Steering in the same direction effectively lengthens the wheelbase and generates a lower yaw rate, which improves stability, driving dynamics, and driving safety [10]. Figure 3.1 shows the effects.

− Greater degree of agility
− Easier handling when
  parking and in city traffic
− Smaller turning circle

− Greater stability
− Increased driving dynamics
− Increased driving safety
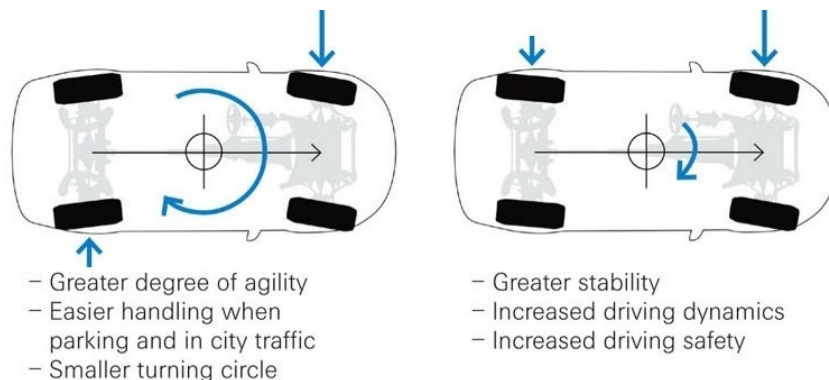
Figure 3.1: Effects of RWS at low speeds (left) and high speeds (right) [10].

Figure 3.2: Vehicle steering response [11].

3.1.1 Decrease Phase Lag

As described in [7], a vehicle is subjected to an increase in time delay in lateral acceleration and yaw rate responses to steering as its speed increases. To maintain its stability, the steering input must have an increasing phase lead to compensate these vehic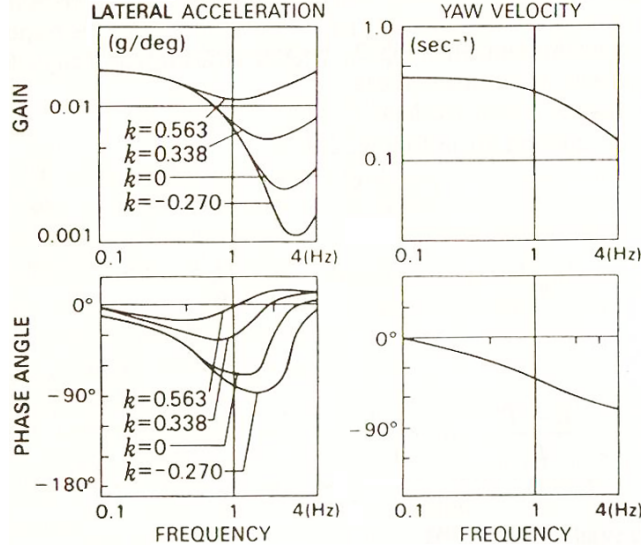le response delays. So a method to achieve phase lag reduction is to look at the response of the yaw rate and lateral acceleration to steering input, as explained in [11] and [12]. Figure 3.2 shows that this response is influenced by the steering angle ratio k, defined as $k = \delta_2/\delta_1$. The lateral acceleration response is improved with a large positive k. The yaw rate response is not influenced by this ratio. So the phase lag between the yaw rate and lateral acceleration can be decreased if the lateral acceleration response is improved, and thus a large positive k is desirable. This means that the rear wheels steer in the same direction as the front wheels at any speed. This negatively influences the vehicle's agility, which is undesirable at low speeds. So this method is not further investigated.

Another variant of this method is proposed in [13], which states that steering the rear wheels in the same direction as the front wheels will slightly increase the phase lag in yaw rate response if the vehicle is understeered. The proposed RWS control method delays the steering action of the rear wheels compared to the front wheels. This reduces the phase lag in both yaw rate and lateral acceleration. However, this variant is not further investigated for the same reason as the previously described variant of this method.

A different method is to analyse the phase lag between the yaw rate and lateral acceleration themselves, explained in [7], [11], and [13]. Ideally, there is no phase lag between the two. So the yaw rate and simultaneously the lateral acceleration increase during cornering. These are related by the side-slip angular velocity $\dot{\beta}$ [5] [6]:

$$a_y = \dot{v}_y + r v_x \approx v_x \left(-\dot{\beta} + r \right) \tag{3.1}$$

As can be seen, the phase lag between the yaw rate and lateral acceleration will decrease when the side-slip angular velocity is reduced. This can be achieved by decreasing the side-slip angle β, which is described in the next subsection.

20

3.1.2 Decrease Side-Slip

A method to control the rear-wheel steering angle is to decrease the side-slip angle, as described in [7], [11], and [13]. To achieve this, the steady-state side-slip angle response in (2.17) is set to zero. From the resulting expression, one can find the relation between the front-wheel and rear-wheel steering angles such that the side-slip angle is equal to zero and thus decreased:

$$\delta_2 = K_\beta \left(\frac{\dfrac{amv_x^2}{C_2 l} - b}{\dfrac{bmv_x^2}{C_1 l} + a} \right) \delta_1 \tag{3.2}$$

where K_β is a gain that scales the resulting rear-wheel steering angle.

3.1.3 Yaw Rate Dependent

Another method to control the rear-wheel steering angle is to make the angle dependent of the yaw rate, as explained in [7]. This means multiplying the yaw rate with a certain constant value to determine the rear-wheel steering angle, which results in:

$$\delta_2 = K_r r - \delta_{2,\max} \frac{\delta_1}{\delta_{1,\max}} \tag{3.3}$$

where K_r is a gain that scales the resulting rear-wheel steering angle. The second term in the expression moves the resulting rear-wheel steering angle to the desirable operation range of the RWS system.

3.2 Controller Designs

This section highlights the RWS controller designs that are implemented. The controller designs described in subsections 3.1.2 and 3.1.3 are both implemented. The rear-wheel steering angle of the method that decreases the side-slip angle is limited to stay within the RWS system's physical limits of $\pm 5°$ and a moving average filter is applied to make the transition to the limitation of the rear-wheel steering angle smoother. The following subsections introduce three new RWS control methods.

3.2.1 Linear

This relatively simple method is primarily developed for quick testing and as a reference for other RWS control methods, since it is relatively simple and predictable. Its steering angle ratio is negative at low speeds, linearly increases when the speed increases, and is positive at higher speeds. To achieve this, the slanted part where the steering angle ratio changes is developed first:

$$\delta_2 = \left(\frac{2\delta_{2,\max}}{v_{x,2} - v_{x,1}} (v_x - v_{x,1}) - \delta_{2,\max} \right) \frac{\delta_1}{\delta_{1,\max}} \tag{3.4}$$

where $\delta_{1,\max}$ and $\delta_{2,\max}$ are the maximum front-wheel and rear-wheel steering angles respectively, and $v_{x,1}$ and $v_{x,2}$ are the longitudinal velocities between which the rear-wheel steering angle goes from its minimum to its maximum value or vice versa.

The longitudinal velocities $v_{x,1}$ and $v_{x,2}$ can be used to tune the resulting rear-wheel steering angle. The rear-wheel steering angle is limited to stay within the RWS system's physical limits of $\pm 5°$ and a moving average filter is applied to make the transition to the limitation smoother.

3.2.2 Adapted Decrease Side-Slip

The method that decreases the side-slip angle described in subsection 3.1.2 is adapted to create a new RWS control method. This new method approximates the method that decreases the side-slip angle at high speeds. However, at low speeds, it is developed to have a larger negative steering angle ratio, which results in enhanced manoeuvrability. The expression for the rear-wheel steering angle that delivers this behaviour is:

$$\delta_2 = K_{\beta,1} \frac{(v_x/v_{x,0})^3 - K_{\beta,2}}{(v_x/v_{x,0})^3 + 1} \frac{\delta_1}{\delta_{1,\max}} \tag{3.5}$$

where $K_{\beta,1}$ is a gain that scales the resulting rear-wheel steering angle, $K_{\beta,2}$ is a gain that adjusts the rear-wheel steering angle at 0 km/h, and $v_{x,0}$ is the longitudinal velocity where the rear-wheel steering angle is equal to zero. So $v_{x,0}$ can be used as a third value to tune the resulting rear-wheel steering angle. Again, the rear-wheel steering angle is limited to stay within the RWS system's physical limits of $\pm 5°$ and a moving average filter is applied to make the transition to the limitation smoother.

3.2.3 Mimic Smaller Vehicle's Behaviour

This RWS control method uses a relatively small vehicle without RWS as a basis to tune the rear-wheel steering angle of a larger vehicle. This way, the behaviour and handling characteristics of the small vehicle can be mimicked in the large vehicle. The Ford Fiesta is used as the small vehicle and the Ford F-150 as the large vehicle. The vehicle parameters of both vehicles can be found in Appendix B. The steady-state yaw rate gains of both vehicles are used, taking (2.11) for the steady-state yaw rate gain of the Ford Fiesta and (2.12) to find the steady-state yaw rate gain of the Ford F-150 with RWS, such that:

$$G_{\text{Fiesta}} = G_{\text{F-150}} \frac{\delta_1 - \delta_2}{\delta_1} \tag{3.6}$$

where G_{Fiesta} and $G_{\text{F-150}}$ are the steady-state yaw rate gains without RWS of the Ford Fiesta and Ford F-150 respectively. The notations Fiesta and F-150 are used to distinguish the vehicles. The steady-state yaw rate gain for each vehicle without RWS is shown in (2.11) and can be expressed as:

$$G_{\text{Fiesta}} = \frac{v_x/l_{\text{Fiesta}}}{1 + \frac{\eta_{\text{Fiesta}}}{gl_{\text{Fiesta}}} v_x^2} \; , \quad G_{\text{F-150}} = \frac{v_x/l_{\text{F-150}}}{1 + \frac{\eta_{\text{F-150}}}{gl_{\text{F-150}}} v_x^2} \tag{3.7}$$

Having (3.6) and (3.7), the relation between the front-wheel and rear-wheel steering angles can be determined:

$$\delta_2 = \left(1 - \frac{G_{\text{Fiesta}}}{G_{\text{F-150}}}\right) \delta_1 \tag{3.8}$$

After implementation, it is found that this RWS control method steers the rear wheels in the opposite direction of the front wheels at any speed. This negatively influences the vehicle's stability, which is undesirable at high speeds. So this method is not further investigated.

3.3 Controller Implementation for Two Vehicles

For the implementation of the RWS control methods, the gains and tunable velocities are chosen for the Ford Fiesta and Ford F-150, using the linear single track vehicle model. The chosen values are shown in Table 3.1.

Table 3.1: Gains and tunable velocities for the RWS control methods.

RWS Control Method	Ford Fiesta	Ford F-150
Linear	$v_{x,1} = 20$ km/h $v_{x,2} = 100$ km/h	$v_{x,1} = 20$ km/h $v_{x,2} = 100$ km/h
Decrease Side-Slip	$K_\beta = 0.25$	$K_\beta = 0.25$
Adapted Decrease Side-Slip	$K_{\beta,1} = 0.079$ $K_{\beta,2} = 3.08$ $v_{x,0} = 48$ km/h	$K_{\beta,1} = 0.052$ $K_{\beta,2} = 4.51$ $v_{x,0} = 64$ km/h
Yaw Rate Dependent	$K_r = 0.0635$	$K_r = 0.0766$

For the linear method, it is chosen to have the steering angle ratio linearly change from 20 km/h to 100 km/h, so the ratio switches sign at 60 km/h. This is inspired by the method that decreases the side-slip angle for the Ford Fiesta, which also changes sign around 60 km/h.

For the method that decreases the side-slip angle, if $K_\beta = 1$, the side-slip angle will be zero. However, this leads to large rear-wheel steering angles that have to be limited due to the RWS system's physical limits of $\pm5°$, even at high speeds. So K_β is set to 0.25, in order to decrease the maximum steering amplitude of the rear-wheel steering angle while still allowing to reach the maximum rear-wheel steering angle of $\pm5°$ up to 16.4 km/h during road driving ($a_y \leq 3$ m/s^2).

The adapted method that decreases the side-slip angle is tuned in such a way that it has the same behaviour as the non-adapted method at high speeds, but has a stronger effect at low speeds. The value of $K_{\beta,1}$ is chosen to mimic the behaviour of the non-adapted method if that method uses $K_\beta = 0.25$. The value of $K_{\beta,2}$ is tuned to make the resulting rear-wheel steering angle at 0 km/h equal to the rear-wheel steering angle of the non-adapted method at 0 km/h. Theoretically, $v_{x,0}$ is the longitudinal velocity where the rear-wheel steering angle is equal to zero. However, due to the effect of $K_{\beta,2}$, this is not exactly the case. Still, $v_{x,0}$ is used to alter the speed at which the rear-wheel steering angle is zero. The value of $v_{x,0}$ is chosen to create a more pronounced effect of RWS at low speeds, compared to the non-adapted method that decreases the side-slip angle. In short, $K_{\beta,1}$ and $K_{\beta,2}$ are tuned to mimic the non-adapted method, and $v_{x,0}$ is tuned to achieve a stronger effect at low speeds.

Finally, for the yaw rate dependent method, K_r is tuned to scale the resulting rear-wheel steering angle exactly within the RWS system's physical limits of $\pm5°$. This is necessary, since this RWS control method is not limited, like the other methods.

The resulting steering angle ratio k, defined as $k = \delta_2/\delta_1$, of the RWS control methods using the values in Table 3.1 is shown in Figures 3.3 and 3.4 for the Ford Fiesta and Ford F-150 respectively. Two comments must be made about these figures. Firstly, $\pm 35°$ and $\pm 5°$ are assumed to be the maximum front-wheel steering angle $\delta_{1,\max}$ and rear-wheel steering angle $\delta_{2,\max}$ respectively. At certain combinations of longitudinal velocity and front-wheel steering angle, some RWS control methods exceed these physical limits, the rear-wheel steering angle is then limited, as stated in the previous section. Secondly, the figures show the steering angle ratios at two front-wheel steering angles. If a front-wheel steering angle of 20° is displayed for example, the steering angle ratios would be limited to ± 0.25 if needed.

Comparing the Ford F-150's RWS control methods with those of the Ford Fiesta, the Ford F-150's methods have a negative steering angle ratio up to a higher speeds. Except the linear method, which is equal for both vehicles. Because of the Ford F-150's considerably longer wheelbase compared to the Ford Fiesta, it benefits more from a negative steering wheel ratio to enhance its agility and manoeuvrability.

(a) Limited ($\delta_1 = 35°$)   **(b)** Not limited ($\delta_1 = 5°$)
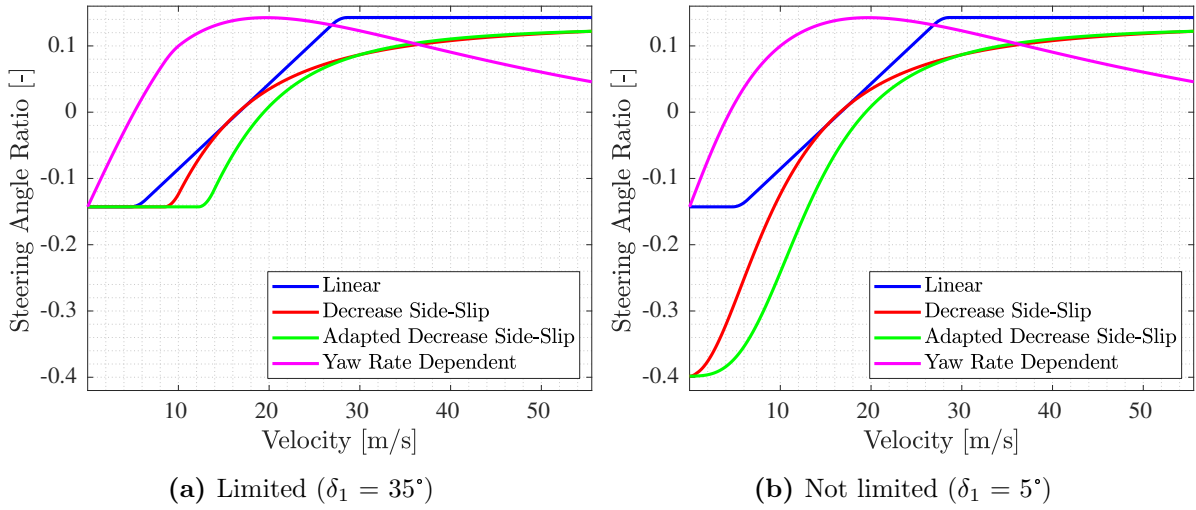
Figure 3.3: Steering angle ratios for the Ford Fiesta.

(a) Limited ($\delta_1 = 35°$)   **(b)** Not limited ($\delta_1 = 5°$)
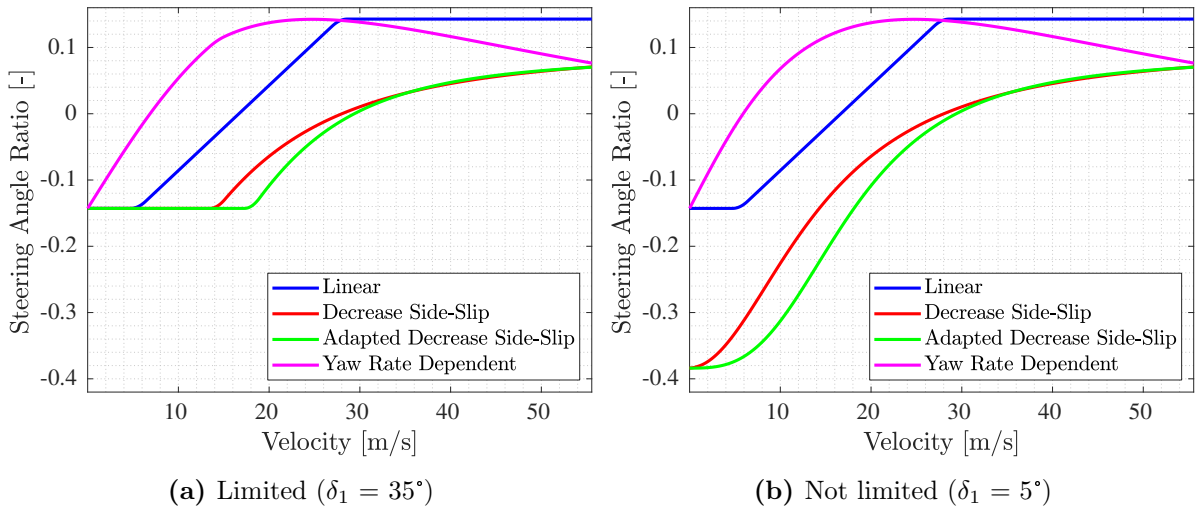
Figure 3.4: Steering angle ratios for the Ford F-150.

3.4 Simulations

To see the effect of the RWS control methods on the handling characteristics of a vehicle, linear simulations are executed using the linear single track vehicle model to obtain the steady-state gains, which will be discussed in the first subsection. The second subsection shows results of non-linear simulations using the non-linear two track vehicle model.

The Ford Fiesta will be used for all further simulations and calculations. Appendix B shows its vehicle parameters. Furthermore, the adapted method that decreases the side-slip angle will be used for all simulations with RWS that are executed to compare a vehicle with and without RWS. This RWS control method is chosen, because it has the smallest steering angle ratio at low speeds and a relatively large ratio at high speeds, as shown in Figure 3.3, making the effect of RWS more noticeable compared to other methods.

3.4.1 Steady-State Gains

To assess the effect of the RWS control methods on the vehicle's handling characteristics, the steady-state gains of the yaw rate, lateral acceleration, and side-slip angle using all methods are obtained, as Figure 3.5 shows. The desirable effect of RWS on the steady-state yaw rate gain is that its value increases at low speeds for improved agility and manoeuvrability. At high speeds, its value should decrease for improved stability. For the steady-state lateral acceleration gain, the same effect is desirable. The desirable effect of RWS on the steady-state side-slip gain is that its value moves closer to zero. Besides the yaw rate dependent method, all methods achieve the desired effects.
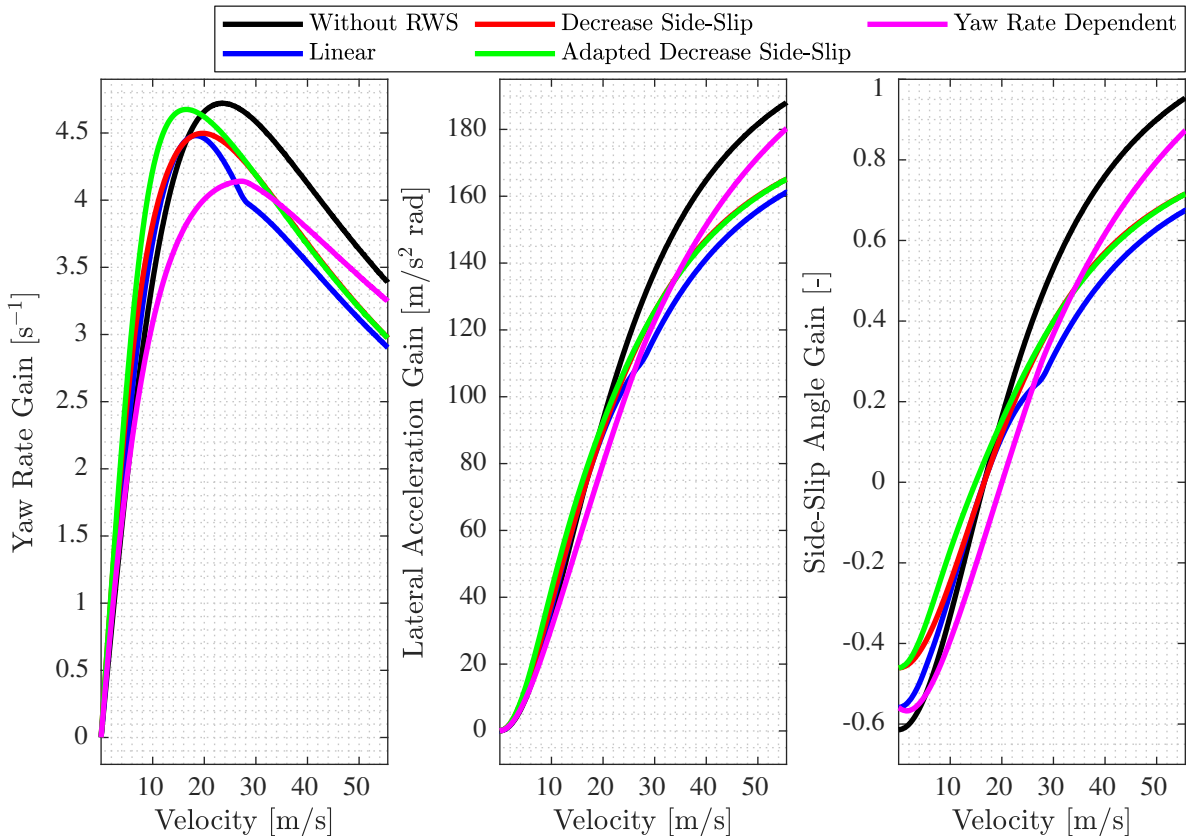
Figure 3.5: Steady-state gains.

Taking a closer look at each method, several comments can be made. Firstly, the yaw rate dependent method has an undesirable effect at low speeds. This can be explained by the fact that this method has a positive steering angle ratio above about 16 km/h, making the vehicle less agile. This happens earlier than with the other methods, as can be seen in Figure 3.3.

Secondly, the linear method has an indent in all steady-state gains around 100 km/h. This is caused by the method's limitation of the rear-wheel steering angle, as shown in Figure 3.3. The moving average filter smooths this transition, but it is still visible.

Lastly, the standard and adapted methods that decrease the side-slip angle are extremely close to each other at high speeds. At low speeds, the adapted method has a more pronounced effect. This is desirable, since the adapted method is developed to have a larger rear-wheel steering angle at low speeds compared to the standard method.

Closer examining the steady-state yaw rate gain gives more inside about the change in the handling characteristics. The adapted method that decreases the side-slip angle is used for the simulation with RWS, as explained in the introduction of this section. Figure 3.6 shows the steady-state yaw rate gain with and without RWS, along with the neutral steer lines. A neutral steer line shows the steady-state yaw rate gain if the vehicle would be neutrally steered, which means its understeer coefficient η is equal to zero. Above this line, a vehicle is oversteered ($\eta < 0$), and under this line, a vehicle is understeered ($\eta > 0$). A neutrally steered vehicle can maintain a constant corner radius while increasing its speed without changing its front-wheel steering angle. An oversteered vehicle has to decrease its front-wheel steering angle to achieve this, and an understeered vehicle must increase the angle [5].

It can be concluded that both vehicles are understeered and that this handling characteristic increases with speed. However, only considering the steady-state yaw rate gains of the vehicles relative to each other, the vehicle with RWS has a larger steady-state yaw rate gain up to 60 km/h and a smaller one at higher speeds. This effect is desirable, because it makes the vehicle more agile at low speeds and more stable at high speeds.
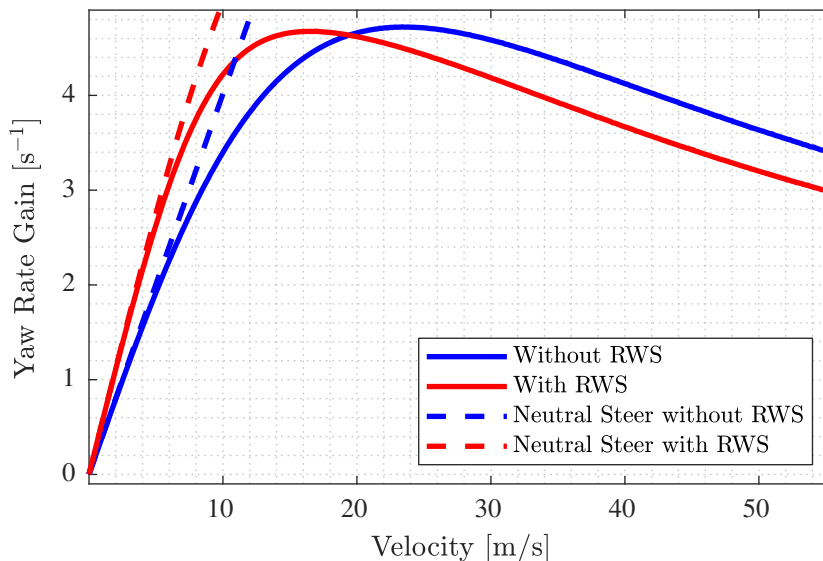
Figure 3.6: Steady-state yaw rate gain and neutral steer line.
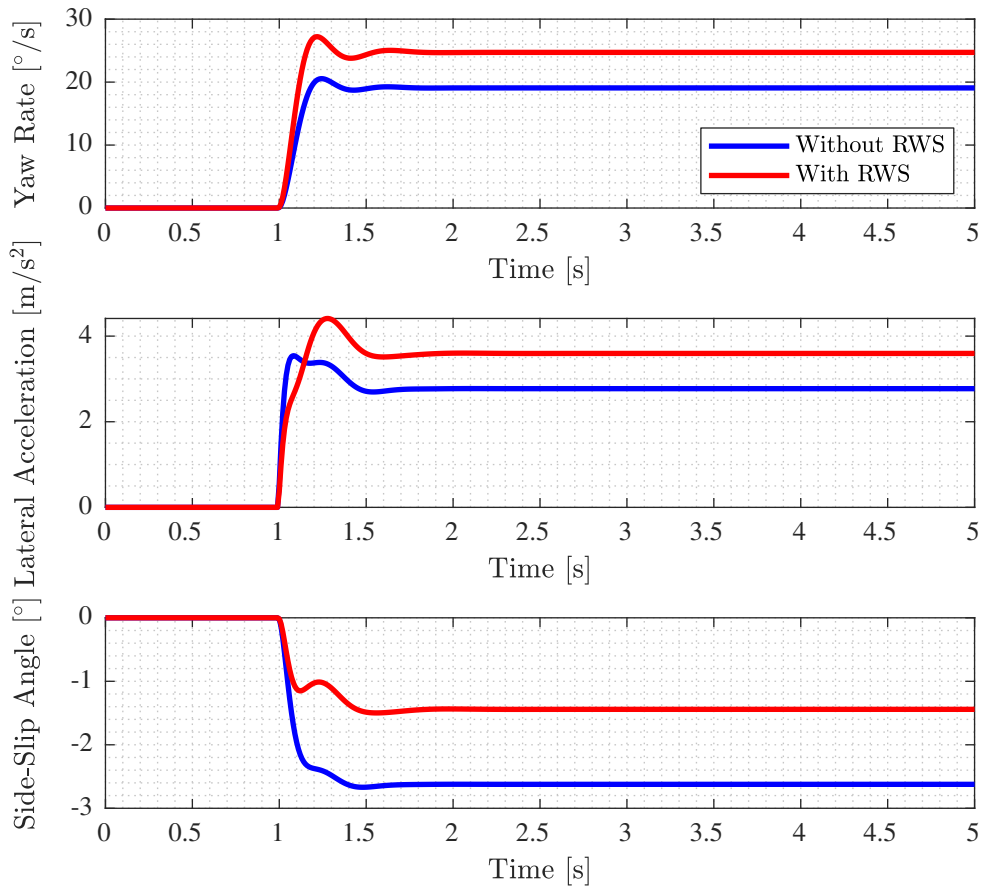
Figure 3.7: Step response at 30 km/h with δ_{sw} at 90°.

3.4.2 Step Response and Moose Test

During the next three simulations, the lateral acceleration is close to or over 4 m/s^2, so the non-linear two track vehicle model is used. For the simulations with RWS, the adapted method to decrease the side-slip angle is used, as explained in the introduction of this section. Starting with the first simulation, a step response at 30 km/h with a steering wheel angle of 90°. The concept of a step response is already explained in subsection 2.3.2. The results of this simulation are shown in Figure 3.7.

The test is executed at 30 km/h, meaning the steering angle ratio is negative when using RWS. Due to this, the overshoot and the steady-state value of the yaw rate and lateral acceleration with RWS are larger than without RWS. From this, it can be concluded that the vehicle with RWS is more agile, which is desirable at this speed. The side-slip angle is smaller with the use of RWS. This is also desirable, since the adapted method to decrease the side-slip angle is used.

During the second simulation, a step response at 100 km/h with a steering wheel angle of 45° is executed. Figure 3.8 shows the results. The opposite effect of RWS is reflected in these results, because at 100 km/h the steering angle ratio is positive, improving the vehicle's stability. Therefore, this is the desired result of the simulation.

27
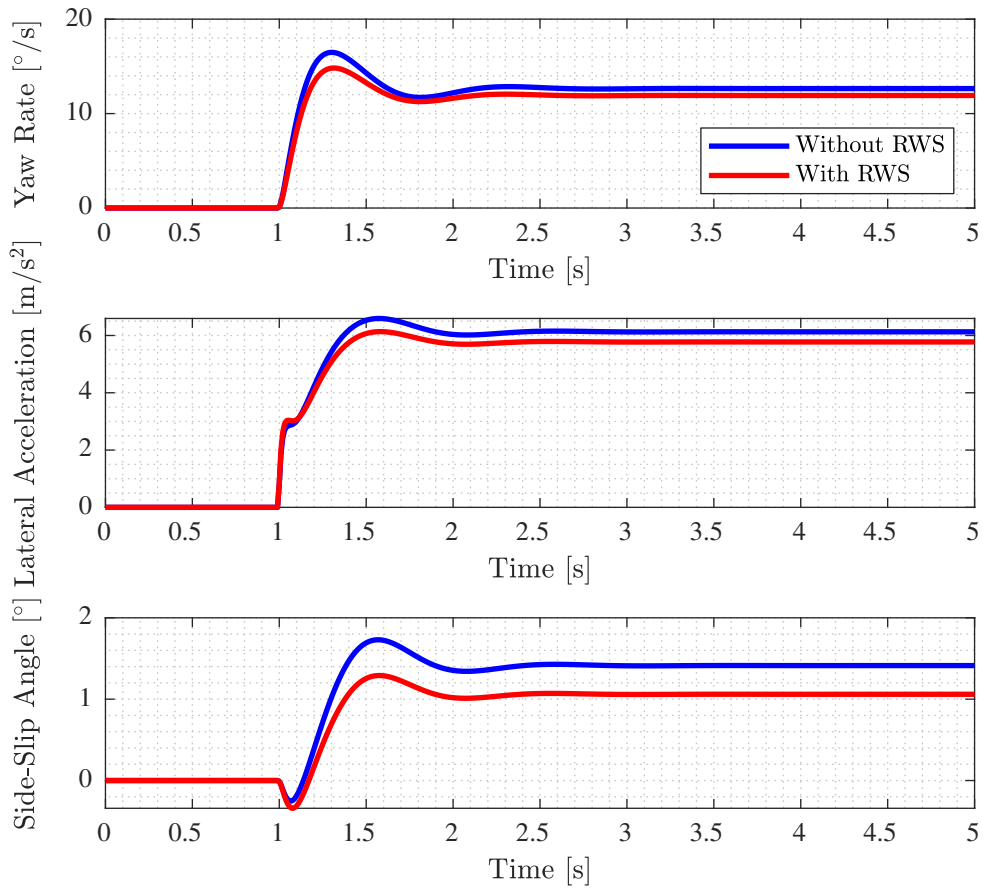
Figure 3.8: Step response at 100 km/h with δ_{sw} at 45°.

The third simulation mimics a so-called moose test. During this test, the avoidance of a moose on the road is simulated. Figure 3.9 depicts what the vehicle does during the moose test at 100 km/h, including the steering wheel angle δ_{sw} at each time t. The simulation inputs are the longitudinal velocity and the front-wheel steering angle, which is determined using δ_{sw}.

Simulating the moose test at 100 km/h gives the results in Figure 3.10. These show the same effect of RWS as discussed the second simulation, since this test is also executed at 100 km/h. All in all, it can be concluded that the effects of RWS explained in the first paragraph of this chapter are actually achieved during the simulations.
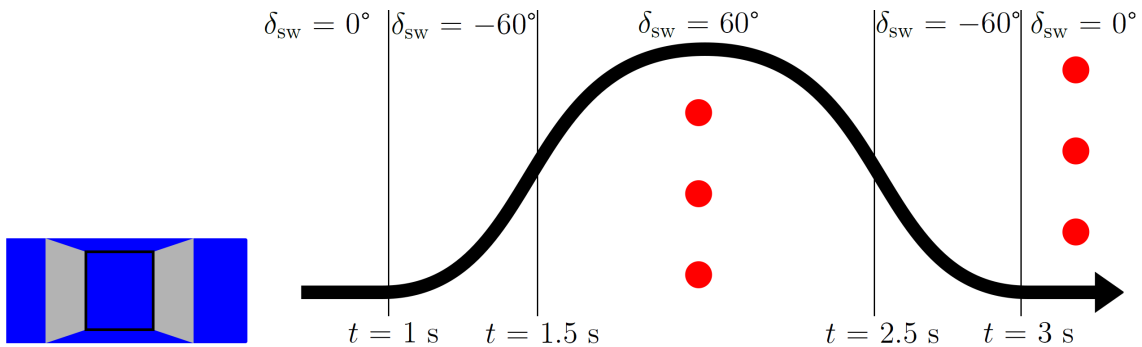
Figure 3.9: Illustration of a moose test at 100 km/h. Adapted from [16].
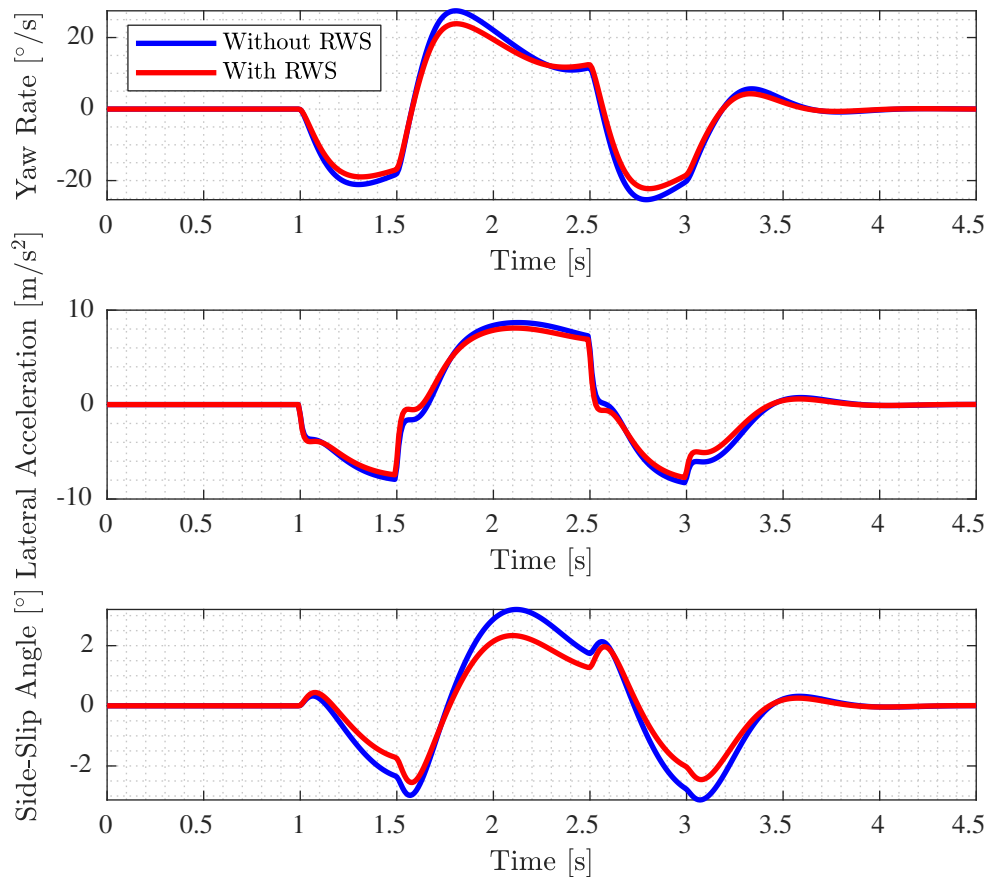
Figure 3.10: Moose test at 100 km/h.

3.5 Summary

A vehicle with RWS cannot only steer its front wheels, but also its rear wheels, introducing a rear-wheel steering angle. This angle depends on two variables, the front-wheel steering angle, which is coupled to the steering wheel angle, and the longitudinal velocity. Multiple RWS control methods are researched in literature, developed and implemented to later determine and quantify their effect on ADAS. This way, the outcome is not based on just one method. To get a better understanding of developing RWS control methods and their effect, methods are developed for a small and large vehicle.

A total of four RWS control methods is developed for a relatively small vehicle, a Ford Fiesta, and for a Ford F-150, which is a larger vehicle. The methods for the Ford F-150 steer the rear wheels in the opposite direction of the front wheels up to higher speeds when compared to the Ford Fiesta. This can be explained by the Ford F-150's longer wheelbase. It is chosen to use the Ford Fiesta and its RWS control methods for all further simulations and calculations.

Using the vehicle parameters and RWS control methods of the Ford Fiesta, simulations are performed to analyse the effect of RWS on the vehicle's handling characteristics. At low speeds, RWS improves the vehicle's agility and manoeuvrability. At higher speeds, the stability of the vehicle increases when using RWS.

Chapter 4

Advanced Driver Assistance Systems

This chapter focusses on ADAS and mainly on Lane Centring (LC), which is a system that can detect the lane markings to help the driver with keeping the vehicle in the lane centre [3]. So the system detects the lane markings, determines the lane centre, which is the desired path, and controls the vehicle to track the path as closely as possible. In this research, three assumptions are made concerning the LC system in general and the corresponding model used for simulating the system:

- The system's operation range is between 50 km/h and 130 km/h.
- The system only controls lateral movement, so there is no longitudinal control. To be more precise, the system's controller determines the steering angle δ_c, which is defined as $\delta_\mathrm{c} = \delta_1 - \delta_2$. So effectively, δ_c is the total steering effort determined by the system's controller that is distributed between the front-wheel and rear-wheel steering angles to correctly implement RWS.
- The system knows the path, which means that this chapter does not discuss the detection of lane markings or the determination of the lane centre. Only the process from knowing the path to controlling the steering angle δ_c is modelled, simulated, and discussed.

Furthermore, this chapter addresses Automated Lane Change (ALC), a system capable of performing a lane change autonomously. This system will be simulated by letting the vehicle follow a predefined path of a lane change manoeuvre. The LC model is used for these simulations. Therefore, ALC will not be further discussed separately, but instead used as one of the driving scenario for the LC simulations.

The first section of this chapter presents a literature survey on path tracking control, which is the essence of LC. The second section explains the LC controller. Next, the third section discusses the error, which is the input of the controller. The fourth section explains the look-ahead distance. The simulation model of LC, driving scenarios, and simulation results are presented in the fifth, sixth, and seventh section respectively. Finally, the eighth section gives a summary.

4.1 Literature Survey

This section discusses a literature survey on error definitions and path tracking control methods that can be used for the development of the LC controller.
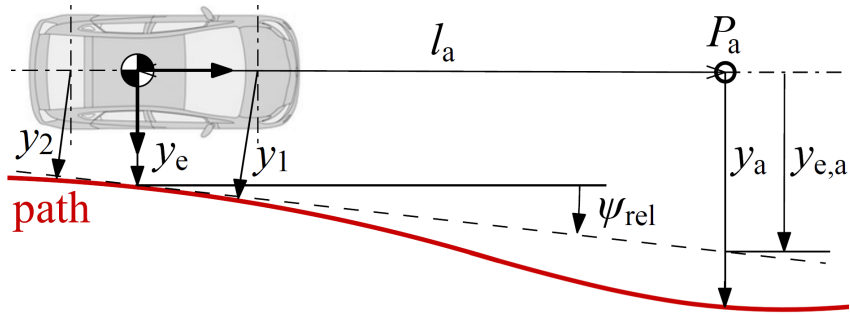
Figure 4.1: Lateral offsets y_e, y_a, $y_{e,a}$, y_1, and y_2. Adapted from [17].

4.1.1 Controller Error Definitions

The main goal is to make the vehicle follow the desired path as accurately as possible, which is realised by minimising the path tracking error, which is the input of the controller. This error can be defined in several ways. Figure 4.1 shows five different lateral offsets that can be used as the error. These error definitions will be discussed now.

The first three error definitions are explained in [17]. The first one takes the lateral offset y_e between the vehicle's centre of gravity and the path, perpendicular to the vehicle's direction of travel, as the error. The second error definition takes the lateral offset y_a between the look-ahead point P_a and the path as the error, again perpendicular to the vehicle's direction of travel. The lateral offset $y_{e,a}$ for the third definition is defined as:

$$y_{e,a} = y_e + l_a \sin \psi_{rel} \tag{4.1}$$

where l_a is the look-ahead distance and ψ_{rel} is the relative yaw angle between the path and the vehicle. So this third error definition tries to predict the lateral offset at the look-ahead point using the current lateral offset and relative yaw angle. The road curvature is not used, since it is relatively hard to determine.

The fourth definition, presented in [18], [19], [20], and [21], is measured from the vehicle's front-axle centre to the nearest path point, perpendicular to the path, and is named y_1. The fifth lateral offset y_2, explained in [19], is similar to y_1. However, it is measured from the vehicle's rear-axle centre to the nearest path point, perpendicular to the path.

When comparing the definitions, it can be concluded that lateral offsets y_e, y_a, and $y_{e,a}$ are defined perpendicular to the vehicle's direction of travel. In contrast to y_1 and y_2, which are defined perpendicular to the path. Furthermore, y_a and $y_{e,a}$ are defined at a look-ahead point ahead of the vehicle, which makes these definitions attractive to use, since defining the offset ahead of the vehicle makes it possible to anticipate on future path changes. Now that the errors are explained, the control methods can be discussed.

4.1.2 Pure Pursuit Control

The pure pursuit control method is among the most common approaches to path tracking. It consists of geometrically calculating the curvature of a circular arc that connects the vehicle's rear-axle centre to a goal point ahead of the vehicle. A circle is the easiest path for the car to reach the goal point. Two variants of this control method will be explained. Figure 4.2 illustrates the geometry for the first variant, presented in [17].
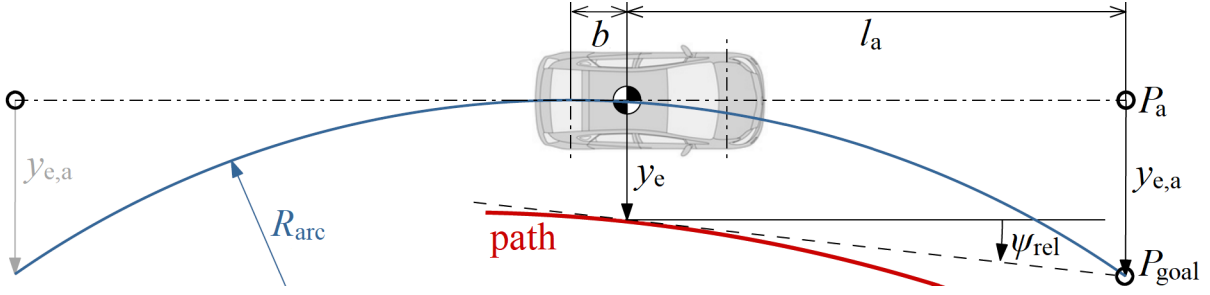
Figure 4.2: First variant of pure pursuit control. Adapted from [17].

This first variant places the goal point P_{goal} at look-ahead distance l_a in front of the vehicle with the lateral offset $y_{e,a}$. The arc curvature κ_{arc} is defined as:

$$\kappa_{\text{arc}} = \frac{1}{R_{\text{arc}}} = \frac{2y_{e,a}}{(b + l_a)^2} \tag{4.2}$$

where R_{arc} is the arc radius. Substituting the arc curvature into the following expression for the front-wheel steering angle during steady-state cornering, which is found using (2.11) and knowing that $R_{\text{arc}} = v_x/r$, gives the control law for the steering angle δ_c:

$$\delta_c = \left(l + \eta v_x^2\right) \kappa_{\text{arc}} = \frac{2\left(l + \eta v_x^2\right)}{(b + l_a)^2} \, y_{e,a} \tag{4.3}$$

The lateral offset $y_{e,a}$ is used as the error in this variant of pure pursuit control. However, $y_{e,a}$ in (4.3) could be replaced by the lateral offset y_a, which is the case in the second variant of pure pursuit control. This second variant places the goal point P_{goal} on the actual path instead of at a predicted location as with the lateral offset $y_{e,a}$. However, a different notation of the second variant is presented in [19] and [20]. Length L is introduced as the length from the vehicle's rear-axle centre to the goal point. Figure 4.3 shows the geometry for this variant. The arc curvature κ_{arc} is defined as:

$$\kappa_{\text{arc}} = \frac{1}{R_{\text{arc}}} = \frac{2\sin\gamma}{L} \tag{4.4}$$

which is substituted into the kinematic part of the front-wheel steering angle during steady-state cornering to obtain the control law for the steering angle δ_c:

$$\delta_c = \arctan\left(\kappa_{\text{arc}}l\right) = \arctan\left(\frac{2l\sin\gamma}{L}\right) \tag{4.5}$$

Figure 4.3: Second variant of pure pursuit control. Adapted from [17].

4.1.3 PID Control

As [22] describes, a proportional–integral–derivative (PID) controller has three parts:

- **Proportional:** the proportional part simply multiplies the error by the proportional gain K_P to get the controller output. If the error is non-zero, the proportional term results in a steering action that steers the vehicle towards the path. The further away the vehicle is from the path, the larger the resulting steering action will be.
- **Integral:** the integral part multiplies the integral of the error by the integral gain K_I. The goal of adding this term to the controller is to minimise the steady-state error. For example, if there is a residual error after the application of the proportional term, the integral term eliminates this by adding a control effect due to the cumulative error value. When the error is eliminated, the integral term stops increasing.
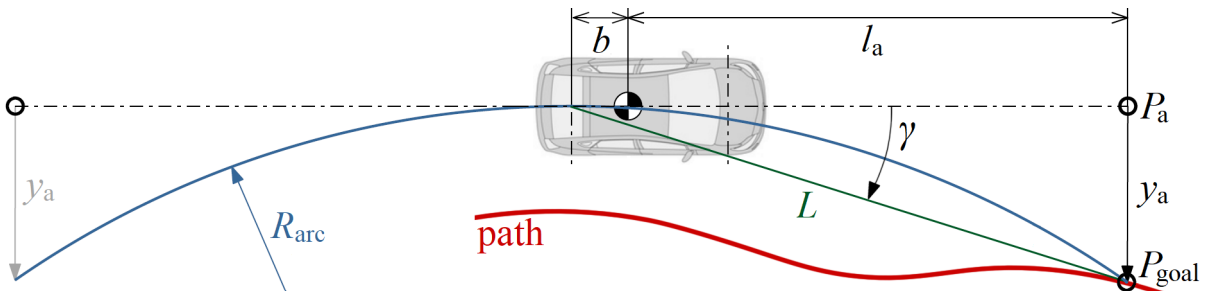- **Derivative:** the derivative part multiplies the derivative of the error by the derivative gain K_D. The derivative of the error is the rate at which the lateral offset changes. So the higher the rate of change, the larger the effect of the derivative term. When the vehicle moves towards the path and therefore a risk of overshoot is present, the steering action is damped by the derivative term. When the vehicle moves away from the path, the derivative part accelerates the change of the steering action to steer towards the path.

The control law is found by taking the sum of the three parts:

$$\delta_c(t) = K_P\, e(t) + K_I \int_0^t e(t)\, \mathrm{d}t + K_D\, \frac{\mathrm{d}e(t)}{\mathrm{d}t} \tag{4.6}$$

where e is the error, which can be set to any lateral offset. The three gains can be tuned to achieve the desired path tracking performance. However, not all gains have to be used. In [23] for example, a PD controller is used for path tracking, so the integral term is neglected.

4.1.4 Stanley Control

The Stanley control method, described in [18], [19], [20], and [21], is the path tracking approach used by Stanford University's autonomous vehicle that won the 2005 DARPA Grand Challenge, a competition for autonomous vehicles. The method is a non-linear feedback function of the lateral offset y_1, which is taken as the error. The control law is:

$$\delta_c = \psi_{\mathrm{rel}} + \arctan\left(\frac{K y_1}{v_x}\right) \tag{4.7}$$

where K is a gain that can be tuned to achieve the desired look-ahead distance. The first term of the control law simply keeps the wheels aligned with the path by setting the steering angle δ_c equal to the relative yaw angle between the vehicle and path ψ_{rel}. When y_1 is non-zero, the second term adjusts the steering angle δ_c such that the intended trajectory intersects the tangent of the nearest path point. The Stanley control method is best suited for low speeds, since it does not take parameters like the understeer coefficient into account, which could change its behaviour with speed. Furthermore, this method has to be tuned for one specific vehicle, since it does not include any vehicle parameters like the wheelbase, only K is tunable.

4.1.5 Rear-Wheel Feedback Control

The Stanley control method effectively is front-wheel feedback control. However, a less well-known alternative is rear-wheel feedback control, which [19] presents. This alternative method is similar to the Stanley control method, but it uses the lateral offset y_2 instead of y_1. The control law of the rear-wheel feedback control method is:

$$ r = \frac{v_x \kappa_{\text{path}} \cos \psi_{\text{rel}}}{1 - \kappa_{\text{path}} y_2} - K_{\psi_{\text{rel}}} v_x \psi_{\text{rel}} - \left(K_{y_2} v_x \frac{\sin \psi_{\text{rel}}}{\psi_{\text{rel}}} \right) y_2 \qquad (4.8) $$

where κ_{path} is the path curvature, and $K_{\psi_{\text{rel}}}$ and K_{y_2} are gains that can be tuned to achieve the desired controller performance.

4.1.6 Model Predictive Control

Model predictive control (MPC), explained in [19], [24], and [25], is a control method that controls a system while satisfying the system's constraints. The capability of handling constraints makes MPC attractive for path tracking, because vehicles are subjected to physical constraints, like maximum steering angles or velocities. Conceptually, the approach is to solve the path tracking problem over a short time horizon, take an interval of the resulting open-loop control, and apply it to the system. While executing, the path tracking problem is resolved to find the most suitable control action to minimise the tracking error. To do this, MPC uses a dynamic vehicle model, a history of past control actions, and a cost function that has to be minimised.

When comparing MPC to the simpler path tracking control methods, the main advantage of MPC is its ability to anticipate future events and adapt the control action accordingly. For example, the relatively simple PID control method does not have this predictive ability. However, the additional complexity of MPC might not be needed to provide adequate control in most path tracking situations, which are often adequately controlled by simpler control methods, like PID control.

4.1.7 Iterative Learning Control

Iterative learning control (ILC), discussed in [23], can be used for tracking a specific path that is repeated many times, like a race track. By using information, like the lateral offset or relative yaw angle, from prior attempts, ILC can be used to gradually determine the control inputs that cause the system's output to track a path with minimal error. This method has not been further researched, since a path must be driven several times before the error is minimised. Therefore, it is unsuitable for the public road.

4.2 Controller Design

It is chosen to use the first variant of pure pursuit control, described in subsection 4.1.2, as basis for the LC controller, mainly because it uses a look-ahead distance, which is desired for the research goal to quantify the effect of RWS. Furthermore, its control law is relatively simple, meaning no unnecessary complexity is added. However, using the pure pursuit controller did not lead to good path tracking behaviour. So a PID controller, explained in subsection 4.1.3, is added, because an integral and derivative term can be added to possibly further improve the path tracking performance.

The proportional gain is based on the term in front of $y_{e,a}$ in (4.3):

$$K_P = 1.1 \frac{2\left(l + \eta v_x^2\right)}{\left(b + l_a\right)^2} \tag{4.9}$$

The term is multiplied by 1.1 for two reasons. Firstly, to compensate the increased rise time and settling time caused by the added derivative gain. The rise time and settling time will be explained in subsection 4.7.1. Secondly, to compensate for the dynamics in the response of the vehicle. Simulations show that the rise time of the yaw rate on a step input of steering angle is 0.14 s. The value 1.1 in (4.9) is found to be the optimal mix between improved path tracking performance and keeping the proportional gain small, because larger values hardly show any improvement in path tracking performance compared to the extent to which the gain value increases. A small proportional gain is desired, because otherwise possible noise is amplified too much.

The integral term is neglected, so K_I is zero. Making it non-zero influences the path tracking performance negatively. Due to the increasing cumulative error value during cornering, the vehicle has trouble settling quickly on the path after exiting a corner.

It was found that the front-wheel steering angle fluctuates during simulations of multiple different driving scenarios. Two examples of this are shown in Figure 4.4, which shows the front-wheel steering angle at 100 km/h during a step response and ALC simulations without RWS. These fluctuations indicate damping needs to be added, so a derivative term is added. The derivative gain should be as small as possible in order not to increase the rise time and settling time too much. Then the proportional gain would have to be increased further, which is not desirable, as explained before. However, the derivative gain has to be large enough to improve stability and remove fluctuations in the front-wheel steering angle. The value of K_D that meets these requirements is 0.012.

For this variant of pure pursuit control, the lateral offset $y_{e,a}$ and optionally y_a can be used, and any lateral offset can be used for PID control. So the choice has to be made between lateral offsets $y_{e,a}$ and y_a. This will be explained in the next section.

(a) Step response

(b) ALC
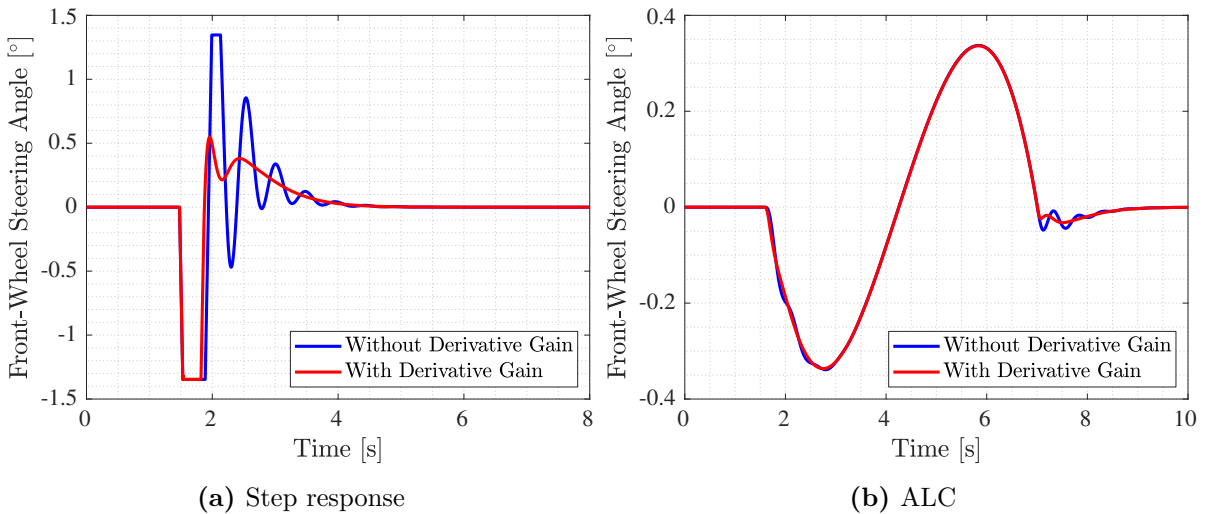
Figure 4.4: Front-wheel steering angle at 100 km/h without RWS.

4.3   Controller Error Definition

The lateral offset $y_{e,a}$ is chosen to be used, because for the goal of this research, a look-ahead distance is desired, since the effect of RWS is more noticeable if the vehicle looks far ahead. This means only lateral offsets y_a and $y_{e,a}$ are options. After performing simulations with both offsets, the path tracking performance with $y_{e,a}$ is found to be superior. Moreover, this lateral offset is used in [17] as the error for pure pursuit control, which is used as the basis of the LC controller of this research, as discussed in the previous section.

The lateral offset $y_{e,a}$ is shown in (4.1), in which the look-ahead distance l_a is known when determining $y_{e,a}$. However, the relative yaw angle ψ_{rel} and lateral offset y_e have to be calculated. Only the coordinates and yaw angle of the vehicle and the path in the global coordinate system, at the current vehicle's global x-coordinate, are known during simulations. So the relative yaw angle ψ_{rel} and length l_1, shown in Figure 4.5, can be determined using:

$$\psi_{rel} = \psi_{path,g} - \psi_g \tag{4.10}$$

$$l_1 = y_{path,g} - y_g \tag{4.11}$$

where $\psi_{path,g}$ is the yaw angle between the global x-axis and the path, ψ_g is the yaw angle between the global x-axis and the vehicle, and $y_{path,g}$ and y_g are the global y-coordinates of the path and vehicle respectively. Length l_1 is defined perpendicular to the x-axis of the global coordinate system, indicated with g, instead of perpendicular to the vehicle's direction of travel. To determine the actual desired lateral offset y_e, perpendicular to the vehicle's direction of travel, several steps are needed. It is assumed that the path between the intersection points of y_e and l_1 with the path is straight.

Figure 4.5: Overview for calculations of the lateral offset y_e. Adapted from [17].

Firstly, lengths l_2 and l_3 are calculated using l_1:

$$l_2 = l_1 \cos \psi_{\mathrm{g}} \, , \quad l_3 = l_1 \sin \psi_{\mathrm{g}} \tag{4.12}$$

Secondly, length l_4 is determined using length l_3:

$$l_4 = l_3 \tan \psi_{\mathrm{rel}} = l_1 \sin \psi_{\mathrm{g}} \tan \psi_{\mathrm{rel}} \tag{4.13}$$

Finally, the lateral offset y_{e} is found using lengths l_2 and l_4:

$$y_{\mathrm{e}} = l_2 - l_4 = l_1 \cos \psi_{\mathrm{g}} - l_1 \sin \psi_{\mathrm{g}} \tan \psi_{\mathrm{rel}} \tag{4.14}$$
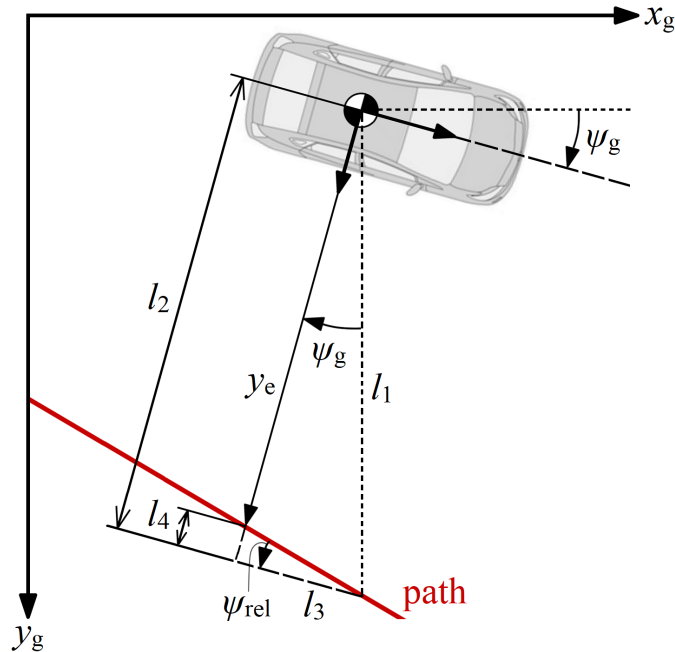
which is used in (4.1) to find the lateral offset $y_{\mathrm{e,a}}$.

4.4 Look-Ahead Distance

The goal of this research is to study the effect of RWS on ADAS. Therefore, controller designs with a large look-ahead distance are preferred, because the effect of RWS is more noticeable if the vehicle looks far ahead. For example, a change in yaw angle creates more lateral offset at the look-ahead point if it is located far ahead of the vehicle. The look-ahead distance cannot be too large though, since the lateral offset y_{e} would increase too much due to the second term with ψ_{rel} in (4.1) becoming too dominant, which allows y_{e} to increase. Moreover, an increased look-ahead distance reduces the controller's proportional gain, as shown in (4.9). For example, when the look-ahead time is doubled, y_{e} also roughly doubles, but δ_{c} remains practically the same, which means worse path tracking behaviour. So the look-ahead distance should be as large as possible without exceeding a certain y_{e}. For instance, [26] concludes that looking-ahead 30 m is the best compromise between path tracking performance and passenger comfort.

The value of y_{e} that may not be exceeded is chosen to be 0.30 m. It is found during simulations that y_{e} increases with speed, since the rate of change of the path also increases with speed, as will be further explained in section 5.3. So within the LC operation range, the largest offset will occur at 130 km/h, achieved on motorways. The minimum lane width on European motorways is 3.50 m [27] and the width of the Ford Fiesta used for simulations is 1.722 m. So with a lateral offset y_{e} of 0.30 m, the distance that remains between the side of the vehicle and the lane marking is 0.59 m. During simulations at 130 km/h with the curved road driving scenario, which will be explained in section 4.6, and considering the maximum lateral offset of 0.30 m, the maximum look-ahead distance is found to be 26.0 m. Now it has to be decided whether the look-ahead distance should be constant or speed dependent using:

$$l_{\mathrm{a}} = t_{\mathrm{a}} v_x \tag{4.15}$$

where t_{a} is the look-ahead time, which equals 0.72 s at 130 km/h with a look-ahead distance of 26.0 m. Table 4.1 shows the maximum absolute lateral offset $\max|y_{\mathrm{e}}|$ with a constant look-ahead time and a constant look-ahead distance on the curved road driving scenario, without RWS, and using the LC controller design and simulation model.

Table 4.1: Maximum absolute lateral offset $\max|y_\mathrm{e}|$ on the curved road.

$v_\mathbf{x}$ [km/h]	$\max\|y_\mathbf{e}\|$ [m]	
	$t_\mathbf{a} = 0.72$ s	$l_\mathbf{a} = 26.0$ m
50	0.045	0.177
80	0.099	0.183
100	0.159	0.217
130	0.297	0.297

As can be seen, a constant look-ahead time provides better path tracking performance compared to a constant look-ahead distance. Simulations with other driving scenarios provided the same conclusion. So a constant look-ahead time of 0.72 s is used.

4.5 Simulation Model

To simulate LC, a simulation model is developed in SIMULINK. Figure 4.6 shows a high-level overview of the model. The model's main outputs are the vehicle position and orientation, so x_g, x_g, and ψ_g, which can be used for the evaluation of the path tracking error. The model applies the theory of the previous sections, but also adds more parts. Those newly developed parts will be mainly discussed in this section. Figure 4.6 illustrates each part as a block. The simulation model uses the `ode4` ODE solver with a fixed step size of 0.001 s. This solver uses the fourth-order Runge-Kutta formula [28]. Each block will now be explained, starting with the so-called error block.

The error block determines the lateral offset $y_\mathrm{e,a}$, which is used as the error, as explained in section 4.3. The inputs $x_\mathrm{path,g}$ and x_g are the global x-coordinates of the path and vehicle respectively. These are used to interpolate the global y-coordinates of the path and yaw angle of path at the current vehicle position. This allows that the error can be determined at every vehicle position along the path. The interpolation method used is `spline`, which means that the interpolated value at a query point is based on a cubic interpolation of the values at neighbouring grid points in each respective dimension. This method is continuous to the second order, but for simulations of a step response, a less smooth interpolation method is desired. So for step response simulations, the `nearest` method is used, which means that the interpolated value at a query point is the value at the nearest sample grid point [8]. Now that $y_\mathrm{e,a}$ is determined in this block, it is sent to the controller, along with the look-ahead time and longitudinal velocity.
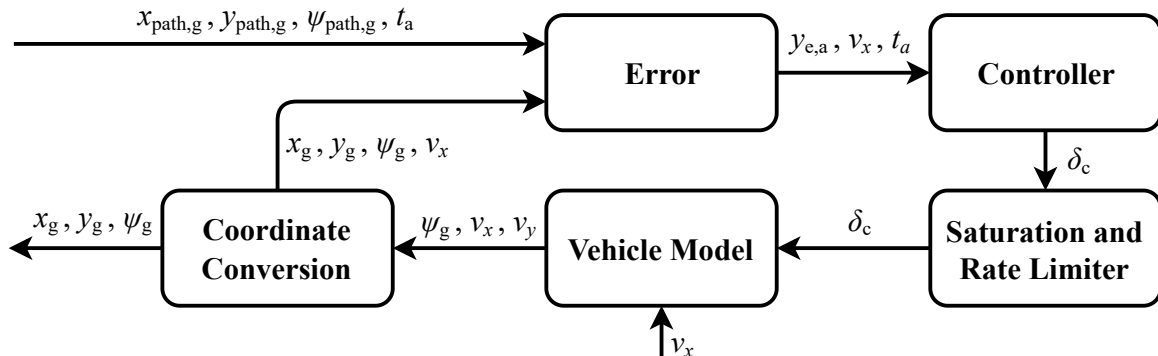
Figure 4.6: Overview of the LC model as implemented in SIMULINK.

The controller block contains the LC controller presented in section 4.2. Its only output is the steering angle δ_c. The value of the steering angle δ_c is then limited in the next block, so that the vehicle's lateral acceleration does not exceed 3 m/s^2. This value is chosen to prevent excessive steering actions and limit the lateral acceleration within an acceptable range for road driving. The upper saturation value $\delta_{c,\text{sat}}$ of the steering angle δ_c is found using (2.13), neglecting the rear-wheel steering angle, and using a lateral acceleration of 3 m/s^2:

$$\delta_{c,\text{sat}} = a_y \,/\, \frac{v_x^2/l}{1 + \dfrac{\eta}{gl}\, v_x^2} = 3 \,/\, \frac{v_x^2/l}{1 + \dfrac{\eta}{gl}\, v_x^2} \tag{4.16}$$

which is multiplied by -1 for the lower saturation value. Furthermore, a rate limiter is used. It limits the rate of the steering angle δ_c to ± 25.9 °/s, which equals one steering wheel rotation per second. This prevents excessive steering rates during simulations, like during a step response. If the rate limiter limits the steering angle δ_c too much, a phase delay is created in the steering angle δ_c, causing non-linearity in the model. All in all, the value is chosen not to be too strict, but still to prevent excessive steering rates. After limiting, if necessary, the steering angle δ_c is sent to the vehicle model block.

The vehicle model block uses the linear single track vehicle model, because the lateral acceleration is limited to 3 m/s^2 and thus stays in the linear area. This block has two inputs, the steering angle δ_c from the LC controller and the predefined longitudinal velocity v_x, which is constant, since there is no longitudinal control. In the block, the front-wheel and rear-wheel steering angles are determined first, using δ_c. As discussed in the introduction of this chapter, the steering angle δ_c determined by the controller is:

$$\delta_c = \delta_1 - \delta_2 \tag{4.17}$$

and using one of the RWS control methods explained in Chapter 3, the steering angle ratio k between the front-wheel and rear-wheel steering angles is used:

$$\delta_2 = k\delta_1 \tag{4.18}$$

To determine the front-wheel and rear-wheel steering angles while satisfying (4.17) and (4.18), the following expressions are used:

$$\delta_1 = \frac{\delta_c}{1 - k} \tag{4.19}$$

$$\delta_2 = \frac{\delta_c}{1 - k}\, k \tag{4.20}$$

Having the steering angles, the equations of motion of the linear single track vehicle model, shown in (2.5) and (2.6), are used to find $\dot{v}_y$ and $\dot{r}$. Right after the vehicle model block, $\dot{v}_y$ is integrated to find the lateral velocity and $\dot{r}$ is integrated twice to find the yaw angle between the global x-axis and the vehicle. These are then sent to the next block, along with the predefined longitudinal velocity.

This next block converts the coordinates from the local coordinate system of the vehicle to the global one. To be more exact, it uses the yaw angle between the global x-axis and the vehicle to convert the velocities to the global coordinate system using [17]:

$$v_{x,\mathrm{g}} = v_x \cos \psi_\mathrm{g} - v_y \sin \psi_\mathrm{g} \ , \quad v_{y,\mathrm{g}} = v_x \sin \psi_\mathrm{g} + v_y \cos \psi_\mathrm{g} \tag{4.21}$$

where $v_{x,\mathrm{g}}$ and $v_{y,\mathrm{g}}$ are the longitudinal and lateral velocities with respect to the global coordinate system respectively. These velocities are then integrated to obtain x_g and y_g, which are the global x-coordinate and y-coordinate of the vehicle respectively. These are sent to the error block, along with the longitudinal velocity and global yaw angle.

4.6 Driving Scenarios

Four driving scenarios, shown in Figure 4.7, are used for simulations with the LC model. These scenarios are predefined paths that the model loads before performing a simulation. The global path coordinates and yaw angle are interpolated to determine the error at every vehicle position along the path, as stated in the previous section.

(a) Straight road

(b) Step response

(c) Curved road

(d) ALC at 100 km/h
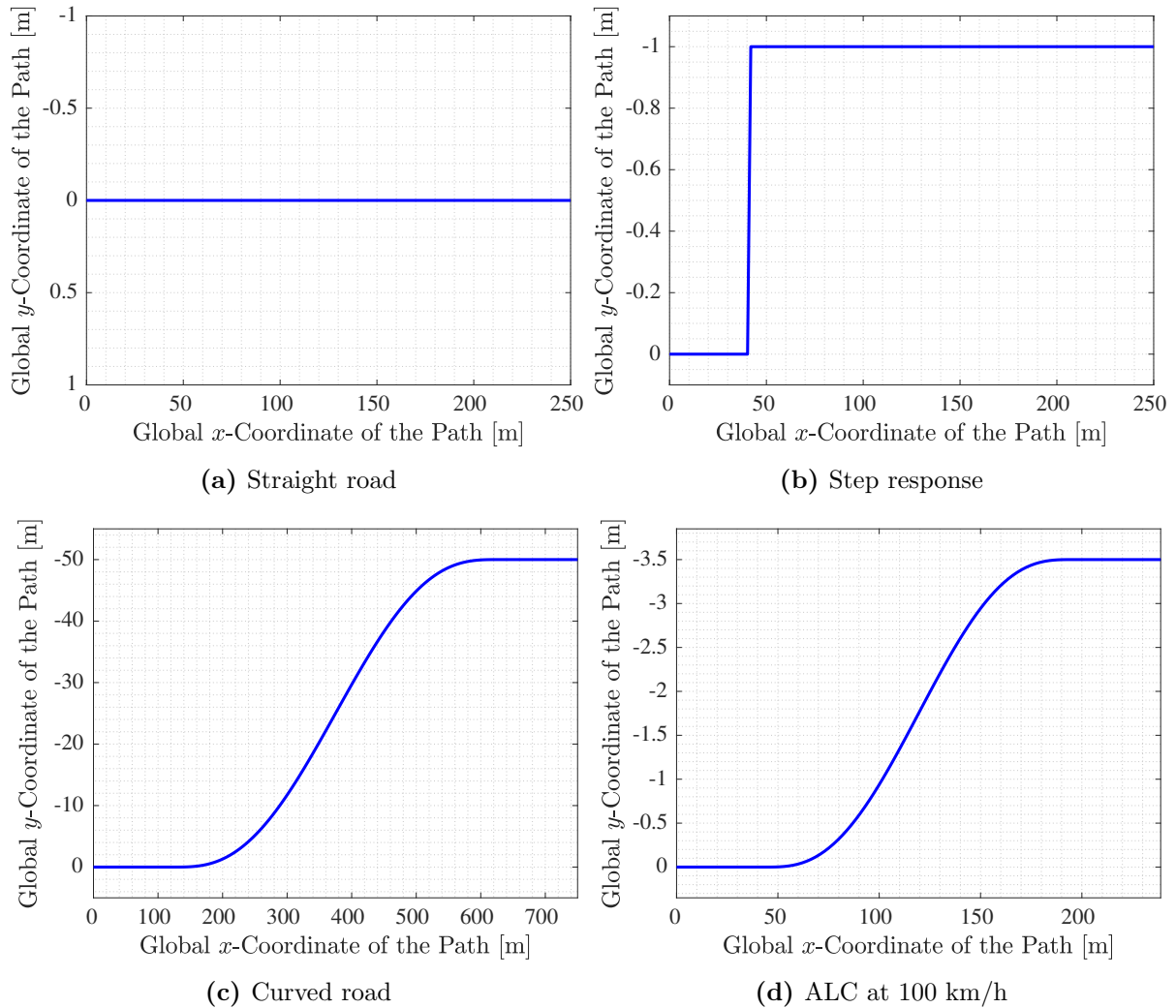
Figure 4.7: Paths of driving scenarios.

The four driving scenarios are:

- **Straight road:** this scenario simulates a straight path and is solely used during controller development to validate if no steering effort is performed while driving straight. Therefore, no results of the simulations using the straight road driving scenario will be discussed.

- **Step response:** the vehicle drives straight at constant speed and at a certain time, a certain input value is chosen and maintained. The input value that changes is the path. It makes a step with a lateral amplitude of 1 m. So the path is now predefined, in contrast to the step responses in Chapters 2 and 3, where the front-wheel steering angle is predefined.

- **Curved road:** this scenario starts and ends with a straight. In between the two straights, a left-hand and right-hand turn are placed.

- **ALC:** this scenario also starts and ends with a straight. In between the straights, a lane change is performed.

The first two driving scenarios, straight road and step response, do not need further explanation. However, the curved road driving scenario and the scenario that simulates ALC will be explained in more detail.

For the curved part between the straights of these two driving scenarios, a fifth order polynomial is used. This polynomial is continuous until the second derivative. This is desirable, since the second derivative of the path represents the shape of the resulting steering angles, lateral acceleration, and yaw rate for example. So if the second derivative of the path is continuous, these results are also continuous. The fifth order polynomial for the global y-coordinate of the path $y_{\mathrm{path,g}}$ is [29]:

$$y_{\mathrm{path,g}}(x_{\mathrm{path,g}}) = K_y \left(10 \left(\frac{x_{\mathrm{path,g}}}{K_x} \right)^3 - 15 \left(\frac{x_{\mathrm{path,g}}}{K_x} \right)^4 + 6 \left(\frac{x_{\mathrm{path,g}}}{K_x} \right)^5 \right) \tag{4.22}$$

where K_x and K_y are gains that can be adapted to create the desired path. Path parameter K_x defines the length of the polynomial in the x-direction and K_y defines the width of the path in y-direction. For the curved road driving scenario, K_y is set to 50 m and K_x is set to 500 m. These values allow to simulate the entire LC operation range without causing unrealistically high lateral accelerations.

For the ALC scenario, K_y equals 3.5 m, which is the minimum lane width on European motorways [27]. Path parameter K_x is created to be speed dependent, because it is chosen that the lane change takes 5 s. So $K_x = 5v_x$ for the driving scenario of ALC.

4.7 Simulations

This section presents the results of several simulations, which are obtained using the LC simulation model, to see how the LC controller performs. The first subsection presents the simulation results of the step response driving scenario. The second subsection discusses the results of the curved road driving scenario and the ALC driving scenario. All simulations are performed using a vehicle without RWS at a speed of 100 km/h and, as discussed before, using the linear single track vehicle model.
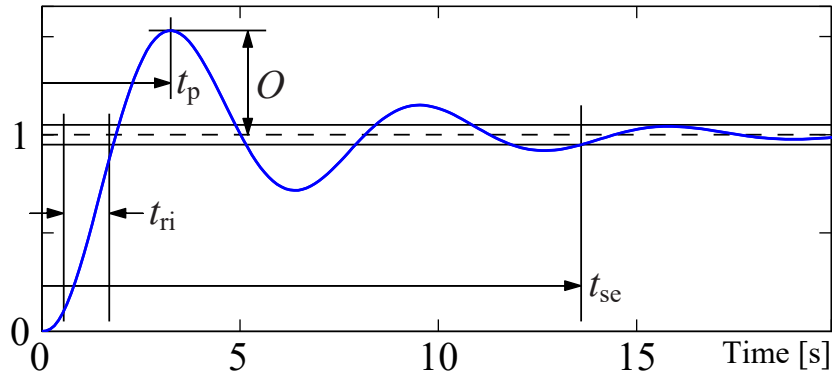
**Figure 4.8:** Rise time, settling time, peak time, and overshoot. Adapted from [31].

4.7.1 Step Response

Using a step response, the controller's path tracking performance is typically specified by parameters in the time domain [30] [31] [32] [33]:

- **Rise time t_{ri}:** the rise time is the amount of time required for the response to go from 10 % of its final value to 90 % of its final value.

- **Settling time t_{se}:** the settling time is defined as the time for the response to reach, and stay within, 2 % of its final value. The settling time is also sometimes defined as reaching 1 % or 5 % of the final value. For this research, 2 % will be used.

- **Peak time t_p:** the peak time is the time required for the response to reach the first peak of the overshoot. Quantifying the peak time is only relevant for underdamped system, since critically damped and overdamped systems have no overshoot. This means the peak time is not relevant for the LC system and it will therefore not be further discussed.

- **Overshoot O:** the overshoot is the percentage of the final value by which the response initially rises above the final value. Overshoot will not be further discussed, because only underdamped systems have overshoot, as explained with the peak time.

- **Time constant τ:** the time constant represents the time needed by the system to reach its final value if the system had continued increasing at the initial rate. However, the time constant can only be used for first order systems, which the LC system is not.

Figure 4.8 shows the rise time, settling time, peak time, and overshoot. The time constant is not depicted, because the response in the figure is from a second order system. All in all, the rise time and settling time will be used to specify the performance of the LC controller with step response simulations. The main model input during such simulation is the step response driving scenario, explained in the previous section. The main model output for the step response is the vehicle position. The LC controller's main input and output are the lateral offset $y_{e,a}$ and the steering angle δ_c respectively.

The results of the step response without RWS are shown in Figure 4.9. The rise time and settling time are determined using the global y-coordinate of the vehicle y_g and applying the definitions of the rise time and settling time listed above. The mean rise time and mean settling time within the LC operation range are found to be 1.345 s and 2.469 s respectively. Chapter 5 explains these results in more detail.
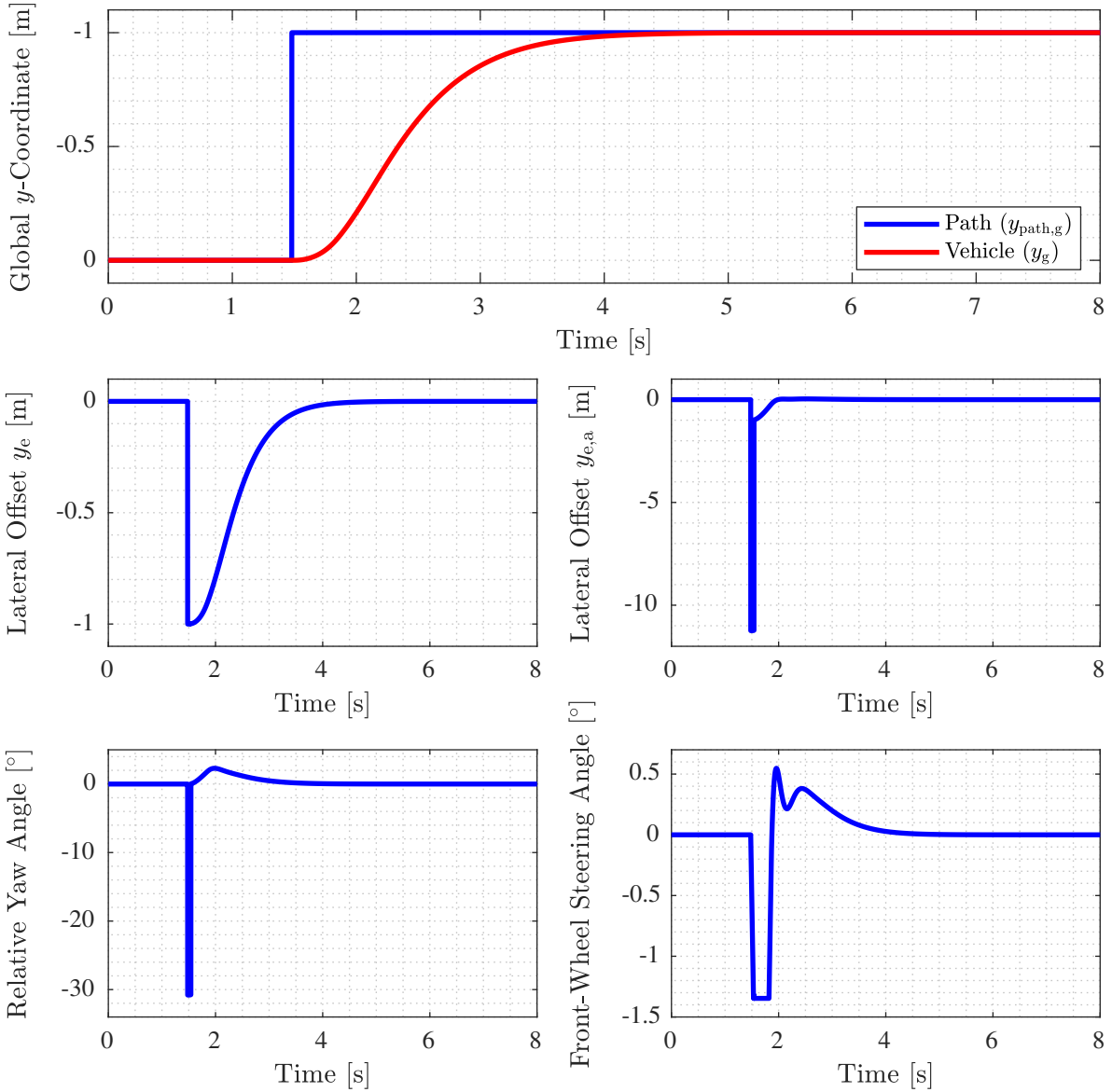
Figure 4.9: Step response at 100 km/h without RWS.

When further analysing the global y-coordinate of the vehicle, it can be seen that its value does not change until the vehicle is positioned at the actual step in the path. This is due to the definition of the controller input, the lateral offset $y_{e,a}$. As explained in subsection 4.1.1, $y_{e,a}$ tries to predict its value at the look-ahead point using the lateral offset y_e and relative yaw angle at the current vehicle position. This means that a sudden path change, like a step, cannot be predicted by $y_{e,a}$. During simulations of smoother driving scenarios, like the curved road, the prediction ability of $y_{e,a}$ is more accurate.

It can also be seen in Figure 4.9 that the lateral offset $y_{e,a}$ has a sharp dip when the step starts. This is caused by the relative yaw angle, which suddenly increases enormously due to the step of the path. However, the lateral offset $y_{e,a}$ settles around 0 m within 0.5 s, which is faster than y_e. This can be explained by considering the effect of the relative yaw angle in (4.1). When the lateral offset y_e is still negative, the relative yaw rate is positive, resulting in a lateral offset $y_{e,a}$ close to 0 m.

Furthermore, the front-wheel steering angle clearly shows the effect of the rate limiter and saturation value. Due to the rate limiter, the initial dip of the front-wheel steering angle is not perfectly vertical, but it has a slightly slanting decrease and increase. The effect of the saturation value can be seen between 1.5 s and 1.9 s. The initial dip of the front-wheel steering angle is limited at the saturation value, which is equal to 1.34° at 100 km/h. The saturation value is defined in (4.16).

4.7.2 Curved Road and Automated Lane Change

Since the simulation results of the curved road and ALC driving scenarios are comparable, these will be discussed together using the results of the curved road simulation without RWS in Figure 4.10. The ALC simulation results without RWS can be found in Appendix D. It can be seen in Figure 4.10 that y_e is negative during left-hand cornering and positive during right-hand cornering. This indicates that the vehicle is positioned slightly towards the outside of the bend during cornering.

Furthermore, the amplitude of the lateral offset y_e is noticeably larger than the amplitude of the lateral offset $y_{e,a}$. This is can be explained by the effect of the relative yaw angle. When the lateral offset y_e is positive, the relative yaw angle is negative and vice versa. This lowers the resulting lateral offset $y_{e,a}$, as described in (4.1). The opposite sign of the relative yaw angle compared to the lateral offset y_e effectively means that when the vehicle has a certain offset from the path, the vehicle is pointed towards the path. This is desirable to minimise the error, which is equal to the lateral offset $y_{e,a}$.
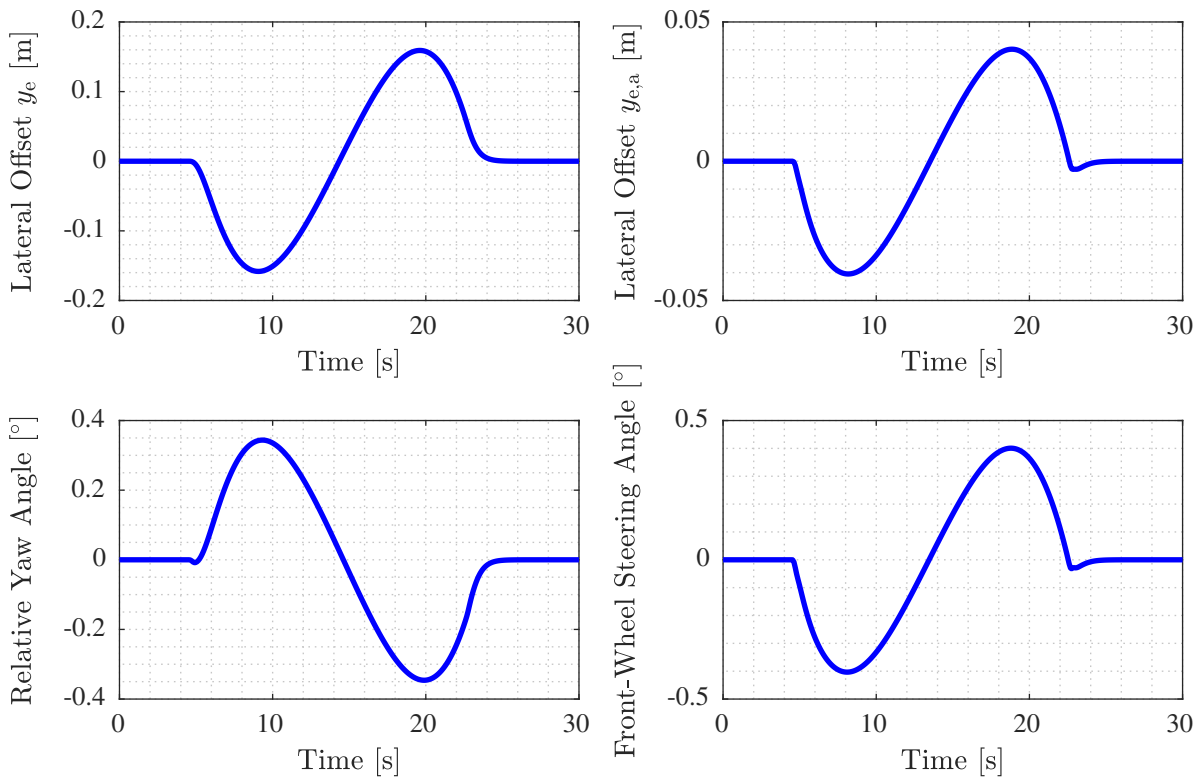
Figure 4.10: Curved road at 100 km/h without RWS.

4.8 Summary

LC, which detects the lane markings to help the driver with keeping the vehicle in the lane centre, is modelled in SIMULINK with an operation range of 50 km/h to 130 km/h. It is assumed that the LC model already knows the desired path, which is the lane centre, and only controls the steering angle δ_c, which is defined as $\delta_c = \delta_1 - \delta_2$. After researching numerous path tracking control methods in literature, pure pursuit control and PID control are combined for the LC controller. The controller minimises an error that is defined at a point 0.72 s ahead of the vehicle.

To check the path tracking performance and later quantity the effect of RWS on ADAS, four driving scenarios are created. One of the driving scenarios is used to simulate a second ADAS, namely ALC. A vehicle equipped with ALC is able to autonomously perform a lane change. ALC is simulated by letting the vehicle follow a predefined path of a lane change manoeuvre using the LC model. Another driving scenario simulates a step response to determine the rise time and settling time, which partly specify the controller's path tracking performance.

Chapter 5

Effect of Rear-Wheel Steering

The research goal is to quantify the effect of RWS on ADAS. This chapter will quantify that effect by performing simulations with the chosen RWS control methods of Chapter 3, and using the LC controller design and simulation model of Chapter 4. The first section discusses step response simulations. The second section presents simulation results of the curved road driving scenario and discusses how the results are affected by RWS. The third section does the same for ALC. Finally, the final section gives a summary.

5.1 Step Response

Step response simulations, explained in detail in subsection 4.7.1, are used to quantify the effect of RWS on the rise time and settling time. These times, which are also explained in subsection 4.7.1, partly specify the controller's path tracking performance. Figure 5.1 shows the rise time and settling time for the chosen RWS control methods, using the LC controller design and simulation model. It can be seen that all RWS control methods, besides the yaw rate dependent method, are faster up to about 60 km/h. This can be explained by the fact that the steering angle ratio is negative up to that speed for these methods. This results in more agile handling, and thus decreased rise times and settling times. Due to RWS, the largest decreases in rise time and settling time are 0.056 s and 0.103 s respectively, using the adapted method that decreases the side-slip angle at 50 km/h. These values equal a decrease of 3.95 % and 3.83 % respectively. So the largest decreases in rise time and settling time due to RWS are relatively marginal.
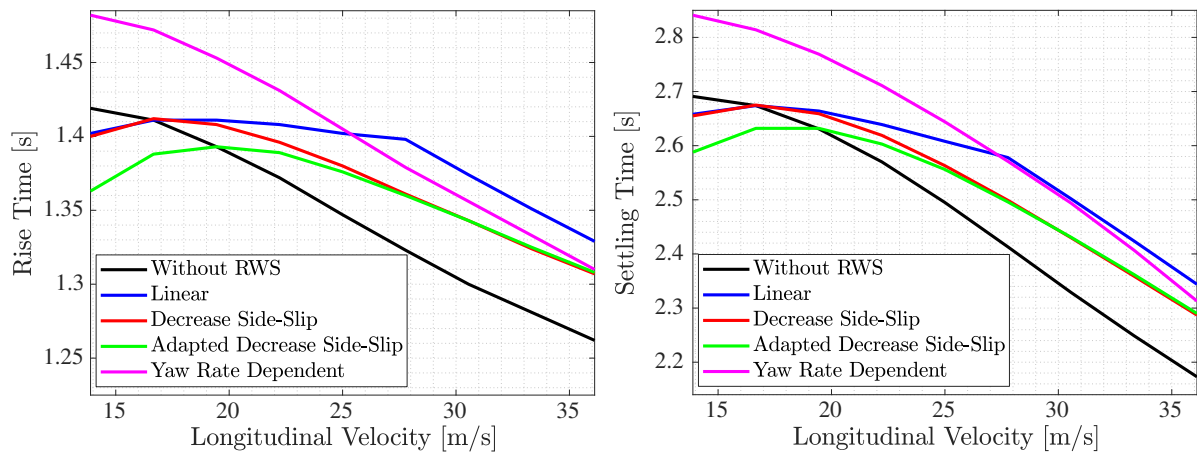

Figure 5.1: Rise time and settling time.

At speeds above 60 km/h, all RWS control methods are slower, because the steering angle ratio is positive. This improves the vehicle's stability, but lowers the agility, making the vehicle slower to react during a step response. The most substantial increase in rise time and settling time is caused by the linear RWS control method. Using this method, the largest increases in rise time and settling time are 0.075 s at 100 km/h and 0.175 s at 120 km/h respectively. These values equal an increase of 5.67 % and 7.78 % respectively, which is more noticeable than the largest decreases, but still modest.

To further quantify the effect, Tables 5.1 and 5.2 show the mean rise time $t_{ri,mean}$ and mean settling time $t_{se,mean}$ respectively, along with the deviation with respect to a vehicle without RWS. Again, the effect of RWS is relatively small. The mean rise time increases by 1.19 % to 4.24 % and the mean settling time increases by 1.66 % and 6.04 % when using RWS, depending on the RWS control method. Appendix D shows more results.

Table 5.1: Mean rise time $t_{ri,mean}$ and deviation with respect to without RWS.

RWS Control Method	$t_{ri,mean}$ [s]	Deviation w.r.t. without RWS [%]
Without RWS	1.345	-
Linear	1.387	3.12
Decrease Side-Slip	1.370	1.86
Adapted Decrease Side-Slip	1.361	1.19
Yaw Rate Dependent	1.402	4.24

Table 5.2: Mean settling time $t_{se,mean}$ and deviation with respect to without RWS.

RWS Control Method	$t_{se,mean}$ [s]	Deviation w.r.t. without RWS [%]
Without RWS	2.469	-
Linear	2.566	3.93
Decrease Side-Slip	2.527	2.35
Adapted Decrease Side-Slip	2.510	1.66
Yaw Rate Dependent	2.618	6.04

All in all, the following conclusions regarding the effect of RWS on the LC controller's rise time and settling time can be drawn from the step response simulations:

- If RWS applies countersteering, the rise time and settling time decrease, making the vehicle faster to react. This is done by most RWS controllers up to 60 km/h.

- If RWS steers in the same direction at higher speeds, the rise time and settling time increase, making the vehicle slower to react.

- The change in rise time and settling time due to RWS is under 4 % in most cases, with the greatest change being less than 8 %. Therefore, the effect of RWS on how fast the vehicle reacts is relatively small and often even marginal.

5.2 Curved Road

To quantify the effect of RWS on the controller's path tracking performance during the curved road driving scenario, explained in section 4.6, two simulations will be discussed in detail. Figures 5.2 and 5.3 present the simulation results at 50 km/h and 130 km/h respectively, using the LC controller design and simulation model.

As explained in section 3.4, the adapted method that decreases the side-slip angle is used for the simulations with RWS and for obtaining the rear-wheel steering angle δ_2.
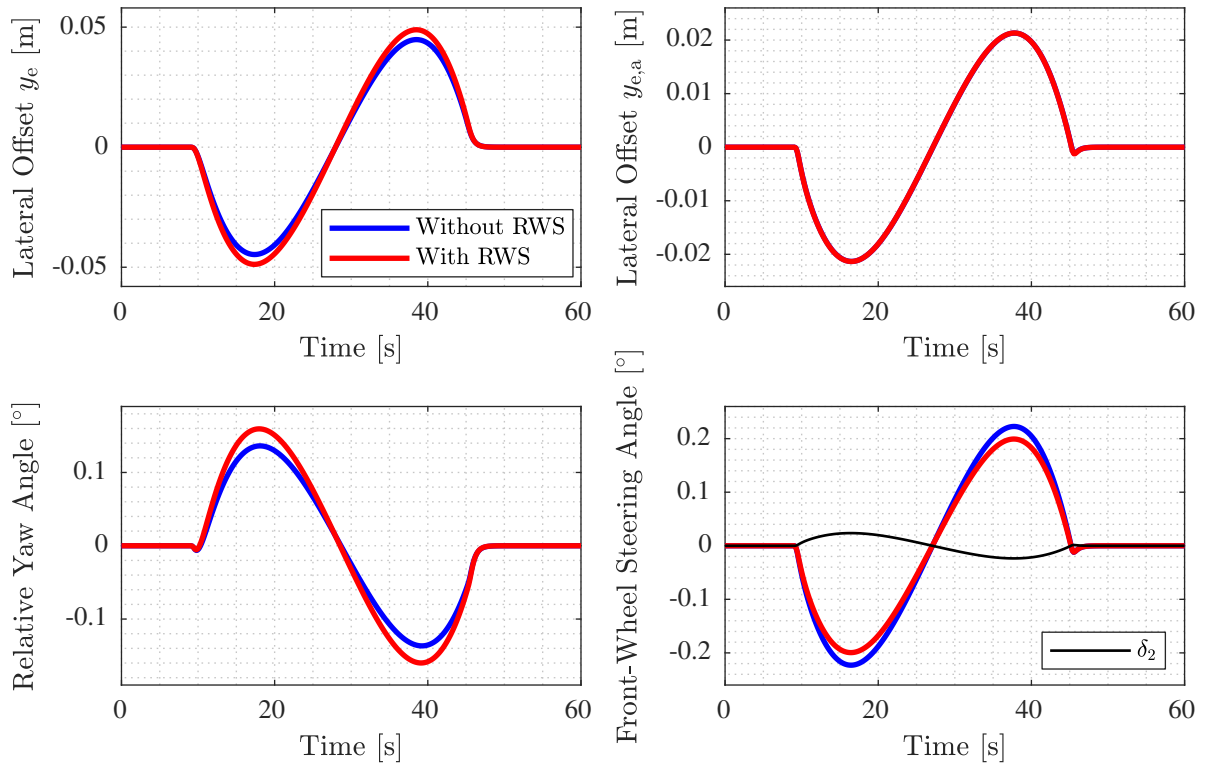

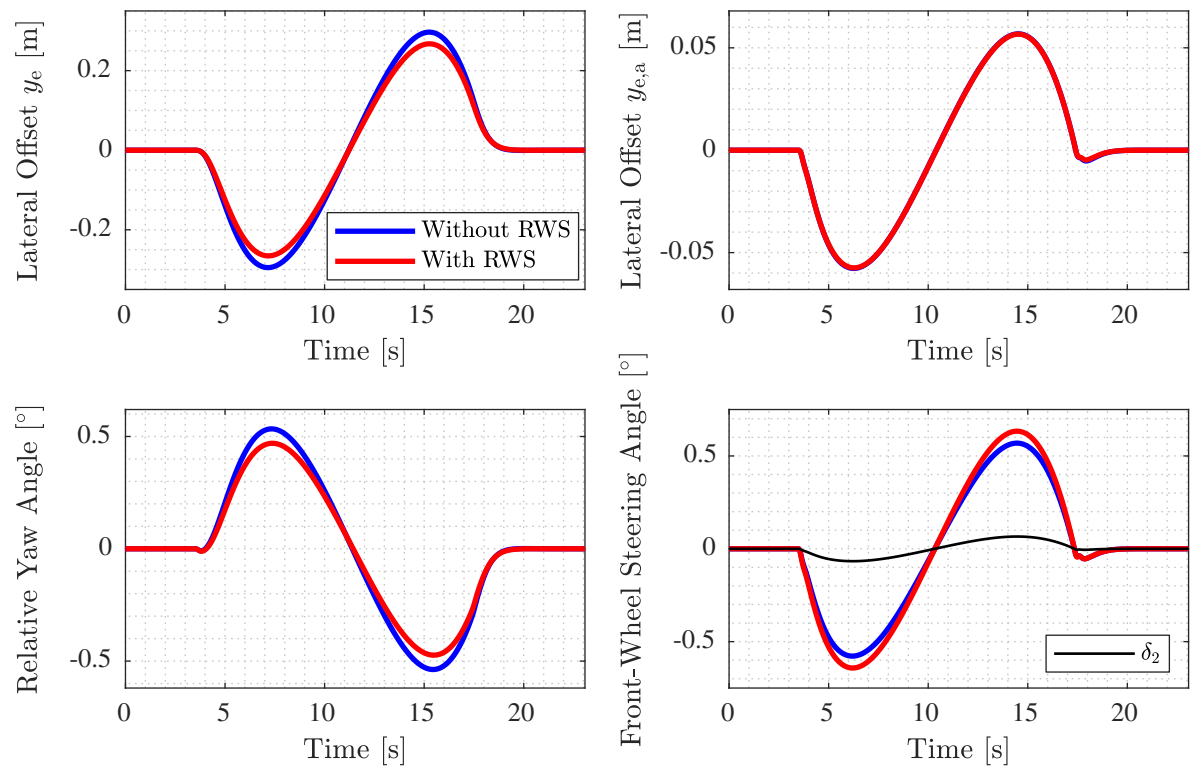**Figure 5.2:** Curved road at 50 km/h.

Figure 5.3: Curved road at 130 km/h.

The general shape of the simulation results is already discussed in subsection 4.7.2 with a curved road simulation at 100 km/h. Now the focus solely lies on the difference in results caused by the use of RWS. The results presented in Figures 5.2 and 5.3 will now be discussed.

Firstly, the relative yaw angle, whose amplitude increases at 50 km/h using RWS. This increase can be explained by the negative steering angle ratio at this speed. Due to the rear wheels steering in the opposite direction of the front wheels, the orientation of the vehicle changes more drastically than without RWS. This results in a larger relative yaw angle. At 130 km/h, the steering angle ratio is positive, resulting in a decrease in the relative yaw angle's amplitude.

Secondly, the lateral offset y_{e}, whose amplitude also increases at 50 km/h using RWS. However, in the opposite direction of the relative yaw angle. Both these effects can be explained by looking at (4.1) and knowing that the lateral offset $y_{\mathrm{e,a}}$ is effectively the same with and without RWS, as shown in Figure 5.2. This means that if the relative yaw angle increases, the lateral offset y_{e} decreases and vice versa. At 130 km/h, the amplitude of the lateral offset y_{e} decreases by using RWS, because of the same reasoning.

Thirdly, as mentioned before, the lateral offset $y_{\mathrm{e,a}}$ is practically the same for a vehicle with and without RWS. The vehicle position y_{g} remains practically the same, if its deviation value is compared to the total size of the path. As a result, the yaw angle ψ_{g} remains practically the same, so the yaw rate also hardly changes. The yaw rate depends directly on the front-wheel steering angle, as seen in (2.5) and (2.5), and that angle in turn depends on the error of the LC controller, the lateral offset $y_{\mathrm{e,a}}$.

Finally, the front-wheel steering angle changes if RWS is used at 50 km/h and 130 km/h. This can be explained by looking at the steering angle that the LC controller controls, which is δ_{c}. The controller receives the same input with or without RWS, namely the lateral offset $y_{\mathrm{e,a}}$. So the controller determines the same δ_{c}, which is distributed between the front-wheel and rear-wheel steering angles, as shown in (4.17) to (4.20). This means that the front-wheel steering angle increases if the rear wheels steer in the same direction and vice versa, resulting in a different front-wheel steering angle when using RWS.

Figure 5.4 shows the maximum absolute results for the chosen RWS control methods, using the LC controller design and simulation model. It can be seen that the findings discussed above are also reflected in the results in this figure. So the maximum absolute lateral offset $\max|y_{\mathrm{e}}|$ and maximum absolute relative yaw angle $\max|\psi_{\mathrm{rel}}|$ increase by using RWS when the steering angle ratio is negative, which is up to about 60 km/h for most RWS control methods. Only the yaw dependent method results in a decrease, which has a positive steering angle ratio at these speeds. A decrease in $\max|y_{\mathrm{e}}|$ and $\max|\psi_{\mathrm{rel}}|$ is a positive and desirable effect, since the vehicle stays closer to the desired path. At higher speeds, all RWS control methods have a positive effect, because $\max|y_{\mathrm{e}}|$ and $\max|\psi_{\mathrm{rel}}|$ decrease while using RWS.

The maximum absolute front-wheel steering angle $\max|\delta_1|$ changes when using RWS, because the steering angle δ_{c} is distributed between the front-wheel and rear-wheel steering angles, as shown in (4.17). Furthermore, the maximum absolute lateral offset $\max|y_{\mathrm{e,a}}|$ stays effectively the same during simulations with RWS, as also previously discussed.
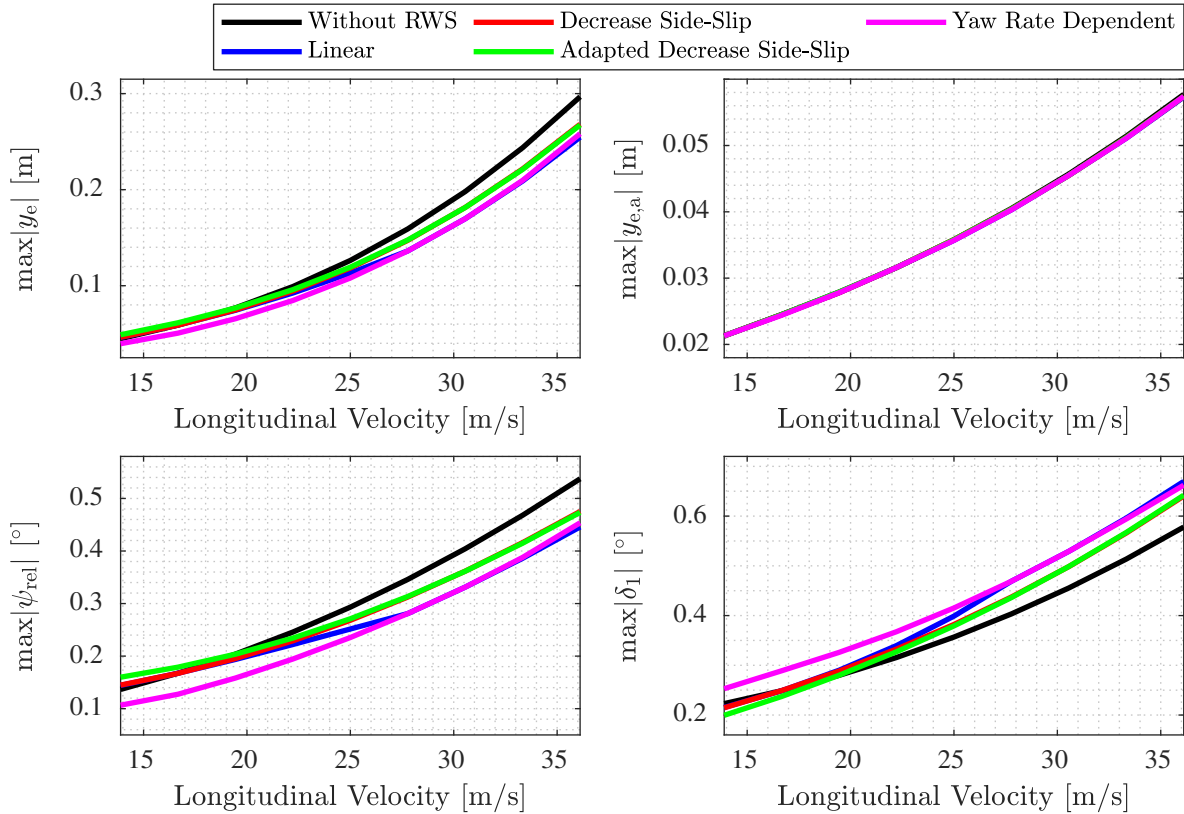
Figure 5.4: Maximum absolute results of curved road.

To further quantify the effect of RWS on the path tracking performance of the LC controller, the largest increase and decrease in $\max|y_e|$ and $\max|\psi_{rel}|$ caused by RWS are the most relevant, because these values specify how well the vehicle follows the path. The largest increases in $\max|y_e|$ and $\max|\psi_{rel}|$ due to RWS are 0.0041 m and 0.0233° respectively, caused by the adapted method that decreases the side-slip angle at 50 km/h. These values equal an increase of 9.15 % and 17.1 % respectively. The largest decreases due to RWS in $\max|y_e|$ and $\max|\psi_{rel}|$ are 0.0421 m and 0.0916° respectively. Both decreases are apparent at 130 km/h using the linear method. These values equal a decrease of 14.2 % and 17.1 % respectively. Overall, the largest percentage change due to the use of RWS is even larger, namely a 23.9 % increase in $\max|\psi_{rel}|$. So the effect of RWS on the path tracking performance during the curved road simulations is relativity large. Appendix D shows more results.

In short, the following conclusions regarding the effect of RWS on the tracking performance of the LC controller can be drawn from the curved road simulations:

- If RWS applies countersteering, $\max|y_e|$ and $\max|\psi_{rel}|$ increase, making the vehicle follow the path worse. This is done by most RWS controllers up to 60 km/h.

- If RWS steers in the same direction at higher speeds, $\max|y_e|$ and $\max|\psi_{rel}|$ decrease, making the vehicle follow the path better.

- The change in $\max|y_e|$ and $\max|\psi_{rel}|$ due to RWS is over 13 % in numerous cases, with the greatest change being almost 24 %. Therefore, the effect of RWS on the path tracking performance during the curved road simulations is relatively large.

5.3 Automated Lane Change

To quantify the effect of RWS on the controller's path tracking performance during the ALC driving scenario, discussed in section 4.6, two simulations are performed at 50 km/h and 130 km/h. These simulation results are shown in Appendix D. The results show the same effects of RWS as in Figure 5.2 and 5.3 for the curved road simulations, which have been extensively discussed in the previous section. Therefore, the effect of RWS during these simulations will not be discussed again.

Figure 5.5 shows the maximum absolute results for the chosen RWS control methods, using the LC controller design and simulation model. Compared to the curved road simulation results in Figure 5.4, the results of ALC show the same effect of RWS and will not be explained again either. However, there is a major difference between the curved road and ALC results. Unlike the ALC results, all curved road results rise when the speed increases. The rising curved road results can be declared by two main reasons. The first reason is that the look-ahead distance increases with speed, which negatively influences the tracking performance, as seen in Table 4.1. As also shown in Table 4.1, even with a constant look-ahead distance, the results rise as the speed increases. This can be largely explained by the second reason, the rate of change of the path increases with speed. This means that the path remains the same, but due to the increasing speed, direction changes such as curves will pass faster. Moreover, as discussed in section 5.1, the rise time and settling time decrease relatively minimally as the speed increases. At least not enough to compensate the increased rate of change. This leads to increasing results for the curved road simulations as the speed increases.
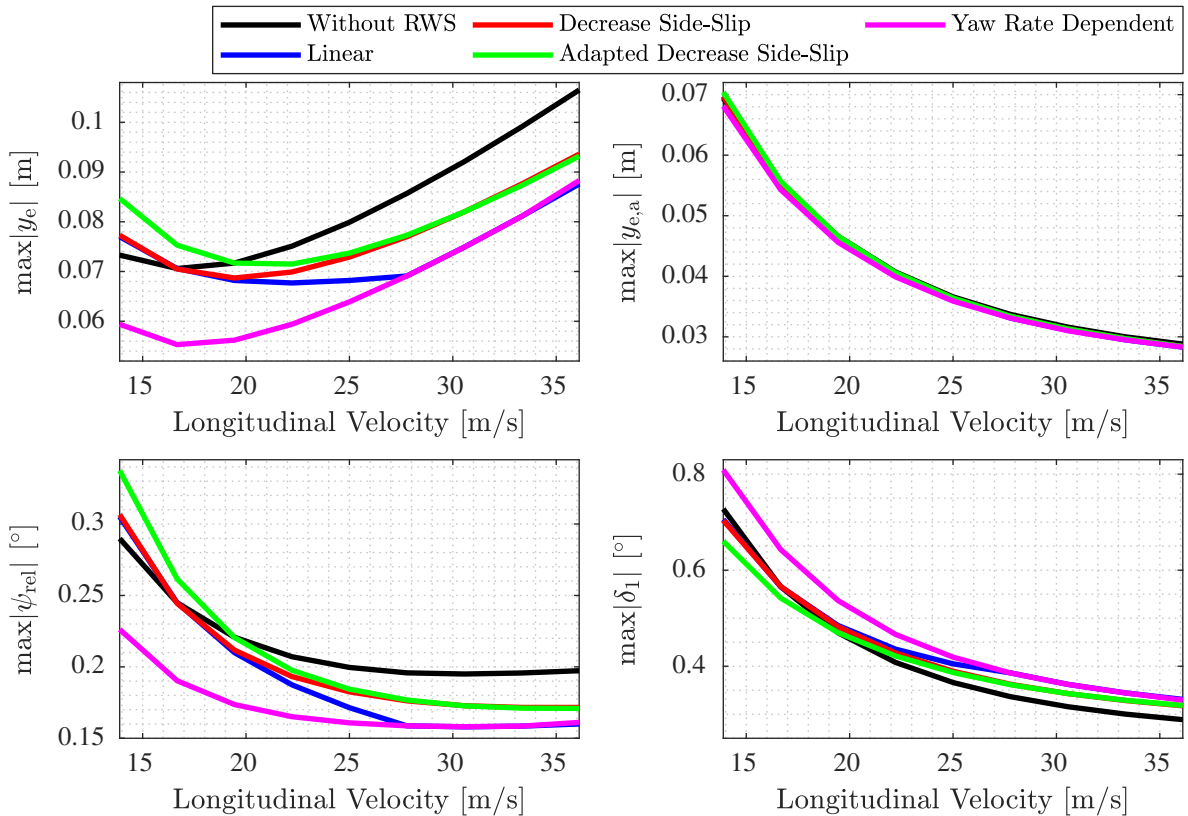

Figure 5.5: Maximum absolute results of ALC.

On the other hand, the maximum absolute results of the ALC simulation do not show an increase with vehicle speed, which is illogical according to the reasoning above. However, the path of ALC changes with speed, as explained in section 4.6. This means that the second reason, about the path's rate of change, is no longer valid. This explains the difference between the curved road and ALC results.

To further quantify the effect of RWS on the LC controller's path tracking performance during ALC simulations, the largest increase and decrease in $\max|y_\mathrm{e}|$ and $\max|\psi_\mathrm{rel}|$ caused by RWS are determined, as with the curved road simulations. The largest increases in $\max|y_\mathrm{e}|$ and $\max|\psi_\mathrm{rel}|$ due to RWS are 0.0114 m and 0.0476° respectively, caused by the adapted method that decreases the side-slip angle at 50 km/h. These values equal an increase of 15.6 % and 16.4 % respectively. The largest decrease due to RWS in $\max|y_\mathrm{e}|$ is 0.0189 m, which is apparent using the linear method at 130 km/h and is a decrease of 17.8 %. The biggest decrease due to RWS in $\max|\psi_\mathrm{rel}|$ is 0.0636°, which is caused by the yaw rate dependent method at 50 km/h. This equals a decrease of 22.0 %. Overall, the largest percentage change due to RWS is even larger, namely a 22.3 % increase in $\max|\psi_\mathrm{rel}|$. The effect of RWS expressed as a percentage is comparable to that of the curved road simulations, so again, the effect on the path tracking performance is relativity large. Appendix D shows more results.

To conclude, these are the major findings regarding the effect of RWS on the tracking performance of the LC controller during the ALC simulations:

- If RWS applies countersteering, $\max|y_\mathrm{e}|$ and $\max|\psi_\mathrm{rel}|$ increase, making the vehicle follow the path worse. This is done by most RWS controllers up to 60 km/h.
- If RWS steers in the same direction at higher speeds, $\max|y_\mathrm{e}|$ and $\max|\psi_\mathrm{rel}|$ decrease, making the vehicle follow the path better.
- The change in $\max|y_\mathrm{e}|$ and $\max|\psi_\mathrm{rel}|$ due to RWS is over 15 % in multiple cases, with the greatest change being slightly over 22 %. Therefore, the effect of RWS on the path tracking performance during the curved road simulations is relatively large.

5.4 Summary

To quantify the effect of RWS on the LC controller's path tracking performance, three driving scenarios are investigated. The first scenario simulates a step response to determine the rise time and settling time. Generally, using RWS makes the vehicle react faster up to about 60 km/h and react slower at higher speeds, compared to a vehicle without RWS. However, the effect is relatively small. The change in rise time and settling time when adding RWS to a vehicle is under 4 % in most cases, with the greatest change being less than 8 %.

To quantify the effect of RWS during the curved road and ALC simulations, the maximum absolute results are analysed. In particular, the maximum absolute offset $\max|y_\mathrm{e}|$ and maximum absolute relative yaw angle $\max|\psi_\mathrm{rel}|$, because their values specify how well the vehicle follows the path. In general, the path tracking performance deteriorates up to about 60 km/h and improves at higher speeds due to RWS. During the curved road simulations, the change in $\max|y_\mathrm{e}|$ and $\max|\psi_\mathrm{rel}|$ due to RWS is over 13 % in numerous cases, with the greatest change being almost 24 %.

During the ALC simulations, the change in $\max|y_{\mathrm{e}}|$ and $\max|\psi_{\mathrm{rel}}|$ caused by RWS is over 15 % in multiple cases, with the greatest change being slightly over 22 %. So in contrast to the step response simulations, the effect of RWS on the path tracking performance during these simulations is relatively large.

Chapter 6

Conclusions and Recommendations

The first section discusses the most important conclusions and the second section presents the recommendations for future research.

6.1 Conclusions

The goal of this research is to quantify the effect of RWS on ADAS. This goal is set to determine whether RWS affects the operation of ADAS such that the ADAS controllers must be retuned, since these controllers do not take RWS into account.

At low speeds, up to about 60 km/h, the chosen RWS controllers steer the rear wheels in the opposite direction of the front wheels, improving the vehicle's agility and manoeuvrability. For ADAS, this means:

- Decreased response times, making the vehicle faster to react. The largest decreases in response time due to RWS are all under 4 %, so a marginal influence of RWS.
- Deteriorated path tracking performance, which means the lateral offset and the relative yaw angle between the path and vehicle increase due to RWS. The greatest increases slightly exceed 17 %, so RWS has a relatively large effect.

At higher speeds, the chosen RWS controllers steer the rear wheels in the same direction as the front wheels, increasing the stability of the vehicle. For ADAS, this means:

- Increased response times, making the vehicle slower to react. The largest increases in response time due to RWS do not exceed 8 %, so again, a marginal influence of RWS.
- Improved path tracking performance, which means the lateral offset and the relative yaw angle between the path and vehicle decrease due to RWS. The largest decreases are slightly under 24 %, so a relatively large effect of RWS.

Even though the maximum relative deviation is quite large at 24 %, the maximum absolute deviation in lateral offset is 4.21 cm. Therefore, it can be concluded that the control of the simulated ADAS, LC and ALC, does not have to be retuned when RWS is added, if the steering angle δ_c determined by the ADAS controller is distributed between the front-wheel steering angle δ_1 and rear-wheel steering angle δ_2, such that $\delta_c = \delta_1 - \delta_2$.

6.2 Recommendations

For future research, it is recommended to:

- Investigate using a different controller for LC and ALC to check if the same effect of RWS is quantified as in this research. This can be done in two ways. Firstly, using the actual lateral offset at a look-ahead distance as the controller's error, instead of using information of the vehicle's current position to predict the lateral offset at a look-ahead distance. Secondly, develop a new controller that uses a different path tracking control method.

- Investigate using a larger vehicle, like a Ford F-150, to check if the same effect of RWS is quantified as in this research. Typically, RWS control on vehicles with a long wheelbase do more countersteering al low speeds.

- Investigate using different driving scenarios to check if the same effect of RWS is quantified as in this research. It is suggested to change the corner radii of the driving scenarios and develop new driving scenarios, like a figure eight or moose test. Furthermore, simulations could be executed at speeds outside the assumed operation range of LC and ALC, which is 50 km/h to 130 km/h.

- Investigate decoupling the control of RWS from the front-wheel steering angle. This allows the steering angles of the front and rear wheels to be the same, causing crab-like movement. This could have potential benefits during lane changes for example, since the yaw movement and lateral movement are decoupled.

- Quantify the effect of RWS on Automated Parking, since steering the rear wheels could have great potential for parking manoeuvres. It is expected that the system's control and corresponding trajectory planning have to be altered to fully benefit from the improved manoeuvrability and agility, and a smaller turning circle caused by RWS. Moreover, the potential benefits of decoupling the control of RWS from the front-wheel steering angle should be investigated, such as applying crab-like movement during parallel parking.

- Compare the closed-loop stability of the LC controller with and without RWS to find if RWS affects the system's stability. This can be done using the Nyquist stability criterion and thus using the open-loop transfer function to assess the closed-loop stability [34]. Furthermore, simulations of a moose test could be used, since stability is of great importance during such highly dynamic manoeuvres.

- Add a camera model to the simulation model used for LC and ALC, which simulates a camera in the vehicle by detecting the lane markings of a predefined path and subsequently determining the lane centre. This would make it possible to simulate the full functionality of the systems.

- Investigate using controller designs for RWS and ADAS of actual vehicles to check if the same effect of RWS is quantified as in this research.

- Perform tests with actual vehicles equipped with RWS and ADAS to verify the simulation results and the corresponding conclusions.

Bibliography

[1] Kyriakidis, M., van de Weijer, C., van Arem, B., & Happee, R. (2015). The Deployment of Advanced Driver Assistance Systems in Europe. *SSRN Electronic Journal.* doi: 10.2139/ssrn.2559034

[2] Jermakian, J. S. (2011). Crash Avoidance Potential of Four Passenger Vehicle Technologies. *Accident Analysis and Prevention, 43*(3), pp. 732-740. doi: 10.1016/j.aap.2010.10.020

[3] Ford Motor Company. *Adaptive Cruise Control with Stop-and-Go and Lane Centering.* Retrieved from
www.ford.com/technology/driver-assist-technology/adaptive-cruise-control/

[4] Ford Motor Company. *Enhanced Active Park Assist.* Retrieved from
www.ford.com/technology/driver-assist-technology/enhanced-active-park-assist/

[5] Besselink, I. J. M. (2017). *Lecture Notes of Vehicle Dynamics.* Eindhoven: Eindhoven University of Technology.

[6] Pacejka, H. B. (2012). *Tire and Vehicle Dynamics* (3rd ed.). Amsterdam: Elsevier.

[7] Veldhuizen, T. J. (2017). *Yaw Rate Feedback by Active Rear Wheel Steering* (master thesis). Eindhoven: Eindhoven University of Technology.

[8] MathWorks. *interp1.* Retrieved from
www.mathworks.com/help/matlab/ref/interp1.html

[9] Shampine, L. F., & Reichelt, M. W. (1997). The MATLAB ODE Suite. *SIAM Journal on Scientific Computing, 18*(1), pp. 1-22. doi: 10.1137/s1064827594276424

[10] ZF Friedrichshafen AG. *AKC - Active Kinematics Control.* Retrieved from
www.zf.com/products/en/cars/products_29123.html

[11] Sano, S., Oguchi, Y., & Furukawa, Y. (1979). The Effect of Improved Vehicle Dynamics on Drivers' Control Performance. *7th International Technical Conference on Experimental Safety Vehicles.*

[12] Vanderploeg, M. J., Trom, J. D., & Bernard, J. E. (1988). Evaluation of Four-Wheel Steer Path Following Performance Using a Linear Inverse Vehicle Model. *SAE Technical Paper Series, 880644.* doi: 10.4271/880644

[13] Takiguchi, T., Yasuda, N., Furutani, S., Kanazawa, H., & Inoue, H. (1986). Improvement of Vehicle Dynamics by Vehicle-Speed-Sensing Four-Wheel Steering System. *SAE Technical Paper Series, 860624.* doi: 10.4271/860624

[14] NetCarShow. *2009 Ford Fiesta 5-door*. Retrieved from
www.netcarshow.com/ford/2009-fiesta_5-door/1600x1200/wallpaper_02.htm

[15] NetCarShow. *2016 Ford F-150 Limited*. Retrieved from
www.netcarshow.com/ford/2016-f-150_limited/1600x1200/wallpaper_03.htm

[16] Mercury. *Moose Test*. Retrieved from
www.wikipedia.org/wiki/Moose_test#/media/File:Moose_test.svg

[17] Ploeg, J. (2017). *Lecture Notes of Vehicle Control: Lateral Dynamics and Controller Design*. Eindhoven: Eindhoven University of Technology.

[18] Thrun, S., Montemerlo, M., Dahlkamp, H., Stavens, D., Aron, A., Diebel, J., ... Mahoney, P. (2007). Stanley: The Robot That Won the DARPA Grand Challenge. *Springer Tracts in Advanced Robotics*, pp. 1-43. doi: 10.1007/978-3-540-73429-1_1

[19] Paden, B., Čáp, M., Yong, S. Z., Yershov, D., & Frazzoli, E. (2016). A Survey of Motion Planning and Control Techniques for Self-Driving Urban Vehicles. *IEEE Transactions on Intelligent Vehicles*, *1*(1), pp. 33-55. doi: 10.1109/tiv.2016.2578706

[20] Snider, J. M. (2009). *Automatic Steering Methods for Autonomous Automobile Path Tracking*. Pittsburgh, PA: Carnegie Mellon University.

[21] Törő, O., Bécsi, T., & Aradi, S. (2016). Design of Lane Keeping Algorithm of Autonomous Vehicle. *Periodica Polytechnica Transportation Engineering*, *44*(1), pp. 60-68. doi: 10.3311/pptr.8177

[22] Johnson, L., Lopez, B., Liu, S. Y., Miller, J., & How, J. P. (2015). Controlling Self-Driving Cars. *2015 IEEE CSS Video Clip Contest*.

[23] Kapania, N. R., & Gerdes, J. C. (2015). Path Tracking for an Autonomous Race Vehicle via Iterative Learning Control. *2015 American Control Conference (ACC)*. doi: 10.1109/acc.2015.7171151

[24] Ji, J., Khajepour, A., Melek, W. W., & Huang, Y. (2017). Path Planning and Tracking for Vehicle Collision Avoidance Based on Model Predictive Control with Multiconstraints. *IEEE Transactions on Vehicular Technology*, *66*(2), pp. 952-964. doi: 10.1109/tvt.2016.2555853

[25] García, C. E., Prett, D. M., & Morari, M. (1989). Model Predictive Control: Theory and Practice - A Survey. *Automatica*, *25*(3), pp. 335-348. doi: 10.1016/0005-1098(89)90002-2

[26] Lee, K., Li, S. E., & Kum, D. (2019). Synthesis of Robust Lane Keeping Systems: Impact of Controller and Design Parameters on System Performance. *IEEE Transactions on Intelligent Transportation Systems*, *20*(8), pp. 3129-3141. doi: 10.1109/tits.2018.2873101

[27] Schoon, C. C. (1994). *Road Design Standards of Medians, Shoulders and Verges*. Leidschendam: SWOV Institute for Road Safety Research.

[28] MathWorks. *Solver*. Retrieved from
www.mathworks.com/help/simulink/gui/solver.html

[29] Zegelaar, P. W. A. (2019). *Lecture Notes of Vehicle Control: Collision Mitigation.* Eindhoven: Eindhoven University of Technology.

[30] Franklin, G. F., Powell, J. D., & Emami-Naeini, A. (2009). *Feedback Control of Dynamic System* (6th ed.). Upper Saddle River, NJ: Pearson Prentice Hall.

[31] Åström, K. J., & Murray, R. M. (2010). *Feedback Systems: An Introduction for Scientists and Engineers.* Princeton, NJ: Princeton University Press.

[32] Nise, N. S. (2010). *Control Systems Engineering* (6th ed.). Hoboken, NJ: John Wiley & Sons.

[33] Dorf, R. C., & Bishop, R. H. (2010). *Modern Control Systems* (12th ed.). Upper Saddle River, NJ: Pearson Prentice Hall.

[34] Witvoet, G. (2016). *Lecture Notes of Control Engineering: Stability.* Eindhoven: Eindhoven University of Technology.

Appendix A

Sign Conventions

Figure A.1 shows an overview of several commonly used sign conventions. The adapted SAE sign convention, used in this report, is shown in the second column.
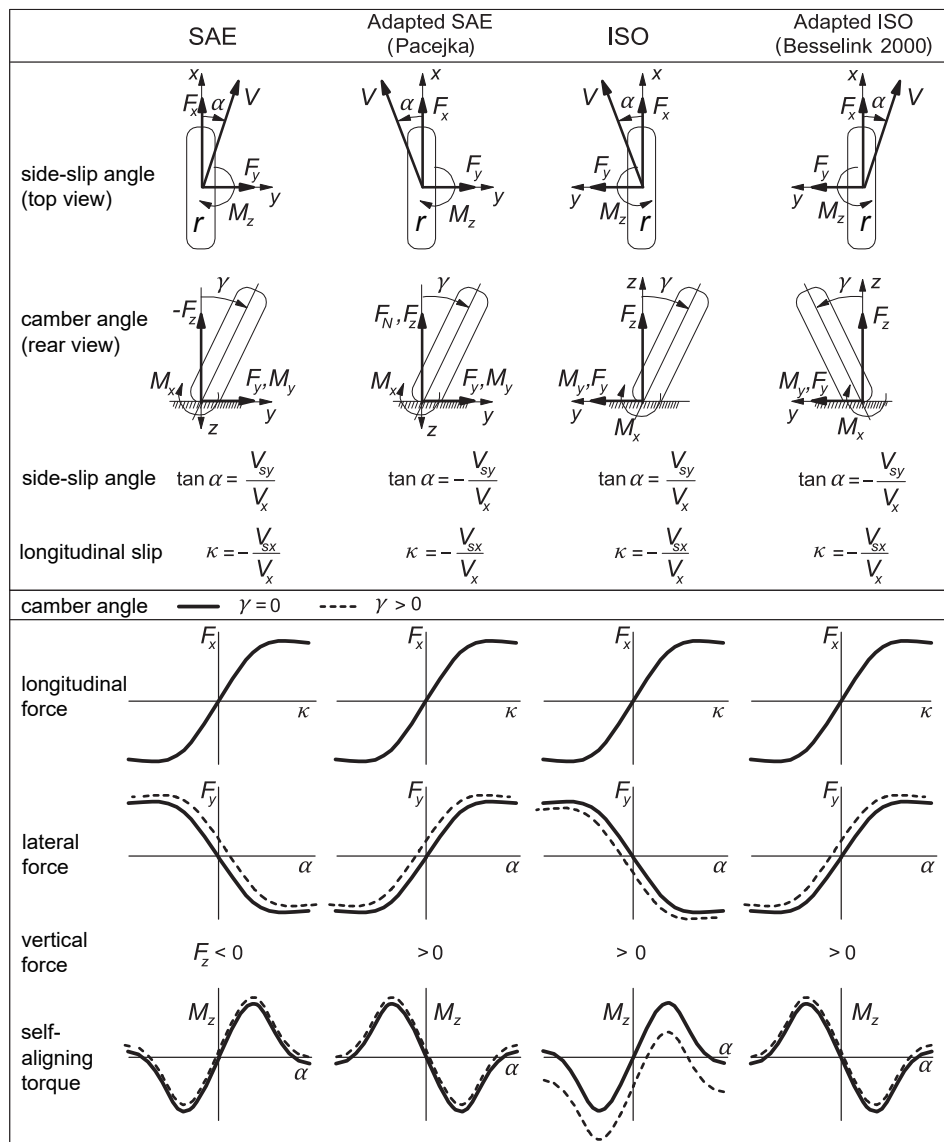
Figure A.1: Overview of sign conventions. Adapted from [6].

Appendix B

Vehicle Parameters

This appendix shows and explains the vehicle parameters, starting with those of the seventh generation Ford Fiesta, shown in Figure B.1, in the first section. The second section presents the parameters of to the thirteenth generation Ford F-150, shown in Figure B.2. All parameters are provided by Ford Motor Company, unless stated otherwise.

Figure B.1: Seventh generation Ford Fiesta [14].

Figure B.2: Thirteenth generation Ford F-150 [15].

Ford Fiesta

The vehicle parameters of the seventh generation Ford Fiesta, built from 2008 to 2017, are chosen for most calculations and simulations throughout the research. Since the Ford Fiesta's parameters are used in the linear single track and non-linear two track vehicle model, a comprehensive list of parameters is required, as shown in Table B.1.

Table B.1: Vehicle parameters of the seventh generation Ford Fiesta.

Parameter	Symbol	Unit	Value
Mass	m	[kg]	1281
Wheelbase	l	[m]	2.490
Distance from the centre of gravity to the front axle	a	[m]	0.960
Distance from the centre of gravity to the rear axle	b	[m]	1.530
Half front track width	s_1	[m]	0.733
Half rear track width	s_2	[m]	0.724
Roll centre height of the front axle*	$h_{\varphi,1}$	[m]	0.0297
Roll centre height of the rear axle*	$h_{\varphi,2}$	[m]	0.1341
Height from the centre of gravity to the ground*	h	[m]	0.550
Height from the centre of gravity to the roll axis**	h'	[m]	0.480
Roll axis inclination angle**	θ	[°]	2.40
Roll stiffness at the front axle*	$k_{\varphi,1}$	[N·m/rad]	56866
Roll stiffness at the rear axle*	$k_{\varphi,2}$	[N·m/rad]	38623
Roll damping at the front axle**	$c_{\varphi,1}$	[N·m·s/rad]	4815
Roll damping at the rear axle**	$c_{\varphi,2}$	[N·m·s/rad]	3270
Cornering stiffness of the front tyres	C_1	[N/rad]	78100
Cornering stiffness of the rear tyres	C_2	[N/rad]	88700
Moment of inertia in x-direction*	I_{xx}	[kg·m^2]	436
Moment of inertia in y-direction*	I_{yy}	[kg·m^2]	1643
Moment of inertia in z-direction*	I_{zz}	[kg·m^2]	1808
Steering ratio	i_{st}	[-]	13.90

Four vehicle parameters in Table B.1 have been calculated, namely the roll axis inclination angle, the height from the centre of gravity to the roll axis, and the roll damping at the front and rear axle. The calculations used to find these parameters will be discussed now. Starting with the roll axis inclination angle θ, which is geometrically determined:

$$\theta = \arctan\left(\frac{h_{\varphi,2} - h_{\varphi,1}}{l}\right) \tag{B.1}$$

The roll axis inclination angle is found to be 2.40°. Now one can determine the height from the centre of gravity to the roll axis h' with:

$$h' = (h - h_{\varphi,1} - a\tan\theta)\cos\theta \tag{B.2}$$

The height from the centre of gravity to the roll axis is found to be 0.48 m.

---

*Average value of vehicles comparable to the Ford Fiesta
**Calculated, see (B.1) to (B.7)

Knowing the height from the centre of gravity to the roll axis, the roll damping at each axle can be determined. For this, the differential equation for a rotational harmonic oscillator system, which represents the vehicle, is determined first:

$$\left(I_{xx} + mh'^2\right)\ddot{\varphi} + \left(c_{\varphi,1} + c_{\varphi,2}\right)\dot{\varphi} + \left(k_{\varphi,1} + k_{\varphi,2} - mgh'\right)\varphi = 0 \tag{B.3}$$

from which the undamped and damped angular natural frequency, ω_{n} and ω_{d} respectively, can be obtained:

$$\omega_{\mathrm{n}} = \sqrt{\frac{k_{\varphi,1} + k_{\varphi,2} - mgh'}{I_{xx} + mh'^2}} \tag{B.4}$$

$$\omega_{\mathrm{d}} = \omega_{\mathrm{n}}\sqrt{1 - \left(\frac{c_{\varphi,1} + c_{\varphi,2}}{2\sqrt{\left(I_{xx} + mh'^2\right)\left(k_{\varphi,1} + k_{\varphi,2} - mgh'\right)}}\right)^2} \tag{B.5}$$

The undamped and damped angular natural frequency are found to be 11.06 rad/s and 9.47 rad/s respectively. This is validated in upcoming subsection. The undamped angular natural frequency is used to determine the roll damping at both axles using [5]:

$$c_{\varphi,1} + c_{\varphi,2} = 2\left(I_{xx} + mh'^2\right)\omega_{\mathrm{n}}\zeta \tag{B.6}$$

where ζ is the damping ratio, which is chosen to be 0.5. So it is chosen that the roll damping is underdamped, because the damping ratio is under 1. The roll damping at both axles combined is found to be 8085 N·m·s/rad. To determine the distribution of roll damping between the front and rear axle, two methods can be used. The first method distributes the roll damping with respect to the mass distribution, and the second method does it with respect to the distribution of the roll stiffness between the axles. It is chosen to use the second method. Using this method, the roll damping at each axle can be found with:

$$c_{\varphi,1} = \frac{k_{\varphi,1}}{k_{\varphi,1} + k_{\varphi,2}}\left(c_{\varphi,1} + c_{\varphi,2}\right) \ , \quad c_{\varphi,2} = \frac{k_{\varphi,2}}{k_{\varphi,1} + k_{\varphi,2}}\left(c_{\varphi,1} + c_{\varphi,2}\right) \tag{B.7}$$

The roll damping at the front and rear axle are 4815 N·m·s/rad and 3270 N·m·s/rad respectively.

Validation of Natural Frequency

To determine the undamped and damped angular natural frequency, relatively straightforward expressions are found in (B.4) and (B.5). To validate if these expressions are correct, a validation method will be presented now. Firstly, $\dot{\mathbf{x}}$ of the state-space notation of a linear single track vehicle model with roll needs to be determined. This is done to obtain $\mathbf{A}$, because from the eigenvalues of $\mathbf{A}$, the natural frequencies can be determined for the validation. The expression for $\dot{\mathbf{x}}$ is found to be:

$$\dot{\mathbf{x}} = \mathbf{A}\mathbf{x} + \mathbf{B}\mathbf{u} \tag{B.8}$$

with:

$$\mathbf{x} = \begin{bmatrix} v_y \\ r \\ \dot{\varphi} \\ \varphi \end{bmatrix}, \quad \mathbf{u} = \delta_1 ,$$

$$\mathbf{A} = \begin{bmatrix} -\dfrac{C_1 + C_2}{mv_x} & \dfrac{bC_2 - aC_1}{mv_x} - v_x & 0 & 0 \\[4mm] \dfrac{bC_2 - aC_1}{I_{zz}v_x} & -\dfrac{a^2C_1 + b^2C_2}{I_{zz}v_x} & 0 & 0 \\[4mm] \dfrac{h'(C_1 + C_2)}{v_x(I_{xx} + mh'^2)} & -\dfrac{h'(bC_2 + aC_1)}{v_x(I_{xx} + mh'^2)} & -\dfrac{c_{\varphi,1} + c_{\varphi,2}}{I_{xx} + mh'^2} & \dfrac{mgh' - k_{\varphi,1} - k_{\varphi,2}}{I_{xx} + mh'^2} \\[4mm] 0 & 0 & 1 & 0 \end{bmatrix}, \quad \text{(B.9)}$$

$$\mathbf{B} = \begin{bmatrix} \dfrac{C_1}{m} \\[4mm] \dfrac{aC_1}{I_{zz}} \\[4mm] -\dfrac{h'C_1}{I_{xx} + mh'^2} \\[4mm] 0 \end{bmatrix}$$

The first and second row of $\mathbf{x}$, $\mathbf{A}$, and $\mathbf{B}$ are from a standard linear single track vehicle model without roll, shown in (2.9). The fourth row expresses that $\dot{\varphi}$ is equal to $\dot{\varphi}$. However, the third row might need some explanation. For this, the expression for roll of the linearised equations of motion of a two track vehicle model is taken [6]:

$$\left(I_{xx} + mh'^2\right)\ddot{\varphi} + mh'(\dot{v}_y + v_x r) + \left(I_{zz}\theta - I_{xz}\right)\dot{r} \\ + \left(c_{\varphi,1} + c_{\varphi,2}\right)\dot{\varphi} + \left(k_{\varphi,1} + k_{\varphi,2} - mgh'\right)\varphi = 0 \quad \text{(B.10)}$$

The influence of the roll axis inclination angle is neglected, since this influence is also neglected in (B.4) and (B.5). This means that the term $\left(I_{zz}\theta - I_{xz}\right)\dot{r}$ is set to zero. Furthermore, $\dot{v}_y$ in (B.10) is substituted with:

$$\dot{v}_y = -\frac{C_1 + C_2}{mv_x}v_y + \left(\frac{bC_2 - aC_1}{mv_x} - v_x\right)r + \frac{C_1}{m}\delta_1 \quad \text{(B.11)}$$

which is found using the state-space notation of a linear single track vehicle model without roll. After substitution of $\dot{v}_y$ and rewriting, the expression for $\ddot{\varphi}$, used in (B.9), is found:

$$\ddot{\varphi} = \frac{h'(C_1 + C_2)}{v_x(I_{xx} + mh'^2)}v_y - \frac{h'(bC_2 + aC_1)}{v_x(I_{xx} + mh'^2)}r \\ - \frac{c_{\varphi,1} + c_{\varphi,2}}{I_{xx} + mh'^2}\dot{\varphi} + \frac{mgh' - k_{\varphi,1} - k_{\varphi,2}}{I_{xx} + mh'^2}\varphi - \frac{h'C_1}{I_{xx} + mh'^2}\delta_1 \quad \text{(B.12)}$$

Determining the eigenvalues of $\mathbf{A}$ in (B.9), the undamped and damped angular natural frequency are found to be 11.06 rad/s and 9.47 rad/s respectively. This means that (B.4) and (B.5) are correct, since the results are the same. The damping term $c_{\varphi,1} + c_{\varphi,2}$ in (B.9) is set to zero to determine the undamped angular natural frequency.

Ford F-150

The parameters of the thirteenth generation Ford F-150, produced since 2014, are only used to develop RWS control methods. The development of RWS control methods is done using the linear single track vehicle model. The parameters needed for this vehicle model are shown in Table B.2. To be more precise, these vehicle parameters are from a so-called Ford F-150 SuperCrew 6.5 ft, meaning that the cabin has four doors and that the cargo box is 1.98 m long.

Table B.2: Vehicle parameters of the thirteenth generation Ford F-150.

Parameter	Symbol	Unit	Value
Mass	m	[kg]	1877
Wheelbase	l	[m]	4.000
Distance from the centre of gravity to the front axle	a	[m]	1.578
Distance from the centre of gravity to the rear axle	b	[m]	2.422
Cornering stiffness of the front tyres	C_1	[N/rad]	148900
Cornering stiffness of the rear tyres	C_2	[N/rad]	240000
Steering ratio	i_{st}	[-]	18.29

Appendix C

Differences Between Vehicle Models

Using a step response, the effect of the differences in roll, tyres, and a combination of both between the vehicle models are explained. Since the longitudinal velocity is constant during a step response, this difference is not further explained.

Roll

Starting with roll, which is only taken into account in the non-linear two track vehicle model. Figure C.1 shows a step response at 100 km/h with a steering wheel angle of 45°, including the results of a non-linear two track vehicle model without roll.
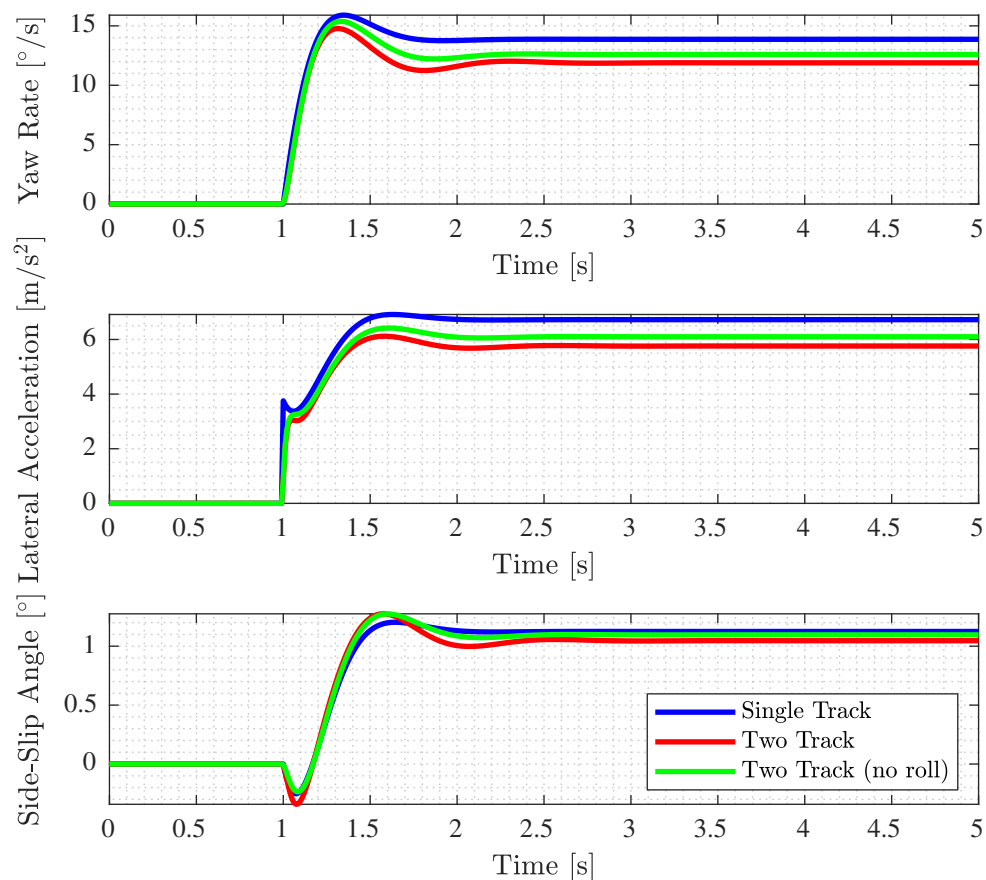
Figure C.1: Step response at 100 km/h with δ_{sw} at 45°.

As can be seen, the results of the non-linear two track vehicle model are closer to those of the linear single track vehicle model if roll is neglected. By neglecting roll, the load transfer due to roll is also neglected, just like in the linear single track vehicle model.

The influence on the yaw rate, lateral acceleration, and side-slip angle can be explained by looking at the effect that roll and load transfer have in the non-linear two track vehicle model. If the vertical force at a wheel increases due to load transfer caused by roll, the lateral force F_y at that wheel increases too. This leads to reaching the tyre's maximum grip level earlier, since non-linear tyres are used. This results in a lower yaw rate and lateral acceleration. The side-slip angle will be larger at the initial steering action, shown in Figure C.1 from 1 s to about 1.7 s, and smaller when vehicle settles due to a lower lateral acceleration. Neglecting roll, and thus load transfer, will not take these effects into account, bringing the results closer to a linear single track vehicle model.

Tyres

The linear single track vehicle model uses linear tyres instead of the non-linear tyres in the non-linear two track vehicle model, which are modelled using the Magic Formula. Figure C.2 shows the same step response as in Figure C.1, but now including the results of a non-linear two track vehicle model with linear tyres.
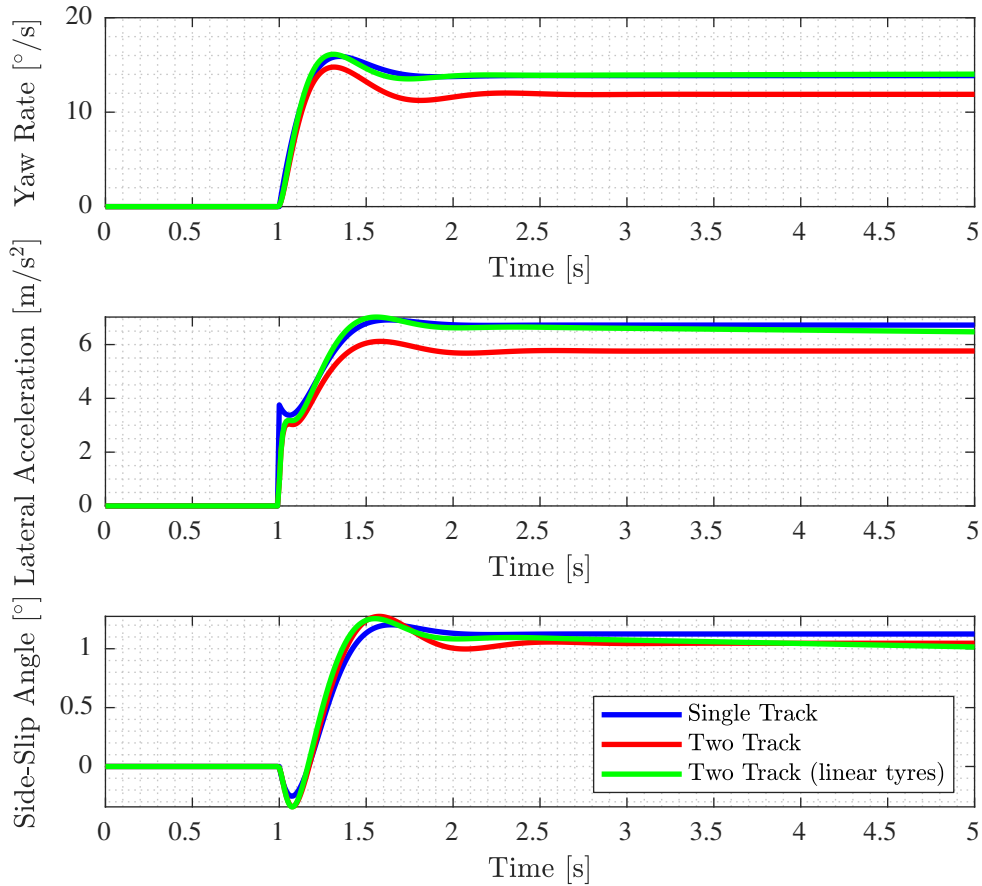
Figure C.2: Step response at 100 km/h with δ_{sw} at 45°.

It can be concluded that the two track vehicle model with linear tyres is closer to the linear single track vehicle model than to the non-linear two track vehicle model. This result can be explained when looking at the Magic Formula. The Magic Formula models non-linear tyres that have a maximum grip level after which a tyre's grip level decreases and settles. A linear tyre model models no maximum, so the force on the tyres can keep increasing. During the step response, the tyres enter the non-linear part of the Magic Formula, which reduces their grip level. However, the forces on linear tyres continue to rise, allowing the yaw rate, lateral acceleration, and side-slip angle to increase further.

Note that the side-slip angle of the two track vehicle model with linear tyres decreases after about 2.5 s. This is due to the drivetrain modelling in the simulation model and it can be ignored.

Combination of Roll and Tyres

The results of neglecting roll and using linear tyres in the two track vehicle model are shown in Figure C.3. To obtain these results, the same step response is simulated again, so at 100 km/h with a steering wheel angle of 45°.

At first glance, these results may seem to be the same as those in Figure C.2. However, when looking at the initial steering action between 1 s and 1.7 s, it can be seen that the results better match those of the linear single track vehicle model.
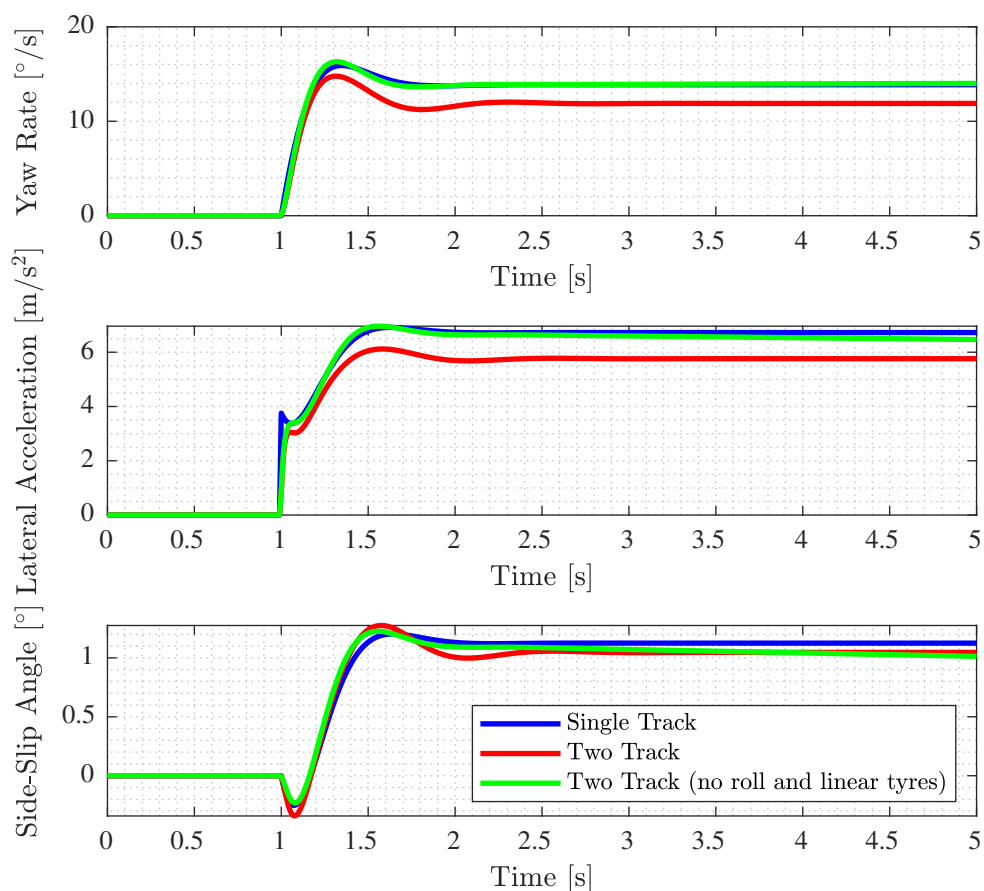
Figure C.3: Step response at 100 km/h with δ_{sw} at 45°.

Again, note that the side-slip angle of the two track vehicle model with linear tyres decreases after about 2.5 s. This is due to the drivetrain modelling in the SIMULINK model and it can be ignored.

It could be expected that the difference between Figures C.2 and C.3 should be bigger when considering the effect of roll seen in Figure C.1. The reason that combining the two effects has relatively little effect compared to just using linear tyres is that by using linear tyres, the effect of load transfer due to roll is already partly dismissed. For example, the lateral force F_y at each tyre in the Magic Formula is influenced by the vertical forces, and thus by load transfer due to roll. However, in the linear tyre model, the lateral tyre force has a linear relation with the side-slip angle at the wheel.

All in all, it can be concluded from Figures C.1, C.2, and C.3 that the difference in tyres between the vehicle models is mainly responsible for the difference between the vehicle models during this step response.

Appendix D

Simulation Results

This appendix shows simulation results in more detail. The first, second, and third section present the results of the step response, curved road and ALC simulations respectively.

Step Response

Table D.1 shows the rise time for the different RWS control methods at multiple speeds within the LC operation range, using the LC controller design and simulation model. Table D.2 does the same for the settling time.

Table D.1: Rise time t_{ri}.

RWS Control Method[†]	$t_{\mathbf{ri}}$ [s]								
	50 km/h	60 km/h	70 km/h	80 km/h	90 km/h	100 km/h	110 km/h	120 km/h	130 km/h
A	1.419	1.411	1.393	1.372	1.347	1.323	1.300	1.281	1.262
B	1.402	1.411	1.411	1.408	1.402	1.398	1.374	1.351	1.329
C	1.400	1.412	1.408	1.396	1.380	1.361	1.343	1.324	1.307
D	1.363	1.388	1.393	1.389	1.376	1.360	1.343	1.325	1.308
E	1.482	1.472	1.453	1.431	1.405	1.379	1.356	1.333	1.310

Table D.2: Settling time t_{se}.

RWS Control Method[†]	$t_{\mathbf{se}}$ [s]								
	50 km/h	60 km/h	70 km/h	80 km/h	90 km/h	100 km/h	110 km/h	120 km/h	130 km/h
A	2.691	2.674	2.631	2.570	2.495	2.413	2.329	2.249	2.173
B	2.658	2.674	2.664	2.639	2.608	2.578	2.502	2.424	2.344
C	2.655	2.675	2.659	2.619	2.563	2.499	2.430	2.359	2.287
D	2.588	2.632	2.632	2.603	2.556	2.496	2.431	2.362	2.290
E	2.841	2.814	2.769	2.711	2.644	2.571	2.494	2.407	2.313

[†]A = Without RWS, B = Linear, C = Decrease Side-Slip, D = Adapted Decrease Side-Slip, E = Yaw Rate Dependent

Curved Road

The tables in this section present the maximum absolute results of the simulations with the curved road driving scenario, using the LC controller design and simulation model.

Table D.3: Maximum absolute lateral offset $\max|y_\mathrm{e}|$.

RWS Control Method[†]	$\max|y_\mathrm{e}|$ [m]								
	50 km/h	60 km/h	70 km/h	80 km/h	90 km/h	100 km/h	110 km/h	120 km/h	130 km/h
A	0.0448	0.0590	0.0769	0.0991	0.1263	0.1591	0.1980	0.2437	0.2967
B	0.0461	0.0590	0.0744	0.0924	0.1131	0.1362	0.1697	0.2090	0.2546
C	0.0463	0.0589	0.0748	0.0944	0.1184	0.1472	0.1815	0.2216	0.2681
D	0.0489	0.0614	0.0768	0.0959	0.1193	0.1476	0.1814	0.2211	0.2673
E	0.0396	0.0506	0.0656	0.0846	0.1080	0.1362	0.1697	0.2097	0.2582

Table D.4: Maximum absolute lateral offset $\max|y_\mathrm{e,a}|$.

RWS Control Method[†]	$\max|y_\mathrm{e,a}|$ [m]								
	50 km/h	60 km/h	70 km/h	80 km/h	90 km/h	100 km/h	110 km/h	120 km/h	130 km/h
A	0.0213	0.0245	0.0279	0.0316	0.0358	0.0405	0.0457	0.0514	0.0577
B	0.0213	0.0245	0.0278	0.0316	0.0357	0.0403	0.0455	0.0511	0.0573
C	0.0213	0.0245	0.0278	0.0316	0.0358	0.0404	0.0455	0.0512	0.0574
D	0.0213	0.0245	0.0279	0.0316	0.0358	0.0404	0.0455	0.0512	0.0574
E	0.0213	0.0244	0.0278	0.0316	0.0357	0.0403	0.0455	0.0511	0.0574

Table D.5: Maximum absolute relative yaw angle $\max|\psi_\mathrm{rel}|$.

RWS Control Method[†]	$\max|\psi_\mathrm{rel}|$ [°]								
	50 km/h	60 km/h	70 km/h	80 km/h	90 km/h	100 km/h	110 km/h	120 km/h	130 km/h
A	0.1366	0.1675	0.2039	0.2458	0.2932	0.3460	0.4043	0.4681	0.5374
B	0.1442	0.1675	0.1937	0.2221	0.2516	0.2810	0.3313	0.3862	0.4458
C	0.1449	0.1672	0.1954	0.2291	0.2682	0.3124	0.3617	0.4160	0.4752
D	0.1599	0.1790	0.2037	0.2344	0.2711	0.3135	0.3615	0.4149	0.4735
E	0.1066	0.1275	0.1583	0.1945	0.2354	0.2810	0.3313	0.3879	0.4537

Table D.6: Maximum absolute front-wheel steering angle $\max|\delta_1|$.

| RWS Control Method[†]	$\max|\delta_1|$ [°]								
	50 km/h	60 km/h	70 km/h	80 km/h	90 km/h	100 km/h	110 km/h	120 km/h	130 km/h
A	0.2230	0.2489	0.2798	0.3157	0.3568	0.4033	0.4555	0.5136	0.5780
B	0.2153	0.2489	0.2901	0.3397	0.3989	0.4690	0.5292	0.5960	0.6697
C	0.2146	0.2492	0.2884	0.3326	0.3821	0.4373	0.4985	0.5660	0.6403
D	0.1995	0.2373	0.2800	0.3273	0.3792	0.4362	0.4987	0.5671	0.6420
E	0.2530	0.2890	0.3260	0.3676	0.4153	0.4690	0.5292	0.5942	0.6621

[†]A = Without RWS, B = Linear, C = Decrease Side-Slip, D = Adapted Decrease Side-Slip, E = Yaw Rate Dependent

Table D.7: Maximum absolute rear-wheel steering angle $\max|\delta_2|$.

RWS Control Method[†]	$\max|\delta_2|$ [°]								
	50 km/h	60 km/h	70 km/h	80 km/h	90 km/h	100 km/h	110 km/h	120 km/h	130 km/h
A	0	0	0	0	0	0	0	0	0
B	0.0077	0.0000	0.0104	0.0243	0.0427	0.0670	0.0756	0.0851	0.0957
C	0.0084	0.0003	0.0087	0.0171	0.0257	0.0346	0.0441	0.0542	0.0651
D	0.0236	0.0117	0.0002	0.0116	0.0227	0.0335	0.0443	0.0553	0.0668
E	0.0303	0.0404	0.0466	0.0525	0.0593	0.0670	0.0756	0.0833	0.0877

Automated Lane Change

Figure D.1 shows the results of the ALC simulation at 100 km/h without RWS, which is discussed in subsection 4.7.2. Figures 5.2 and 5.3 present the ALC simulation results at 50 km/h and 130 km/h respectively, which are discussed in section 5.3. As explained in section 3.4, the adapted method that decreases the side-slip angle is used for the simulations with RWS and for obtaining the rear-wheel steering angle δ_2. Furthermore, the tables in this section present the maximum absolute results of the simulations with the curved road driving scenario, using the LC controller design and simulation model.
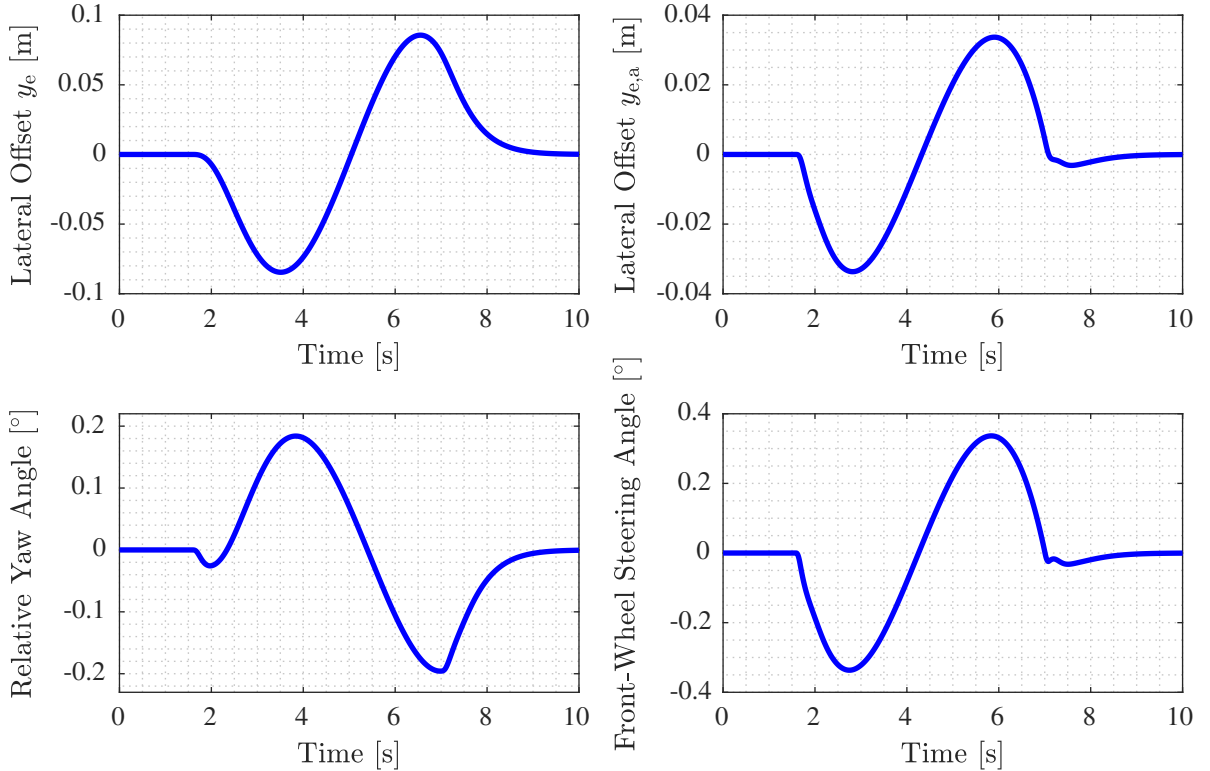
Figure D.1: ALC at 100 km/h without RWS.

[†]A = Without RWS, B = Linear, C = Decrease Side-Slip, D = Adapted Decrease Side-Slip, E = Yaw Rate Dependent
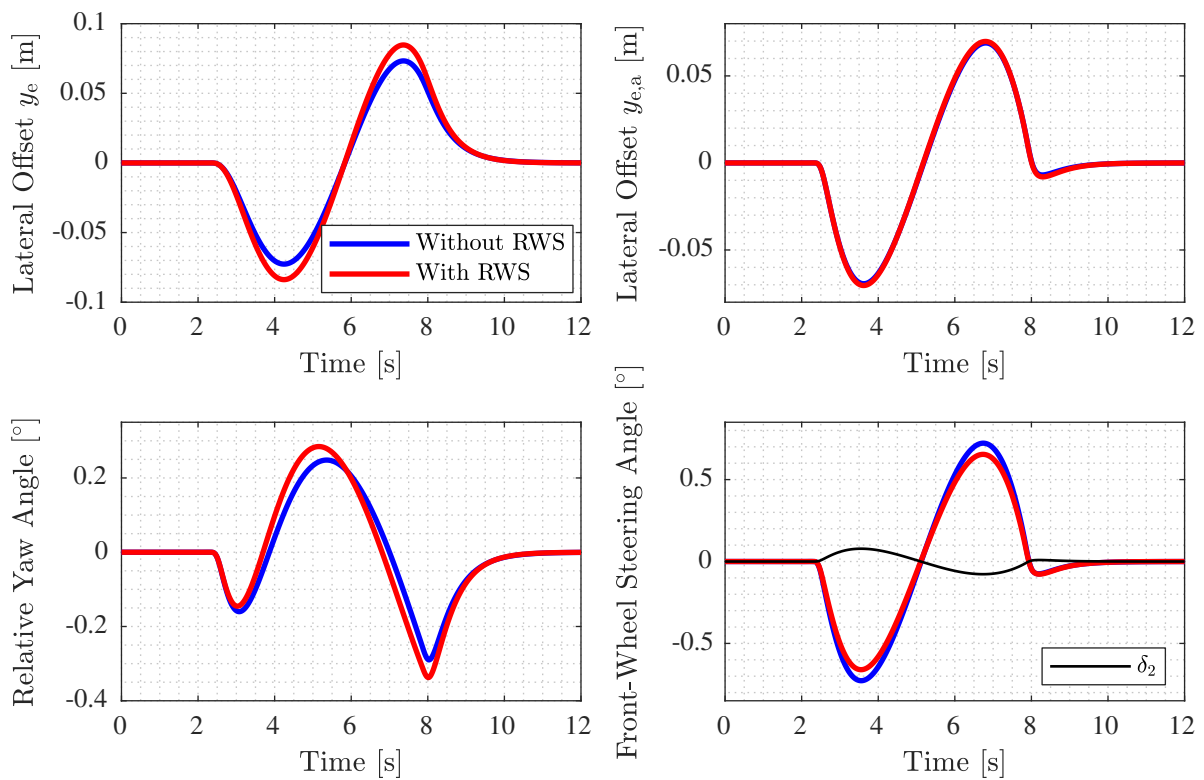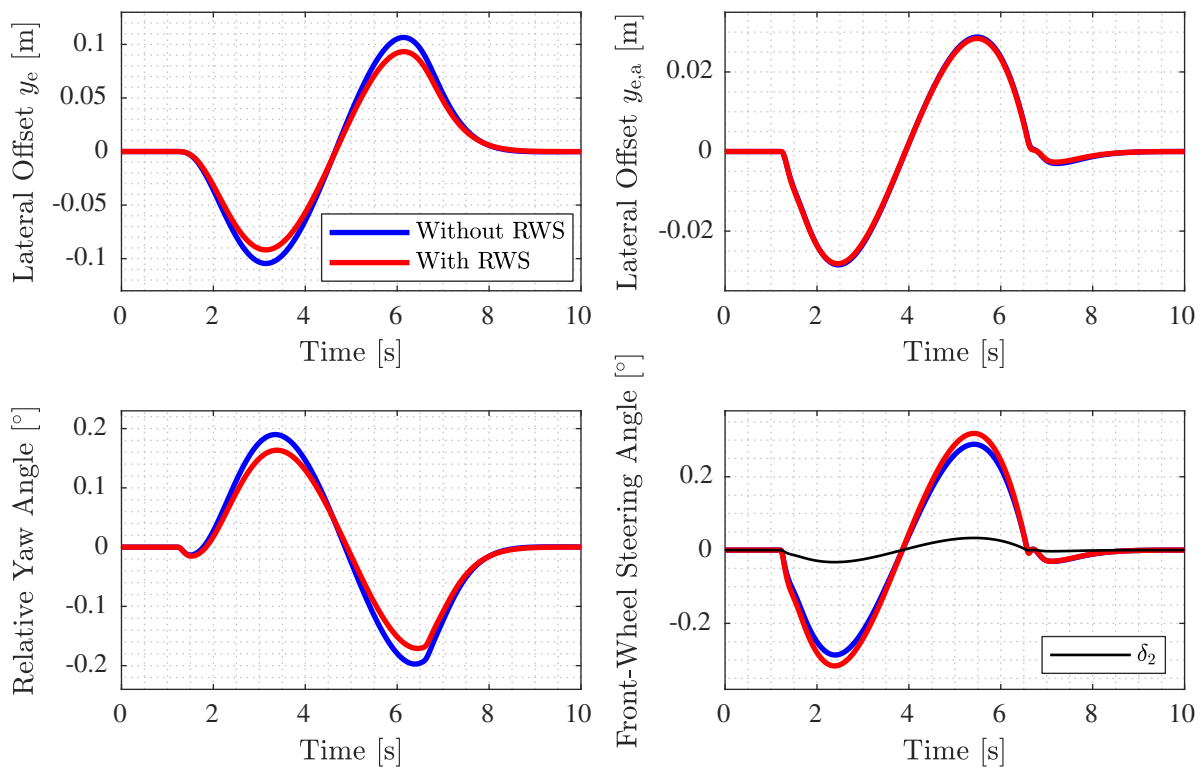
Figure D.2: ALC at 50 km/h.

Figure D.3: ALC at 130 km/h.

Table D.8: Maximum absolute lateral offset $\max|y_\mathrm{e}|$.

RWS Control Method[†]	$\max|y_\mathbf{e}|$ [m]								
	50 km/h	60 km/h	70 km/h	80 km/h	90 km/h	100 km/h	110 km/h	120 km/h	130 km/h
A	0.0733	0.0706	0.0717	0.0751	0.0799	0.0857	0.0921	0.0991	0.1065
B	0.0770	0.0706	0.0682	0.0677	0.0682	0.0691	0.0749	0.0811	0.0876
C	0.0773	0.0705	0.0687	0.0699	0.0729	0.0770	0.0820	0.0876	0.0936
D	0.0847	0.0753	0.0717	0.0715	0.0737	0.0773	0.0820	0.0873	0.0932
E	0.0594	0.0553	0.0562	0.0594	0.0639	0.0691	0.0749	0.0811	0.0883

Table D.9: Maximum absolute lateral offset $\max|y_\mathrm{e,a}|$.

RWS Control Method[†]	$\max|y_\mathbf{e,a}|$ [m]								
	50 km/h	60 km/h	70 km/h	80 km/h	90 km/h	100 km/h	110 km/h	120 km/h	130 km/h
A	0.0694	0.0554	0.0466	0.0407	0.0366	0.0337	0.0316	0.0300	0.0288
B	0.0697	0.0554	0.0464	0.0404	0.0362	0.0331	0.0311	0.0295	0.0283
C	0.0697	0.0554	0.0464	0.0405	0.0364	0.0334	0.0313	0.0297	0.0284
D	0.0704	0.0557	0.0466	0.0406	0.0364	0.0334	0.0313	0.0297	0.0284
E	0.0681	0.0543	0.0456	0.0399	0.0359	0.0331	0.0310	0.0295	0.0283

Table D.10: Maximum absolute relative yaw angle $\max|\psi_\mathrm{rel}|$.

RWS Control Method[†]	$\max|\psi_\mathbf{rel}|$ [°]								
	50 km/h	60 km/h	70 km/h	80 km/h	90 km/h	100 km/h	110 km/h	120 km/h	130 km/h
A	0.2898	0.2449	0.2207	0.2071	0.1996	0.1958	0.1950	0.1957	0.1973
B	0.3051	0.2449	0.2099	0.1874	0.1714	0.1587	0.1580	0.1585	0.1600
C	0.3066	0.2445	0.2117	0.1932	0.1825	0.1762	0.1728	0.1716	0.1716
D	0.3374	0.2616	0.2205	0.1976	0.1844	0.1768	0.1727	0.1711	0.1709
E	0.2262	0.1903	0.1736	0.1651	0.1608	0.1587	0.1581	0.1585	0.1611

Table D.11: Maximum absolute front-wheel steering angle $\max|\delta_1|$.

RWS Control Method[†]	$\max|\delta_\mathbf{1}|$ [°]								
	50 km/h	60 km/h	70 km/h	80 km/h	90 km/h	100 km/h	110 km/h	120 km/h	130 km/h
A	0.7275	0.5655	0.4695	0.4079	0.3661	0.3366	0.3157	0.3003	0.2888
B	0.7058	0.5655	0.4848	0.4356	0.4050	0.3862	0.3623	0.3445	0.3310
C	0.7037	0.5661	0.4823	0.4275	0.3896	0.3624	0.3430	0.3286	0.3176
D	0.6603	0.5421	0.4697	0.4213	0.3869	0.3615	0.3431	0.3291	0.3184
E	0.8088	0.6430	0.5366	0.4663	0.4190	0.3859	0.3621	0.3444	0.3294

[†]A = Without RWS, B = Linear, C = Decrease Side-Slip, D = Adapted Decrease Side-Slip, E = Yaw Rate Dependent

Table D.12: Maximum absolute rear-wheel steering angle $\max|\delta_2|$.

RWS Control Method[†]	$\max|\delta_2|$ [°]								
	50 km/h	60 km/h	70 km/h	80 km/h	90 km/h	100 km/h	110 km/h	120 km/h	130 km/h
A	0	0	0	0	0	0	0	0	0
B	0.0252	0.0000	0.0173	0.0311	0.0434	0.0552	0.0518	0.0492	0.0473
C	0.0276	0.0006	0.0145	0.0220	0.0262	0.0287	0.0303	0.0315	0.0323
D	0.0782	0.0268	0.0003	0.0150	0.0231	0.0278	0.0305	0.0321	0.0331
E	0.0974	0.0905	0.0767	0.0666	0.0599	0.0551	0.0517	0.0492	0.0464

[†]A = Without RWS, B = Linear, C = Decrease Side-Slip, D = Adapted Decrease Side-Slip, E = Yaw Rate Dependent

**Technische Universiteit
Eindhoven
University of Technology**

Declaration concerning the TU/e Code of Scientific Conduct
for the Master's thesis

I have read the TU/e Code of Scientific Conduct[i].

I hereby declare that my Master's thesis has been carried out in accordance with the rules of the TU/e Code of Scientific Conduct

<u>Date</u>

16 - 01 - 2020

<u>Name</u>

Thomas Neilen

<u>ID-number</u>

0852908

<u>Signature</u>

Submit the signed declaration to the student administration of your department.

---

[i] See: http://www.tue.nl/en/university/about-the-university/integrity/scientific-integrity/
The Netherlands Code of Conduct for Academic Practice of the VSNU can be found here also.
More information about scientific integrity is published on the websites of TU/e and VSNU

January 15 2016